
[All ETDs from UAB](#)

[UAB Theses & Dissertations](#)

2023

Investigating the p53 Tumor-Suppressive Network and the Dynamics/Mechanism of p53 Loss of Heterozygosity

Jun Wang
University Of Alabama At Birmingham

Follow this and additional works at: <https://digitalcommons.library.uab.edu/etd-collection>



Part of the [Medical Sciences Commons](#)

Recommended Citation

Wang, Jun, "Investigating the p53 Tumor-Suppressive Network and the Dynamics/Mechanism of p53 Loss of Heterozygosity" (2023). *All ETDs from UAB*. 380.

<https://digitalcommons.library.uab.edu/etd-collection/380>

This content has been accepted for inclusion by an authorized administrator of the UAB Digital Commons, and is provided as a free open access item. All inquiries regarding this item or the UAB Digital Commons should be directed to the [UAB Libraries Office of Scholarly Communication](#).

INVESTIGATING THE p53 TUMOR-SUPPRESSIVE NETWORK AND THE
DYNAMICS/MECHANISM OF p53 LOSS OF HETEROZYGOSITY

by

JUN WANG

ALEXA L. MATTHEYSES, COMMITTEE CHAIR
JOHN M. PARANT, MENTOR
LOUISE T. CHOW
BRUCE R. KORF
BRADLEY K. YODER

A DISSERTATION

Submitted to the graduate faculty of The University of Alabama at Birmingham,
in partial fulfillment of the requirements for the degree of
Doctor of Philosophy

BIRMINGHAM, ALABAMA

2023

Copyright by
Jun Wang
2023

INVESTIGATING THE P53 TUMOR-SUPPRESSIVE NETWORK AND THE DYNAMICS/MECHANISM OF p53 LOSS OF HETEROZYGOSITY

JUN WANG

GRADUATE BIOMEDICAL SCIENCE

ABSTRACT

Tumor suppressor gene TP53 is the most frequently mutated gene across human cancers (~50%). Patients with Li-Fraumeni syndrome (LFS) who carry germline p53 mutations exhibit a diverse spectrum of childhood- and adult-onset malignancies. Despite over 40 years of dedicated studies to understand the role of p53 in tumor prevention, there are still many unanswered questions regarding the underlying mechanisms of p53. Previous studies have supported the notion that p53 exerts its tumor-suppressive function through its transcriptional activities. Therefore, strategies to enhance p53's functions in tumor suppression via manipulating of downstream target gene activities in cancers show promising. To better investigate the *p53* tumor-suppressive network, we first generated *p53^{-/-}*, *p63^{-/-}*, *p73^{-/-}*, *puma^{-/-}*, *noxa^{-/-}* and analyzed their response to genotoxic, ER and ROS stresses. Our studies revealed that PUMA is a common module mediating apoptosis in these stress pathways. Therefore, the induction of PUMA expression may have promising therapeutic applications in p53-mutant human cancers.

p53-mediated apoptosis (via p53 targets PUMA/BBC3 and PMAIP1/NOXA) and cell-cycle arrest (via p53 target CDKN1A/p21) are considered the primary mechanisms downstream of p53 tumor suppression. However, intriguingly, multiple animal models with deficiencies in p53-mediated apoptotic cell death and cell-cycle arrest, while still displaying intact p53 other downstream transcription, still maintain the suppression of tumor onset. These suggest that other non-canonical p53 targets and their effector functions

may play a critical, and possibly even more significant, role in tumor suppression. To study this, we generated zebrafish triple knockouts of *puma*, *noxa*^{-/-} and *p21* and observed that these triple knockouts did not develop spontaneous tumors similar to the loss of *p53*. We next showed that *p21* is not the only p53 downstream target in regulation of cell cycle. To identify the other *p53* targets, we conducted a cross-species transcriptional analysis and defined 132 conserved *p53*-upregulated transcripts. We proposed that they may contribute significantly to p53 tumor suppression. Among these conserved transcripts, our following experiments confirmed that *ccng1*, *fbxw7* and *foxo3b* are important in *p53*-dependent cell-cycle arrest. These findings highlight additional players in p53-mediated tumor-suppressive networks.

Loss of heterozygosity (LOH) is a genetic event where an individual loses the remaining functional allele of a tumor suppressor gene. In the context of tumor suppression, LOH plays a critical role in cancer predisposition, particularly after the loss of one copy of tumor suppressor gene TP53. Cancers associated with LFS patients often lose the remaining wild-type p53 allele. Interestingly, recent comprehensive analysis of p53 mutant sporadic tumors have shown that inactivation of both alleles occurs in more than 90% of TCGA cancers, strongly suggesting that p53 LOH contributes to tumor initiation. The timing of tumor onset varies significantly among p53 heterozygous-null models, and the incidence and frequency of p53 LOH can impact the timing. Notably, ESCO2, which plays a crucial role in the establishment of sister chromatid cohesion during the cell cycle, has emerged as a promising modifier candidate in context of p53 LOH and timing of tumor initiation. Through studies in zebrafish and mouse p53 heterozygous nulls, we showed that *Esco2* haploinsufficiency accelerates the timing of tumor onset. We also demonstrated

esco2 haploinsufficiency resulted in reduced sister chromatid cohesion (SCC) and elevated mitotic recombination(MR)-derived p53 LOH. We proposed that reduced SCC as a promising modifier, contributing to the accelerated tumor penetrance by elevating p53 LOH derived from mitotic recombination. These findings indicate the complex interplay between sister chromatid cohesion and p53 LOH events, providing valuable insights into the molecular mechanisms that govern tumor initiation and progression.

Keywords: p53, Tumor Suppression, Apoptosis, Cell-cycle Arrest, Loss of Heterozygosity

ACKNOWLEDGMENTS

I am filled with immense grateful as I reflect on my journey as a graduate student. First and foremost, my heart overflows with appreciation and thanks for my mentor, Professor Dr. John M. Parant. Your unwavering support and guidance have been a constant source of strength. Your "open-door policy" and boundless patience have always made me feel welcome, providing timely help with scientific questions and life's challenges alike. Your belief in me as a scientist, encouraging me to pursue my hypotheses and defend my ideas in research, has been truly inspiring. In moments of difficulty, you have been there for me, both in the lab and in life. I couldn't have asked for a better mentor.

A special note of thanks goes to Holly, who has been with me from the very beginning, offering exceptional guidance and support when I joined the lab. To all the former and current lab members, Flo, Yongjie, Stephanie, Griffin, and Jack, I extend my heartfelt gratitude. Your presence has not only helped me overcome obstacles in my project but has also provided comfort and encouragement during tough times. Our joyful moments, filled with laughter, funny conversations, and shared experiences in the lab, will forever hold a cherished place in my heart.

I am deeply thankful to my esteemed committee members, Drs. Alexa L. Mattheyses, Louise T. Chow, Bruce R. Korf, and Bradley K. Yoder. Your unwavering support throughout the years has kept me focused on achieving my research goals. Your valuable advice and guidance have been instrumental in shaping the course of my work. To the directors of BSB Theme, Drs. Thomas M. Ryan and Chad Petit, I express my sincere gratitude. The opportunity to pursue my graduate research here and the generous support I have received during my journey have been truly invaluable.

Above all, I dedicate my dissertation to my beloved family. To my mom and dad, thank you for being my unwavering pillars of support throughout my life. Your respect for my decisions and words of encouragement in times of adversity have meant the world to me. To my husband, Zhang Li, you are my best friend, and I am forever grateful for all that you do for me. And to my precious son Ethan, being your mom has been the greatest blessing of my life. You have brought boundless joy into my world, and I wish you nothing, but a life filled with wonder and happiness.

TABLE OF CONTENTS

	<i>Page</i>
ABSTRACT.....	iii
ACKNOWLEDGMENTS	vi
LIST OF FIGURES	x
CHAPTER 1: INTRODUCTION.....	1
p53 Tumor Suppression	1
Regulation of p53 Following Cellular Stress.....	2
p53 Mediated Cell-Cycle Arrest via p21/Cdkn1a.....	7
p53 Mediated Apoptosis via PUMA and NOXA	7
p53 Family Members p63 and p73 Also Mediated Apoptosis via PUMA and NOXA.....	9
p53 is Sufficient to Suppress Tumor Formation in the Absence of PUMA, NOXA, and p21	10
p53 Transcriptome and Non-Canonical Downstream Pathways	12
p53 Tumor Suppression is Conserved in Zebrafish.....	13
p53 Loss of Heterozygosity (LOH).....	16
p53 LOH Modifier: Reduced Sister Chromatid Cohesion.....	19
Concluding Remarks.....	21
CHAPTER 2: PUMA, NOXA, P53 AND P63 DIFFERENTIALLY MEDIATE STRESS PATHWAY INDUCED APOPTOSIS	25
CHAPTER 3: p21, CCNG1, FOXO3B AND FBXW7 CONTRIBUTE TO p53-DEPENDENT CELL-CYCLE ARREST	69
CHAPTER 4: REDUCED SISTER CHROMATID COHESION ACTS AS A TUMOR PENETRANCE MODIFIER.....	125

CHAPTER 5: SUMMARY, CONCLUSIONS AND FUTURE DIRECTIONS	176
p53-Mediated Apoptosis Mainly Occurs through the Activation of Puma in Response to IR-irradiation	178
p53-Independent Apoptosis Mainly Occurs through The Activation of Puma in Response to ER and ROS stress	179
Investigating Tissue-Specific Puma Expression Patterns after p53 Activation.....	181
p21 is Important but Not the Sole Mediator in p53-Mediated Cell Cycle Arrest.....	184
Identified Conserved p53 Target Gene Candidates	186
Identification of ccng1, fbxw7 and foxo3b as Important Components of p53-dependent Cell-Cycle Arrest	189
Overcoming Challenges in Identifying p53 Target Genes and Unraveling Tissue-specific Roles in Tumor Suppression.....	191
Reduced Sister Chromatid Cohesion Acts as Modifier for p53 LOH and Tumor Penetrance in p53 Heterozygous Null Background	194
Monitoring p53 LOH in Somatic Tissues at Single-Cell Level.....	195
 GENERAL LIST OF REFERENCES	 201
APPENDIX: IACUC ANIMAL USAGE APPROVAL.....	216

LIST OF FIGURES

<i>Figure</i>		<i>Page</i>
CHAPTER 1: INTRODUCTION		
1	Figure 1. Simplified model depicting regulation of p53 protein in unstressed cells.....	3
2	Figure 2. Models depicting regulation of p53 protein in response to cellular stresses.	6
CHAPTER 2: PUMA, NOXA, p53 AND p63 DIFFERENTIALLY MEDIATE STRESS PATHWAY INDUCED APOPTOSIS		
1	Figure 1. Quantitative real-time PCR (qRT-PCR) analysis of pro-apoptotic markers after IR- and drug-induction in wild-type zebrafish embryos.....	30
2	Figure 2. The protein structure of 6 mutant alleles in zebrafish generated by Zinc Finger, TALEN or CRISPR-Cas9 gene editing.....	32
3	Figure 3. Loss of <i>puma</i> not <i>noxa</i> rescues IR-induced apoptosis in <i>p53</i> -dependent manner.....	36
4	Figure 4. Loss of <i>puma</i> rescues <i>mdm2</i> -null induced apoptosis at early embryonic stage	39
5	Figure 5. Loss of <i>puma</i> partially rescues Thapsigargin (Thaps.)-induced apoptosis at early embryonic stage	41

6	Figure 6. Loss of <i>p63</i> (not <i>p53</i> and <i>p73</i>) partially rescued Thaps. induced apoptosis at early embryonic stage	44
7	Figure 7. <i>puma</i> and <i>noxa</i> are required for PMA-induced apoptosis	46
8	Figure 8. <i>p63</i> , but not <i>p53</i> and <i>p73</i> , are required for PMA-induced apoptosis	48

CHAPTER 3: p53 MEDIATING CELL-CYCLE ARREST THROUGH p21-DEPENDENT AND INDEPENDENT PATHWAY IN RESPONSE TO STRESS IN ZEBRAFISH MODEL

1	Figure 1. <i>puma</i> ^{-/-} ; <i>noxa</i> ^{-/-} ; <i>p21</i> ^{-/-} zebrafish are not predisposed to spontaneous tumors.....	74
2	Figure 2. Loss of <i>puma</i> , <i>noxa</i> and <i>p21</i> provide completely resistance to <i>p53</i> -mediated induction of apoptosis and partially resistant to <i>p53</i> -mediated cell-cycle arrest	76
3	Figure 3. Loss of <i>p21</i> partially rescues <i>p53</i> -dependent <i>mdm2</i> -null induced cell-cycle arrest	79
4	Figure 4. Defining early-responsive <i>p53</i> -upregulated genes in response to IR-irradiation in zebrafish.....	83
5	Figure 5. Defining conserved <i>p53</i> -upregulated genes in zebrafish and mouse	85
6	Figure 6. The functional enrichment analysis for conserved <i>p53</i> -induced genes in zebrafish and mouse	89
7	Figure 7. Comparing 132 conserved genes with DEGs in <i>mpnp</i> ^{-/-} datasets	93
8	Figure 8. <i>fbxw7</i> , <i>foxo3b</i> and <i>ccng1</i> G0 crispants partially rescued <i>mpnp</i> -null induced cell-cycle arrest	96
9	Figure S1. Generation and validation of a stable <i>cdkn1a/p21</i> mutant in zebrafish.....	108
10	Figure S2. IR-induced cell-cycle arrest at 6 and 9 hpi.....	109
11	Figure S3. Loss of <i>puma</i> , <i>noxa</i> and <i>p21</i> getting rid of their downstream <i>p53</i> indirectly regulated differentially expressed genes (DEGs)	110
12	Figure S4. Transcriptional analysis on IR-treated mouse embryos	111

13	Figure S5. One example of not orthologue but paralogues of zebrafish DEGs upregulated in mice	112
14	Figure S6. Line graphs showing the kinetics for 132 conserved p53-upregulated genes from 1 to 3 hpi in response to IR-irradiation	113
15	Figure S7. Line graphs showing the kinetics for 108 overlapped p53-upregulated genes from 8 to 16 hpf in MPNP and PNP group	114
16	Figure S8. Line graphs showing the kinetics of the rest 24 GOIs in MPNP datasets.....	115
17	Figure S9. Recapitulation of Null phenotypes in G0 embryos by four-guide targeting <i>p53</i>	116
18	Figure S10. None crispants of 24 GOIs rescue morphological abnormality for <i>mpnp</i> ^{-/-} embryos.....	117
19	Figure S11. Representative pH3-stained images for injected <i>mpnp</i> ^{-/-} and sibling controls for all 24 GOIs.	118
20	Figure S12. Rescue/resistance ratio (RR) for all 24 GOIs.....	119

CHAPTER 4: REDUCED SISTER CHROMATID COHESION ACTS AS A TUMOR PENETRANCE MODIFIER

1	Figure 1. <i>Esco2</i> deficiencies are common in multiple tumor types and associated with poor patient survival	131
2	Figure 2. <i>Esco2</i> deficiencies accelerate tumor onset in a LOH-sensitive background.....	136
3	Figure 3. Reduced SCC in <i>esco2</i> and <i>sgoll</i> haploinsufficient animals correlates with accelerated tumor onset.....	139
4	Figure 4. Elevated mitotic segregation errors in <i>esco2</i> haploinsufficient embryos.....	142
5	Figure 5. Elevated micronuclei during embryogenesis does not contribute to enhanced tumor onset.	145

6	Figure 6. Reduced SCC allows for elevated mitotic recombination derived LOH	148
---	---	-----

CHAPTER 5: SUMMARY, CONCLUSIONS, AND FUTURE DIRECTIONS

1	Figure 1. Schematic showing how <i>p53</i> , <i>p63</i> , <i>p73</i> , <i>puma</i> and <i>noxa</i> in response to different cellular stress in zebrafish.....	180
2	Figure 2. Generation of overexpression (OE) zebrafish line.	183
3	Figure 3. Proposed models depicting <i>p53</i> downstream tumor-suppressive network.....	185
4	Figure 4. Generation and validation of transgenic fish to visualize <i>p53</i> LOH in somatic tissues.	198

CHAPTER 1

INTRODUCTION

p53 Tumor Suppression

p53 encoded by TP53 in human, is one of the most widely implicated tumor suppressors in cancer research. The Cancer Genome Atlas (TCGA) data reconfirm that TP53 is the most frequently mutated gene across various cancers (~50%) [1]. p53 mutations were found in approximately 80% of basal-like/triple-negative breast cancer, the most lethal subtype of breast cancer [2]. Clinically, TP53 mutation is linked to poor patient prognosis [3-7]. Even in cancers that contain wild-type TP53, its expression is also repressed through different mechanisms [8, 9].

The significance of p53 in tumor suppression is further supported by an autosomal dominant, highly penetrant cancer predisposition syndrome, the Li-Fraumeni syndrome (LFS). TP53 mutations are a hallmark of LFS diagnosis, and germline mutations in TP53 have been identified in 50-70% of LFS families, with sarcomas being the most prevalent associated disease [10-16]. LFS can bear a diverse spectrum of childhood- and adult-onset malignancies, with a 70% or higher lifetime risk of cancer in men and a 90% or higher lifetime risk of cancer in women [13, 15].

Multiple p53 knockout or mutant mice were generated to model LFS and understand the role of p53 in tumor suppression. p53 heterozygous- and homozygous-null mice develop spontaneous tumors (most are lymphoma, some are sarcoma) at 100%

penetrance [17, 18]. Similar results were observed in zebrafish *p53*-deficient models. We and others have generated different *p53* mutant or null alleles and found *p53* homozygous-mutant or -null zebrafish form tumors spontaneously (100% sarcoma) with 100% penetrance [19, 20]. These data highlight the importance of p53 function in tumor suppression and indicate the conservation of its tumor-suppressive function across vertebrate species.

Regulation of p53 Following Cellular Stress

In “normal” cells, p53 protein level is maintained at low levels by a series of negative regulators. Among them, Murine double minute 2 (MDM2) is the major player, containing RING finger domain at the C-terminal, which functions as an E3 ubiquitin ligase responsible for promoting the degradation of p53 [17-19] (Figure 1). Additionally, MDM2 also can bind the TAD domain of p53 and inhibit its transcriptional activity under homeostatic conditions [19].

unstressed state

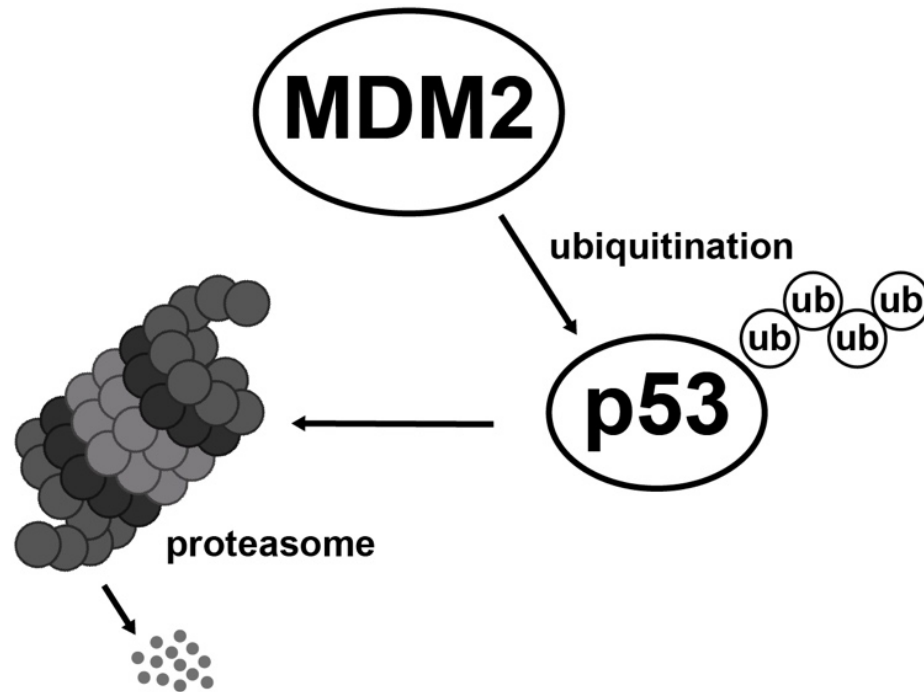


Figure 1. Simplified model depicting regulation of p53 protein in unstressed cells. (Ub, ubiquitin)

In response to a variety of cellular stresses, such as DNA damage or oncogene activation, p53 can be stabilized and activated through different mechanisms, often involving post-translational modifications, such as phosphorylation, acetylation and methylation. These modifications prevent p53 degradation or enhance its transcriptional activity. For instance, in the presence of DNA damage, both p53 and MDM2 can be phosphorylated by ataxia-telangiectasia (ATM) kinase, especially in cases of ionizing radiation (IR)-induced DNA damage. This phosphorylation event leads to p53 activation by inhibiting MDM2-mediated degradation [17].

Upon activation, p53 acts as the “Guardian of the Genome” and activates a wide range of downstream target genes that contain the p53 response element in their promoter region. These activated downstream targets, in turn, orchestrate a diverse array of biological processes, working towards either eliminating damaged cells or inducing cell-cycle arrest [18, 19]. In performing these crucial functions, p53 plays an essential role in limiting the deleterious outcome of mutations and ensuring the safeguarding of genomic integrity.

Furthermore, MDM2 is itself a transcriptional target of p53 and is induced following p53 activation[20-24]. This forms a negative feedback loop between p53 and MDM2 which can regulate the duration of p53 response, leading to its termination once the upstream stress signals cease. In this way, the p53-MDM2 negative feedback loop play a critical role in controlling the dynamic response of p53 in response to cellular stress, ensuing that p53 regulatory network is tightly regulated and finely tuned.

As a key transcription factor, p53 is capable of inducing a diverse array of target genes to facilitate distinct biological outcomes. These outcomes include but not limited to

the regulation of apoptosis, cell-cycle arrest, DNA damage response, autophagy, metabolism, ROS control, tissue remodeling, inflammation/TME, and EMT/invasion [18]. Among them apoptosis (mediated by pro-apoptotic Bcl-2 family members PUMA/BBC3 and NOXA/PMAIP1) and cell-cycle arrest (achieved through the CDK inhibitor p21^{cip}/CDKN1A) are the most extensively studied and are poised to be critical barriers to cancer development downstream of p53 [25-27] (Figure 2).

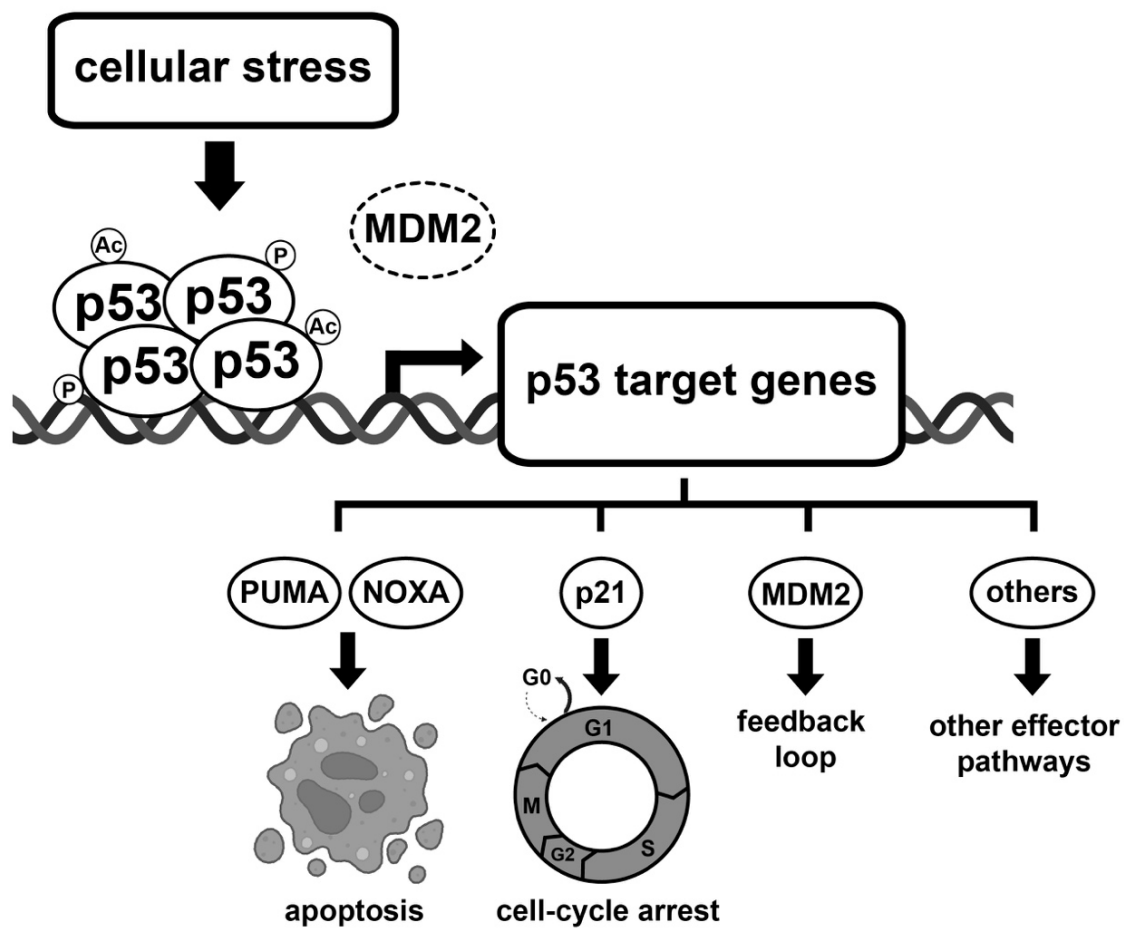


Figure 2. Models depicting regulation of p53 protein in response to cellular stresses.

(P, phosphorylation; Ac, acetylation; dashed circle of MDM2 indicating mdm2 which cannot destabilize p53 protein following cellular stress)

p53 Mediated Cell-Cycle Arrest via p21/Cdkn1a

Cell cycle contains a series of ordered events leading to cell division and can be divided into four stages: G1, S, G2 and M. Throughout this process, there are three major cell-cycle checkpoints that play a crucial role in preventing the transmission of damaged or incomplete chromosomes to daughter cells, ensuring the accurate completion of all important processes. Among these checkpoints, the G1/S checkpoint serves to prevent cells from replicating damaged DNA, whereas the G2/M checkpoint blocks cells from dividing if the damage is deemed irreparable.

p21^{cip}/CDKN1A, also known as p21^{waf1/cip1}, is one of the most important cyclin-dependent kinase inhibitors in cell-cycle arrest. Remarkably, p21 was the first transcriptional target of p53 to be discovered. The p21 gene harbors two conserved p53 responsive elements in its promoter region [25, 28]. Functionally, p21 exerts cell-cycle arrest effects at both G1/S and G2/M transitions by inhibiting the interactions of CDK4/6 with cyclin D and CDK2 with cyclin E, respectively [26, 29-31].

The primary upstream regulator that induces the expression of p21 is p53. Previous studies have shown that various stimuli, including DNA damage and oxidative stresses activate p53, subsequently leading to the induction of p21 and G1 cell-cycle arrest [25, 28, 32, 33]. Notably, the G1/S checkpoint does not exist if either p53 or p21 are absent, suggesting that the G1/S checkpoint is frequently defective in p53-mutant cancer cells. Intriguingly, in several instances during normal tissue development and cellular differentiation, p21 can be upregulated in a p53-independent manner [34].

p53 Mediated Apoptosis via PUMA and NOXA

When the body's equilibrium is disrupted, cellular stress responses are triggered [35]. Often, this results in cell death to eliminate the stressed cell from the body [36-42]. However, when the apoptotic response is either upregulated or dysregulated, it can be linked to various human diseases. Apoptosis, a form of programmed cell death, is evolutionarily conserved and tightly regulated process that plays important roles in homeostasis, development and in response to different cellular stresses. The Bcl-2 family proteins are involved in the controlling the apoptotic processes [43-45]. These proteins can be categorized into three groups: 1) Pro-apoptotic proteins, which contain three Bcl-2 Homology (BH) domains, include Bak, Bad, Bok, Diva and etc; 2) Pro-apoptotic BH3-only proteins, represented by PUMA and NOXA, which play key roles in initiating apoptosis. 3) Anti-apoptotic Bcl-2 family proteins, such as Bcl-2, Bcl-X_L, Bcl-w and Mcl-1, which act to prevent apoptosis and promote cell survival. Apoptosis is generally initiated by the release of cytochrome c from the mitochondria into the cytosol. The release is via the channel formed by the oligomerization of pro-apoptotic proteins BAK or BAX in the outer mitochondrial membrane. In response to various cytotoxic stresses, pro-apoptotic BH3-only proteins act as sensors/inducers. These BH3-only proteins bind to anti-apoptotic family members and inhibit their ability to block the activation of BAX/BAK [46]. By neutralizing the anti-apoptotic proteins, the BH3-only proteins enable BAX/BAK to initiate the apoptotic process and ultimately lead to cell death.

PUMA (p53 Up-regulated Modulator of Apoptosis protein) is encoded by the Bcl-2 binding component 3 (BBC3) gene. Previous studies have shown that PUMA is directly activated by p53, which binds to specific sites in its promoter region in response to diverse cellular stresses like DNA damage, oxidative stress or viral infection [47]. Similarly,

NOXA is encoded by the Phorbol-12-myristate-13-acetate-induced protein 1 (PMAIP1) gene and is also primarily induced by p53. For example, when exposed to X-ray irradiation, wild-type mouse embryonic fibroblasts (MEFs) exhibit a rapid increase in Noxa expression, whereas p53-deficient MEFs do not show such induction [48]. These findings highlight the critical role of p53 in activating PUMA and NOXA as part of the apoptotic response to ensure cellular integrity in response to cellular stresses.

p53 Family Members p63 and p73 Also Mediated Apoptosis via PUMA and NOXA

p63 and p73 are member of p53 family and also play important roles in mediating the apoptotic response [49-53]. They share a conserved DNA binding domain with p53, enabling them to induce p53 target genes in response to different cellular stresses. However, the roles of p53, p63 and p73 in regulating cell death seem to depend on context, showing variations based on the tissue or cell type involved. Furthermore, the functions of p63 and p73 may extend beyond apoptosis regulation, as they are also implicated in various other biological processes such as development, differentiation, and tumor suppression. Their diverse functions highlight their significance in maintaining cellular homeostasis in response to various cellular stresses.

Endoplasmic reticulum (ER) stress, also known as the unfolded protein response (UPR), plays an important role in various diseases, including retinal degeneration, diabetes, obesity, and neurological disorders [36]. When there is an accumulation of unfolded or misfolded proteins in the endoplasmic reticulum, it triggers the activation of the UPR. The main objectives of UPR are to halt protein translation, degrade misfolded proteins, and activate pathways that enhance the production of molecular chaperones to facilitate proper

protein folding. However, if these goals are not met within a specific time frame or if ER stress persists, the UPR will move towards apoptosis.

Oxidative stress arises from an imbalance between the production of reactive oxygen species (ROS) and the capability of the body to neutralize them, which is referred to as the redox state. ROS are highly reactive oxygen-based chemical intermediates that are naturally generated as byproducts of cellular processes. When there is an excessive production of ROS, it can lead to cellular toxicity and initiate apoptosis.

Previous studies have provided evidence indicating that p53 plays a critical role in regulating intrinsic apoptosis in response to ER stress by regulating the expression of Puma [54-56]. On the other hand, p73 can mediate the impact of ROS stress by increasing the BAK/BCL-2 ratio in human cells[57-59]. Furthermore, there are instances where induction of Puma and Noxa occurs independently of p53. For example, under conditions such as hypoxia, infection or cytokine depletion, Puma can be activated to eliminate damaged cells, regulated by p73 or Sp1 depending on the specific cell type [47, 60, 61]. Additionally, the induction of Noxa mRNA has been observed in various p53^{-/-} melanoma cell lines upon treatment of the γ -secretase inhibitor GSI [62].

p53 is Sufficient to Suppress Tumor Formation in the Absence of PUMA, NOXA, and p21

Previously, it has been widely believed that the tumor-suppressive role of p53 primarily relied on its ability to activate apoptosis and induce cell-cycle arrest at the G1/S boundary. However, the significance of these two cellular responses in the tumor-suppressive functions of p53 has been called into questions. The loss of Puma, Noxa or

p21 alone does not appear to be sufficient for tumor development. Mice lacking Puma, Noxa, and both Puma and Noxa do not spontaneously develop tumors [63]. Mutant p53 alleles R175P and E180R, which have defects in apoptosis but retain the ability to arrest the cell cycle, exhibit extended tumor-free survival compared to p53-null mice [64]. Furthermore, p21-null mice do not develop spontaneous tumors within seven months after birth [33]. Additionally, unlike p53, mutations in the p21 gene in human cancers are infrequent, with the highest incidence observed in bladder carcinomas (approximately 10%) [65].

If p53-mediated apoptosis and cell-cycle arrest indeed collaborate to suppress tumors, it would be expected that simultaneous knockout of all three targets regulating these pathways would result in a tumor predisposition similar to that observed with the loss of p53 alone. However, several findings challenge this notion and suggest that p53 alone suffices to suppress tumor formation, even in the absence of its pro-apoptotic effector (Puma and Noxa) and its cell-cycle inhibitor (p21). For instances, mutant mice harboring p53 mutations in the first transactivation domain (TAD) of p53 (L25Q, W26S, referred to as p53^{25,26}) displayed resistance to DNA damage-induced apoptosis and cell-cycle arrest, due to defective transcriptional induction of key p53 targets such as Puma, Noxa and p21. Strikingly, unlike p53-deficient mice that all developed lymphoma or sarcoma within 250 days, homozygous p53^{25,26} mutant animals did not exhibit accelerated tumor formation in a mutant Ras-driven transgenic model of non-small cell lung cancer. Another p53 mutant mouse strain, p53^{3KR}, lacking three conserved amino acid residues critical for acetylation in response to DNA damage, failed to induce apoptosis and cell-cycle arrest, attributed to defective induction of Puma, Noxa, p21 and other p53 targets. Nonetheless, the incidence

of spontaneous tumor formation was low and occurred late in p53^{KR} mice. Furthermore, mice deficient in all three p53-mediated targets (Puma, Noxa and p21) remained tumor-free, in contrast to p53-deficient mice. [66]. Therefore, these findings strongly indicate that p53's tumor-suppressive role extends beyond the regulation of Puma, Noxa and p21, and other downstream targets and/or pathways are critical for its tumor-suppressive actions.

It is important to note that while the loss of Puma, Noxa, and p21 is not enough to fully replicate the tumor predisposition observed in p53 deficiency, this does not rule out their potential involvement in tumor suppression. Therefore, further studies aiming to investigate additional targets or pathways involved in p53-mediated tumor suppression should consider taking advantages of models lacking Puma, Noxa and p21. By utilizing these models, researchers can better explore the contributions and interactions of these other targets and pathways in the tumor-suppressive functions of p53.

p53 Transcriptome and Non-Canonical Downstream Pathways

To elucidate the other targets within the p53 regulatory network involved in tumor suppression, multiple research groups have conducted a large number of Chromatin Immunoprecipitation Sequencing (CHIP-seq) experiments, consisting of at least 132 datasets, as well as extensive gene expression sequencing such as RNA-seq in human cell lines with wild-type p53 following activation of p53 using various stimuli [67]. However, the identification of p53 target genes from these different datasets has yielded inconsistent results, with thousands of candidate genes being reported. To address this, several meta-analyses have been conducted in an attempt to integrate and reconcile the vast amount of sequencing data. However, it is a quite challenging job, especially considering the

variability of cell types, duration, nature of stimuli and experimental techniques employed. Among them the largest-scale meta-analysis to define p53 targets in humans involved the analysis of 41 CHIP-seq datasets and 16 gene expression datasets, ultimately identifying over 943 genes directly targeted by p53 (referred to as the p53 “cristrome”) [68]. These studies have provided a valuable resource of potential direct target genes of p53 in humans.

Furthermore, considerable efforts have also been devoted to characterizing p53-regulated targets in mice. For example, Broz et al. identified p53 binding sites in the promoter region of approximately 3000 genes in MEFs treated with the DNA-damage inducer doxorubicin [69]. Li et al. discovered over 3,500 direct p53 target genes in mouse embryonic stem (ES) cells treated with another DNA-damage inducer Adriamycin [70]. Tonelli et al. profiled the transcriptional responses to p53 restoration in Myc-driven lymphomas and identified over 4000 conserved p53 high-confidence binding sites at the promoters of target genes [71]. However, similar to the analysis conducted in humans, the inconsistent identification of gene candidates across different datasets is also a major concern in mouse studies. Additionally, another concern is that these sequencing data in both humans and mice were obtained using cultured cells, which lack the diversity of cell types, tissue complexity, and organismal physiology. Therefore, a deeper exploration of the p53 target genes involved in tumor prevention is warranted.

p53 Tumor Suppression is Conserved in Zebrafish

Zebrafish, serving as a powerful model, possess several major advantages over other vertebrate models for investigating in vivo pathology associated with human diseases. One notable advantage is their high fecundity, as a mating pair can produce a substantial

number of eggs, ranging from 50 to 300 eggs at a time, in a single reproductive event. Moreover, these pairs can undergo repeated breeding, typically on a weekly basis. The abundance of progeny provides unique opportunities for large-scale genetic screens and facilitates the generation of genetically complex animals, such as quadruple null mutants, within fewer generations compared to rodent models. The large brood size also allows for the generation of sizable tumor cohorts, with up to 96 individuals per genotype, from a single mating pair.

Another advantage of zebrafish is their external fertilization, which simplifies the monitoring of embryonic phenotypes in real time. Furthermore, the transparent nature of zebrafish embryos and larvae further enhances their utility, as it enables the imaging and visualization of cellular and molecular markers throughout the entire organism. This transparency facilitates the examination of various cell types and tissues, providing valuable insights into developmental processes and disease mechanisms.

Furthermore, there is a high degree of shared genome sequence between humans and zebrafish, with approximately 70% of human genes having at least one orthologue in zebrafish (compared to 80% in mice) [72, 73]. Moreover, around 82% of human disease-related genes have homologues in zebrafish [74] and many disease pathways and stress responses are conserved between the two species. Additionally, spontaneous development of cancers can occur in zebrafish following exposure to mutagens or through transgenesis, and these tumors often exhibit histological and genetic similarities to human cancers [75].

In summary, zebrafish provide distinct advantages as a model system, including high fecundity, ease of genetic manipulation, external fertilization, and transparency. Moreover, zebrafish exhibit a high degree of genetic similarity to humans, conservation of

disease-related genes and pathways with humans and have the ability to spontaneously develop cancers. A large number of studies, including our own and those of others, have successfully demonstrated the utility of zebrafish as a model system for investigating a wide range of diseases and biological processes, including cancer predisposition, heart development, and neurodegeneration among others [76-80]. Overall, zebrafish is a highly valuable model for large-scale genetic studies, human disease modeling and visualization of developmental processes and advancing our understanding of disease mechanism and potential therapeutic strategies.

In addition to the previously discussed advantages of zebrafish as a model organism, zebrafish serves as an ideal model to study p53's tumor-suppressive function. First, p53 analogues have been identified in other genetically engineered model systems, such as *Drosophila melanogaster*, *Caenorhabditis elegans* and *Danio rerio* [81-85]. However, there are limitations to using invertebrate models in fully recapitulating the complexity of the p53 regulatory networks observed in mammalian systems, as well as the formation of spontaneous tumors. For example, both drosophila and nematode lack the entire p53 family, including p53, p63 and p73, as well as the negative regulators of p53, MDM2 and MDM4 [85]. These components are crucial modules in the regulatory loops governing p53 activity. In contrast, zebrafish possess the complete p53 regulatory network, encompassing all three p53 family members (p53, p63 and p73) and the negative regulators (mdm2, mdm4 and hausp) [85]. The conservation of the p53 tumor-suppressive pathway and its regulatory network in zebrafish suggests that this model organism holds immense potential for investigating the intricate mechanisms of the p53 tumor-suppressive network.

Furthermore, it is important to highlight the conservation of p53 tumor suppression across species. Studies have showed that p53 tumor suppression is conserved among species, including humans, mice, and zebrafish [13, 27, 86-90]. In mice, the loss of Trp53 (the mouse equivalent of human TP53) results in the developmental of tumors with high penetrance [86, 87, 91]. Congenital homozygous knockout mice for Trp53 develop spontaneous tumors within three to six months of age, while half of the heterozygous null mice develop tumors by 18 months [86, 92]. These findings demonstrate the critical role of p53 in tumor suppression in mice.

Similarly, in zebrafish, diverse tp53 mutant strains, such as I166T [76], M214K [90] and N168K [90], have been generated. These p53 mutant zebrafish strains exhibit heritable cancers, particularly malignant peripheral nerve sheath tumors (MPNSTs), a type of sarcoma. The development of early-onset tumors in zebrafish lacking functional p53 indicates the preservation of p53's transcriptional targets involved in tumor suppression across species.

These observations highlight the conservation of p53-mediated tumor suppression and support the notion that the transcriptional targets responsible for p53's tumor-suppressive function are conserved across humans, mice, and zebrafish. Consequently, zebrafish provide a valuable model for investigating the p53 tumor-suppressive network and further understanding its role in cancer development and progression.

p53 Loss of Heterozygosity (LOH)

Loss of heterozygosity (LOH) is a genetic event commonly observed in cancer development, where one copy of a gene, typically a tumor suppressor (TS) gene, and its

surrounding chromosomal region are lost in diploid organisms. Li-Fraumeni syndrome (LFS) provides an example of LOH. As mentioned earlier, LFS is a genetic disorder that is characterized by individuals who carry germline heterozygous p53 mutations. Previous studies have demonstrated that cancers associated with LFS patients often exhibit loss of the remaining functional wild-type p53 allele [10-12, 16, 93-95]. Initially, individuals with LFS possess one functional and one non-functional copy of the tp53 gene, allowing them to remain partial tumor-suppressive function. However, as they age, the remaining functional copy of p53 can become inactivated through segmental deletion or other mechanisms, resulting in the complete loss of p53 function. This loss of the remaining functional wild-type p53 allele may render the body vulnerable to oncogenic stresses and increase the risk of developing various tumors, particular sarcomas, contributing to the cancer predisposition observed in LFS patients.

Furthermore, in a recent integrated tumor analyses conducted by Donehower et al., they examined various human tumor types to determine the frequency of p53 mutations. Their findings showed that 91.3% of the tumors exhibited loss of both wild-type p53 alleles, while only 8.7% displayed likely retention of the second wild-type p53 allele [8]. This indicates a significant preference for the loss of the remaining wild-type p53 allele following mutation of the first functional allele, suggesting strong selective pressure. However, the exact factors that drive this strong selection are still unclear.

As previously mentioned, p53 homozygous mutants exhibit complete penetrance in developing spontaneous tumors in both mice and zebrafish. Interestingly, p53 heterozygous mutants also show complete penetrance in tumor development [76, 86, 88, 89]. However, in comparison to p53 homozygous mutants, the timing of tumor onset in

p53 heterozygous mutants varies to a greater extent, even under identical experimental conditions and genetic backgrounds. For example, in p53 heterozygous mutant zebrafish, it takes more than 450 days for tumors to appear in the initial 50% of the population. However, within this time frame, all p53 homozygous mutants succumb to tumors [89]. Typically, tumorigenesis requires the complete inactivation of tumor suppressor genes. Therefore, stochastic events may play a critical role in the loss of wild-type p53 allele.

Accumulating evidence emphasizes the significance of p53 LOH in the process of tumorigenesis. Detailed analyses conducted on tumors from p53 heterozygous mutant mice and zebrafish have consistently demonstrated the loss of the p53 wild-type allele in cells derived from these tumor samples [76, 86, 88-90]. Venkatachalam et al. observed that early-onset tumors in a cohort of p53 heterozygous mutant mice frequently exhibit p53 LOH, while late-onset tumors do not. This correlation suggests that the occurrence of p53 LOH in tumors is linked to the timing of tumor onset [96].

Furthermore, the frequency of tumors with p53 LOH in p53 heterozygous-null mice is dependent on the genetic background. For example, p53 LOH is observed in approximately 96% in a BALB/c background, but only around 50% in a mixed C57/129 strain. Additionally, tumor onset tends to occur earlier in BALB/c mice. These results suggest that the loss of the remaining p53 wild-type allele contributes to tumor initiation. These findings suggest that this loss contributes to the initiation of tumors.

However, a critical barrier is that existing models only enable the study of p53 LOH in tumor samples, which are end products in the process of tumorigenesis. Consequently, it remains impossible to ascertain whether the frequency or rate of p53 LOH affects tumor initiation or subsequent events such as promotion, aggressiveness and metastasis. Indeed,

studying p53 LOH in somatic tissues before tumor initiation is crucial. However, considering the extremely low frequency of p53 LOH in somatic tissues, current methods face limitations in accurately assessing such changes. For instance, bulk RNA-seq is unable to detect differences smaller than 1%. Fluorescence in situ hybridization (FISH) can produce a high number of false-positive results. Moreover, since p53 expression is typically very low in normal cells, examining p53 LOH through immunohistochemistry using a p53 primary antibody is undoable. Therefore, the development of a model system that allows the monitoring of p53 LOH in somatic cells is critical. Such a model would provide a valuable tool for studying the dynamics/mechanisms of p53 LOH, shedding light on its role in tumor initiation.

Moreover, multiple avenues can inactivate the second allele of a tumor suppressor gene in human cancers. These mechanisms can be broadly categorized into two major types. The first type is LOH with copy number losses, including the whole or segmental chromosome deletion. The second type is referred to as copy neutral LOH, commonly known as uniparental disomy (UPD). Copy neutral LOH occurs when there is a duplication or homologous recombination event involving the retained allele. The first avenue of inactivating the second allele, particularly segmental deletion, is a major cause of p53 LOH in human cancers [97, 98].

p53 LOH Modifier: Reduced Sister Chromatid Cohesion

Factors that affect genome stability have the potential to be a modifier of p53 LOH. Genomic alterations are generally regarded as cancer hallmarks and are often associated with poor patient outcomes. Three main types of genomic alternations include missegregation,

aneuploidy, and micronuclei formation [99]. These alterations commonly arise from mitotic errors; however, the specific drivers of these changes in tumors remain unclear [100-102]. For instance, defects in microtubule attachment and spindle assembly checkpoint can lead to genomic instability and increase cancer susceptibility [103, 104]. RecQ helicases, such as WRN or BLM, have been demonstrated to elevate the rate of mitotic recombination, making them to be modifiers of p53 LOH and influencing tumor penetrance [105-107].

Furthermore, an aberration in sister chromatid cohesion (SCC) could potentially serve as another modifier for p53 LOH. During the S phase, DNA replication generates two identical copies of DNA molecules known as sister chromatids, which remain connected in their chromatinized form. These sister chromatids remain joined throughout the G2 phase and early stages of M phase. A series of preparations occurs for cell division, and once everything is set, the sister chromatids separate from each other during anaphase and migrate towards opposite spindle poles of the mother cell. This chromosome separation is followed by the division of the mother cell into two genetically identical daughter cells. The physical connection that retains sister chromatids prior to chromosome partitioning is referred to as SCC [108, 109]. SCC is an important process for proper chromosome segregation, ensuring that sister chromatids are equally distributed to two daughter cells during mitosis. Without proper cohesion, sister chromatids cannot be symmetrically segregated, leading to aneuploidy, which represents an abnormal number of chromosomes in a cell [110]. Additionally, cohesion plays a critical role in accurate chromosome segregation during both meiosis I and meiosis II. In human oocytes, defects in cohesion can result in aneuploidy, a significant cause of spontaneous abortion. Only a few types of

aneuploidies, such as trisomy 21, trisomy 18, and trisomy 13, are compatible with viability [111].

During S phase, SCC is established, and the presence of cohesion 1 homolog 2 (ESCO2) is essential for this process. ESCO2 is frequently deleted or altered in human cancers [109, 112]. Mutations in ESCO2 have been linked to Robert/SC phocomelia syndrome, a developmental disorder. Patients with Roberts syndrome have exhibited defects in centromeric cohesion, highlighting the significance of ESCO2 in establishing cohesin. However, the involvement of impaired SCC in cancers has been less extensively studied. This is primarily due to the fact that complete loss of SCC triggers a series of detrimental biological processes, including apoptosis, cell-cycle arrest, and cellular senescence, which are incompatible with tumor development [113]. Furthermore, even mild SCC dysfunction is proposed to be toxic to cells since centromeric cohesion is required for establishing bi-orientation of kinetochores during mitosis [114].

Concluding Remarks

This thesis focuses on unraveling the p53 regulatory network in tumor suppression and investigating how the loss of the wild-type allele of p53 in heterozygous-null zebrafish impacts tumor initiation. The thesis comprises three main research projects: 1) Studying the roles of *puma*, *noxa*, *p53* and *p63* in mediating apoptosis in response to various cellular stresses. This research has been published in *Cell Death and Disease*; 2) Identifying conserved p53-induced genes between mice and zebrafish, and defining that *p21*, *ccng1*, *fbxw7* and *foxo3b* function in p53-mediated cell-cycle arrest. This study is currently prepared for submission to *Cell Death and Differentiation*; 3) Investigating how reduced

sister chromatid cohesion acts as a tumor penetrance modifier. This research has been published in *PLOS Genetics*.

The first piece of work focuses on the regulation of p53 family members (p53, p63 and p73), as well as their downstream transcriptional apoptotic targets (PUMA/BBC3 and NOXA/PMAIP1), in response to various cellular stresses. Our research demonstrates that in response to genotoxic stress, apoptosis requires *p53* and *puma*, while *p63*, *p73*, and *noxa* are not necessary. Interestingly, we have also observed a secondary wave of genotoxic stress-induced apoptosis that occurs independently of *p53* or *puma*. To further investigate the *p53/puma* axis, we developed a zebrafish model with a knockout of *mdm2*, a negative regulator of *p53*. Our findings reveal that the lethality associated with *mdm2* knockout is completely rescued by p53 knockout, while *puma* knockout only partially rescues the phenotype. Furthermore, we have discovered that *p63* and *puma* play essential roles in ER stress-induced apoptosis, whereas *p53*, *p73*, and *noxa* are not required. Similarly, oxidative stress-induced apoptosis relies on *p63*, *noxa*, and *puma*, but not on *p53* and *p73*. Notably, our studies highlight that the neural tube is inclined towards apoptosis under genotoxic stress, while the epidermis is predisposed to apoptosis under ER and oxidative stress. These findings suggest the existence of both shared and distinct molecular pathways driving cell death in response to different types of stress.

Recent studies have shown that p53 alone is sufficient to suppress tumor formation, even in the absence of apoptosis mediated by *puma* and *noxa*, as well as cell-cycle arrest via p21. This finding suggests the existence of additional noncanonical targets of p53 and their critical effector, which contribute to p53's tumor-suppressive function. The focus of the second piece of work is to elucidate the regulatory network of p53 that may play a

crucial role in tumor suppression. Our research findings align with those in mice, as we have observed that zebrafish lacking *puma*, *noxa*, and *p21* are not predisposed to cancer. Furthermore, we have discovered that *p53*-dependent cell-cycle arrest can still occur in the absence of *p21*. Through a cross-species comparative transcriptome, we have identified 132 transcripts that are upregulated by *p53*. In a *mdm2*^{-/-}; *puma*^{-/-}; *noxa*^{-/-}; *p21*^{-/-} background, we employed a CRISPR/Cas9 "crispant" screening approach and identified *ccng1*, *fbxw7*, and *foxo3b* as novel targets involved in *p53*-dependent cell-cycle arrest. We have completed this work and it is now ready for submission to *Cell Death and Differentiation* for review.

Cancers associated with LFS patients frequently exhibit loss of the remaining wild-type *p53* allele, a phenomenon known as loss-of-heterozygosity (LOH). Recent integrated analyses of human *p53* mutant tumors have highlighted the significance of *p53* LOH in tumorigenesis. In more than 90% of TCGA cancers, both alleles of *p53* were found to be inactivated, providing strong evidence for the contribution of *p53* LOH to tumor initiation. In my third study, published in *PLoS Genetics*, I collaborated with Dr. Holly R. Thomas to investigate the potential impact of reduced chromatid cohesin (SCC) on *p53* LOH and tumor penetrance. We specifically focused on *Esco2* haploinsufficiency, which leads to decreased SCC. Our research involved zebrafish and mouse heterozygous mutant models of *p53*. Our results demonstrated that *Esco2* haploinsufficiency resulted in reduced SCC and accelerated the timing of tumor onset in both zebrafish and mouse models. We observed higher levels of chromosome missegregation and micronuclei formation in *esco2* heterozygous mutant animals. However, this alone did not lead to an earlier onset of tumors in *p53* heterozygous mutants. Instead, we found that tumors in *esco2* haploinsufficient

animals demonstrated a higher level of p53 LOH derived from mitotic recombination. Furthermore, bioinformatic analysis revealed an increase in mitotic recombination events throughout the genome in human tumors lacking functional ESCO2. These findings suggest that the defective SCC plays a role in the earlier onset of tumors by promoting elevated mitotic recombination.

Collectively, the research presented in this body of work has employed a diverse range of genetic, molecular and cellular techniques, bioinformatic approaches and downstream analysis to gain a comprehensive understanding of the p53 regulatory network in tumor suppression and the significance of p53 LOH in tumor initiation. By delving into the underlying mechanisms of p53 tumor suppression, our findings hold potential for identifying promising strategies in cancer risk prediction and treatment.

CHAPTER 2

PUMA, NOXA, P53 AND P63 DIFFERENTIALLY MEDIATE STRESS PATHWAY
INDUCED APOPTOSIS.

by

JUN WANG, HOLLY R. THOMAS, ZHANG LI, NAN CHER (FLORENCE) YEO,
HANNAH E. SCOTT, NGHI DANG, MOHAMMED IQBAL HOSSAIN, SHAIDA A.
ANDRABI, JOHN M. PARANT*Cell Death Disease*Wang, J., Thomas, H.R., Li, Z. et al. Puma, noxa, p53, and p63 differentially mediate
stress pathway induced apoptosis. *Cell Death Dis* 12, 659 (2021).
<https://doi.org/10.1038/s41419-021-03902-6>

Copyright

2021

by

Springer Nature

Used by permission

Format adapted for dissertation

ABSTRACT:

Cellular stress can lead to several human disease pathologies due to aberrant cell death. The p53 family (tp53, tp63, and tp73) and downstream transcriptional apoptotic target genes (PUMA/BBC3 and NOXA/PMAIP1) have been implicated as mediators of stress signals. To evaluate the importance of key stress response components in vivo, we have generated zebrafish null alleles in *puma*, *noxa*, *p53*, *p63* and *p73*. Utilizing these genetic mutants, we have deciphered that the apoptotic response to genotoxic stress requires *p53* and *puma*, but not *p63*, *p73* or *noxa*. We also identified a delayed secondary wave of genotoxic stress induced apoptosis that is *p53/puma* independent. Contrary to genotoxic stress, ER stress induced apoptosis requires *p63* and *puma*, but not *p53*, *p73* or *noxa*. Lastly, the oxidative stress induced apoptotic response requires *p63*, and both *noxa* and *puma*. Our data also indicate that while the neural tube is poised for apoptosis due to genotoxic stress, the epidermis is poised for apoptosis due to ER and oxidative stress. These data indicate there are convergent as well as unique molecular pathways involved in the different stress responses. The commonality of *puma* in these stress pathways, and lack of gross or tumorigenic phenotypes with *puma* loss suggest that inhibitor of Puma may have therapeutic application. In addition, we have also generated a knockout of the negative regulator of *p53*, *mdm2* to further evaluate the *p53* induced apoptosis. Our data indicates that the *p53* null allele completely rescues the *mdm2* null lethality, while the *puma* null completely rescues the *mdm2* null apoptosis but only partially rescues the phenotype. Indicating Puma is the key mediator of *p53* dependent apoptosis. Interestingly the *p53* homozygous null zebrafish develop tumors faster than the previously described *p53*

homozygous missense mutant zebrafish, suggesting the missense allele may be hypomorphic allele.

INTRODUCTION:

Cellular stress response occurs when homeostasis is perturbed (1). Prolonged acute stress or chronic stress often results in cell death to remove the stressed cell from the organism. The apoptotic response to stress is often pathological and associated with human diseases (2-8). Among stress pathways, DNA damage stress, unfolded protein stress, and oxidative stress responses have been linked to multiple human pathologies and can be distinguished by distinct proximal signaling components but can also converge downstream on the p53 family of stress sensors and the apoptotic signaling network (9-17). Interestingly, the cellular response to a stress can also be cell/tissues dependent (18-23). Deeper understanding of consequences of cellular stress and mediators of stress pathways in vivo will facilitate avenues to mediate disease pathogenesis.

The p53 family (tp53, tp63, and tp73) acts as mediators of apoptotic stress response (24-28). The tumor suppressor p53 is activated by a number of cellular stresses including but not limited to genotoxic stress, ribosomal stress, and oncogenic stress (29-35). Further, p63 and p73 have been shown to be required for doxorubicin induced neural cell death in mouse embryos (36); however not in irradiated mouse thymocytes (37). This suggests tissue specific influences occur. Additionally, the transcription factor p63 can regulate the intrinsic apoptosis in response to ER stress through mediating Puma expression (19, 38, 39). p73 can also mediate ROS stress to increase the BAK/BCL-2 ratio in human cells (40). These studies suggest not only p53, but also p63 and p73 have the potential to mediate

multiple stress-induced apoptotic outcomes through the induction of the pro-apoptotic Bcl-2 family members, such as PUMA and NOXA (41-43). However, which of the p53 family and/or proapoptotic family are essential for the different stress responses is unclear.

Zebrafish is a useful model to understand the in-vivo pathology associated with human diseases. We and others have demonstrated zebrafish are a model of cancer predisposition, heart development, neurodegeneration, and many others (44-48). Many of diseases and stress pathways are conserved and approximately 82% of human disease genes have zebrafish homologs (49). For example, in the p53 pathway *p53*, *p63*, and *p73*; the negative regulators *mdm2* and *mdm4*; the downstream transcriptional targets such as *p21*, *puma*, *noxa*, *cyclin G*, and *gadd45a* are conserved in 1:1 orthology. Here, we took advantage of the properties of zebrafish embryos to analyze apoptotic outcomes in response to genotoxic stress, ER stress and oxidative stress in a number of genetic null animals. We generated 6 knock-out alleles including *puma/bbc3*, *noxa/pmaip1*, *p53*, *mdm2*, *p63* and *p73* with multiple genome-editing techniques. Utilizing these mutants, we defined: 1) that the apoptosis response to genotoxic stress requires *p53* and *puma*, but not *p63*, *p73* or *noxa*. 2) The ER stress induced apoptosis requires *p63* and *puma*, but not *p53*, *p73* or *noxa*. And 3) the oxidative stress induced apoptotic response requires *p63*, and both *noxa* and *puma*. These data indicate there are convergent as well as unique molecular pathways involved in the different stress responses.

RESULTS:

Multiple cellular stresses induce transcriptional induction of *puma* and *noxa* in zebrafish

To first determine if pro-apoptotic mRNAs were upregulated in zebrafish following diverse cellular stresses, we analyzed the relative expression of *puma*, *noxa*, *bax*, and *bid* (Figure S1 depicts zebrafish orthology analysis) in 24 hours post fertilization (hpf) embryos exposed to either the genotoxic stress (30 Gy ionizing radiation, IR), ER stress (5uM Thapsigargin, Thaps.), or oxidative stress (3.3uM Phorbol 12-myristate 13-acetate, PMA). As with human cells (50, 51), *puma* has the strongest induction following IR, then *noxa*, followed by *bax* and *bid* have mild to no induction (Figure 1A). Similar to IR, following Thaps. and PMA, both *puma* and *noxa* were significantly upregulated, however *bax* and *bid* were not induced (Figure 1B&C). Together these data have indicated that *puma* and *noxa* are strongly transcriptionally regulated by cellular stresses. While the p53 family of stress mediators are largely controlled at the post-translational level we analyzed the relative expression of *p53*, *p63* and *p73* after these stresses (Figure S2). Only after IR did we observe increases in *p53* mRNA, which is self-inducing (Figure S3). *p73* was significantly induced after IR (this induction is *p53* dependent - Figure S3), non-significantly induced with Thapsigargin treatment, and significantly reduced after PMA treatment. However, *p63* mRNA was not significantly induced by all treatments.

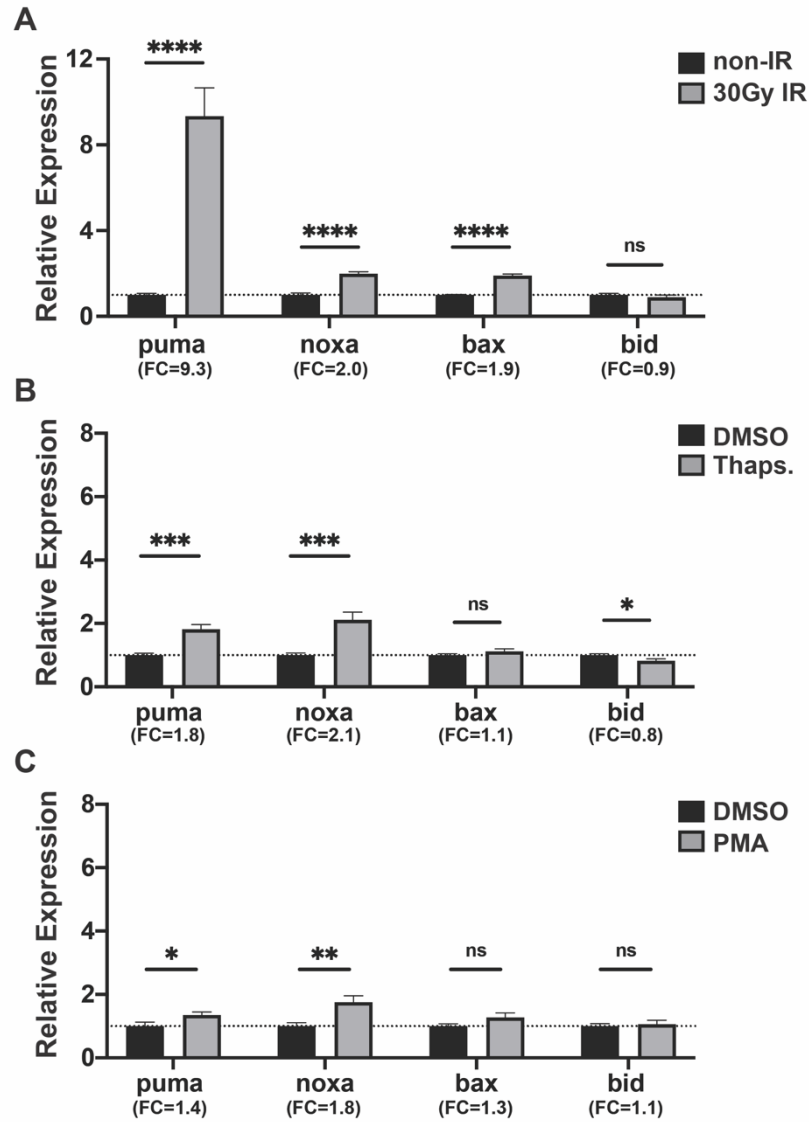


Figure 1. Quantitative real-time PCR (qRT-PCR) analysis of pro-apoptotic markers after IR- and drug-induction in wild-type zebrafish embryos. 24hpf zebrafish embryos were treated with (A) 30Gy IR-irradiation, (B) 5µM Thapsigargin (Thaps.), and (C) 3.3µM Phorbol 12-myristate 13-acetate (PMA); and qRT-PCR was performed at 6h (A) or 4h (B and C) after treatment. Expression levels were normalized to GAPDH. n=9 (A and B) and n=7 (C) from ~30 pooled embryos per sample. Bars represent mean ± SEM. *, p < 0.05; **, p < 0.01; ***, p < 0.001; ****, p < 0.0001. Fold change (FC) is indicated.

Generation of zebrafish null mutants

To further pursue the importance of *puma* and *noxa* in the stress induced apoptotic response in zebrafish, we generated zebrafish *puma* and *noxa* null alleles (Figure 2, S4 and S5). PUMA and NOXA have been described to be transcriptionally induced in a p53 dependent as well as p63 and p73 dependent manner (19, 36-40, 52-54). Therefore, to further evaluate the stress pathways we have also generated a *p53* null allele (Figure 2 and S6), as well as *p63* and *p73* null alleles (Figure 2, and S7 and S8) in zebrafish. To introduce an alternative mechanism of p53 induction and evaluate our new *p53* null allele and *puma* null allele, we also generated a *mdm2* null allele (Figure 2 and S9). MDM2 is E3 Ubiquitin ligase. Mouse and zebrafish genetic experiments have established that deletion of the negative regulator of p53 (55, 56), MDM2, results in embryonic lethality due to unregulated activation of p53 and apoptosis. This lethality can be completely rescued in a p53 null background, solidifying the lethality is p53 dependent (57-59). Important to this model is that p53 is hyper-activated in the absence of a true stress signal. Our overall strategy for all of these knockouts is to generate a small deletion or insertion 5' in the coding region that results in a frame shift that truncates the protein (Figure 2).

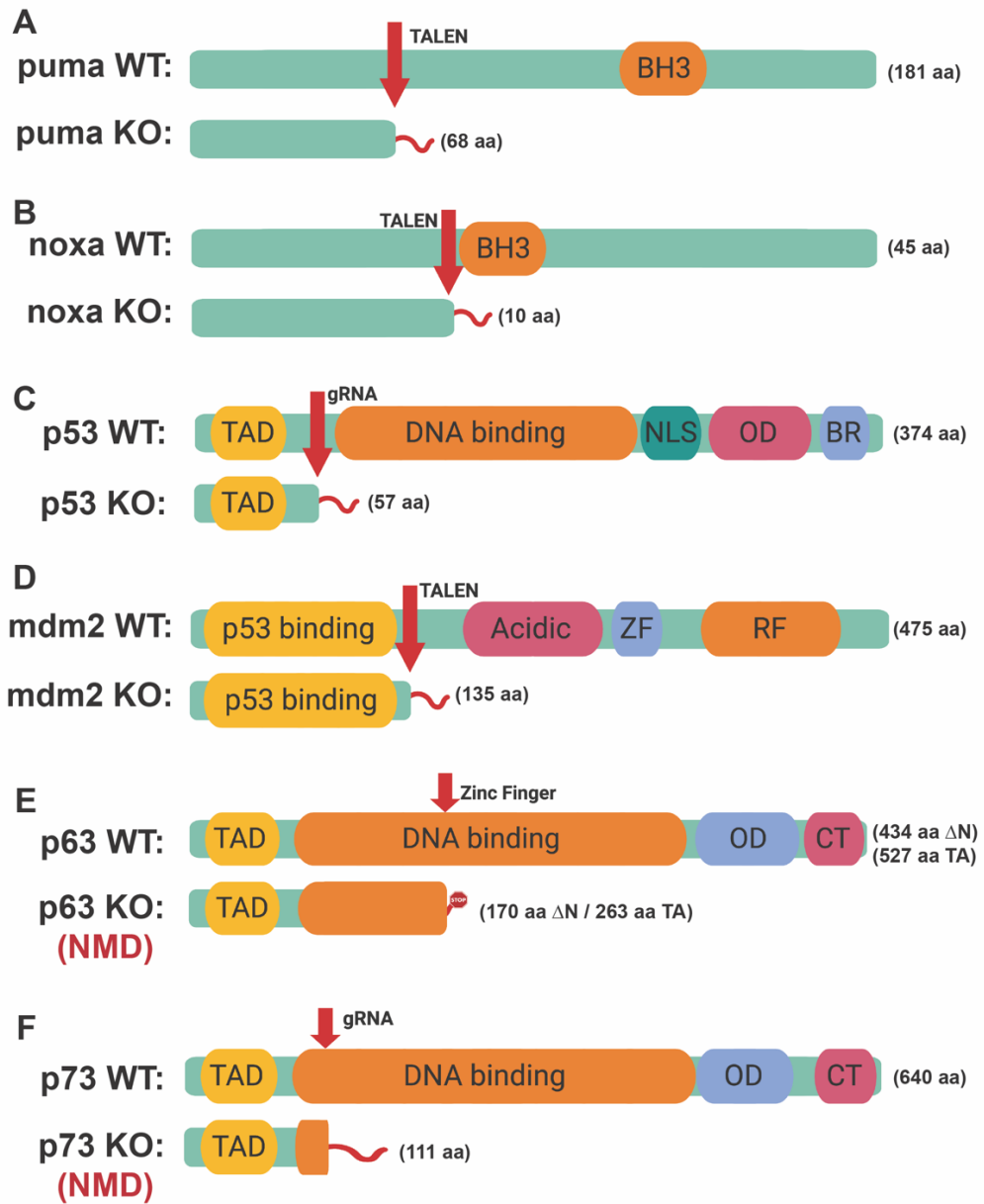


Figure 2. The protein structure of 6 mutant alleles in zebrafish generated by Zinc Finger, TALEN or CRISPR-Cas9 gene editing. **A.** Schematic of Puma wildtype and mutant proteins. (BH3, BH3 domain) **B.** Schematic of Noxa wildtype and mutant proteins **C.** Schematic of p53 wildtype and mutant proteins. (TAD, transactivation domain; DNA-binding, DNA binding domain; NLS, nuclear location signal; OD, Oligomerization domain; BR, basic region) **D.** Schematic of Mdm2 wildtype and mutant proteins (p53 binding, p53 binding domain; Acidic, acidic domain; ZF, zinc finger domain; RF, ring finger domain) **E.** Schematic of p63 wildtype and mutant proteins (CT, C-terminal region; p63 mutant transcripts undergo nonsense mediated decay, NMD) **F.** Schematic of p73 wildtype and mutants. Arrow points out the target site of zinc finger, TALEN or CRISPR-Cas9 gene editing. Orange indicates the key domain in each protein. Light green bar labels full-length wildtype or in-frame truncated mutant protein and the length of amino acid (aa) sequence is indicated. Red tail indicates out-of-frame part of the truncated protein. The figure is created with BioRender.com.

***puma*, but not *noxa*, is essential for *p53* dependent induction of apoptosis following genotoxic stress**

To investigate the genotoxic stress induced apoptotic pathway in zebrafish, we have treated 24hpf embryos with IR. Our data and others have indicated that IR induced apoptosis primarily occurs in the neural tube of 24hpf zebrafish embryos and is *p53* dependent (44, 60-62). This is consistent with mouse studies demonstrating apoptosis predominantly in the neural tube of 13.5dpc embryos after IR treatment (63). To determine if *puma* and *noxa* are required for the *p53* dependent, as well as if *p63* or *p73* contribute to the apoptotic response in zebrafish, we treated zebrafish wild type, *tp53*^{-/-}, *tp63*^{-/-}, *tp73*^{-/-}, *bbc3*^{-/-}, and *pmaip1*^{-/-} embryos with 30 Gy IR-irradiation and stained for the apoptotic marker activated Caspase 3 at 1hpi (hour post irradiation), 6hpi, and 24hpi. In wild-type embryos, we do not observe apoptosis within 1hr, but do by 6hpi and this persists into 24hpi (Figure 3A&S10). We also performed TUNEL staining to validate the active Caspase 3 apoptotic staining on untreated and IR treated wildtype embryos (Figure S11). For *p53* null, we do not observe apoptosis at 1hpi or 6hpi, but do observe apoptosis at 24hpi (Figure 3A&S10). This indicates the primary apoptotic response at 6hpi is in a *p53* dependent manner; however, the later 24 hpi apoptosis is *p53* independent. Interestingly loss of *puma*, but not *noxa*, resulted in loss of apoptosis at 1hpi and 6hpi, but not 24hpf similar to *p53* loss (Figure 3A&S10). These data suggest that *puma* alone, but not *noxa*, is an essential mediator of IR induced *p53* dependent apoptotic response. Note, *puma* loss does not alter the 24 hpi apoptosis suggesting this apoptosis is through a *p53/puma* independent mechanism. *p63* or *p73* null embryos undergo apoptosis similar to wildtype and *noxa* null (Figure 3A&S10) embryos, suggesting they are not essential for IR induced

apoptosis. The fact that *puma* alone mediates the IR induced apoptotic response was surprising and raised the possibility that *puma* loss abrogates apoptosis at milder doses of IR, but at stronger doses *noxa* may also contribute. Therefore, we treated wild type, *tp53*^{-/-}, *tp63*^{-/-}, *tp73*^{-/-}, *bbc3*^{-/-}, and *pmaip1*^{-/-} embryos with either 0, 15, 30, 45, 60, and 100 Gy of IR and stained them with the active Caspase 3 and apoptotic dye acridine orange (Figure 3B and S12). The *puma* null was equally effective at preventing IR induced apoptosis as the p53 null at all doses, again suggesting that *puma* is the essential mediator of p53 dependent apoptosis. To further evaluate the lack of involvement of *noxa* in IR induced apoptosis, we compared wild type and *pmaip1*^{-/-} embryos with a 15Gy low dose and observed a very mild apoptosis in the wild type embryos and similar level of apoptosis in *pmaip1*^{-/-} embryos (Figure 3B and S12); suggesting *noxa* is not essential for IR-induced p53-dependent apoptosis in 24hpf zebrafish embryos. Following IR treatment, the p53 protein levels accumulate due to inhibition of interaction with the E3 ubiquitin ligase mdm2, thereby extending the half-life of the p53 protein. To address the possibility that *puma* loss influences p53 protein accumulation, we performed a western blot for p53 following IR treatment. p53 protein accumulated to equivalent levels in the wild type, *bbc3*^{-/-} and *pmaip1*^{-/-}, but not *p53*^{-/-} following IR treatment (Figure 3C). It indicates the loss of *puma* has no influence on p53 protein levels. Further, using qRT-PCR of RNA extracted from *p53* wild-type and *p53* null embryos either untreated or 6 hours after 30gy IR we demonstrated that *puma* and *noxa* mRNA induction is in a p53-dependent manner (Figure 3D).

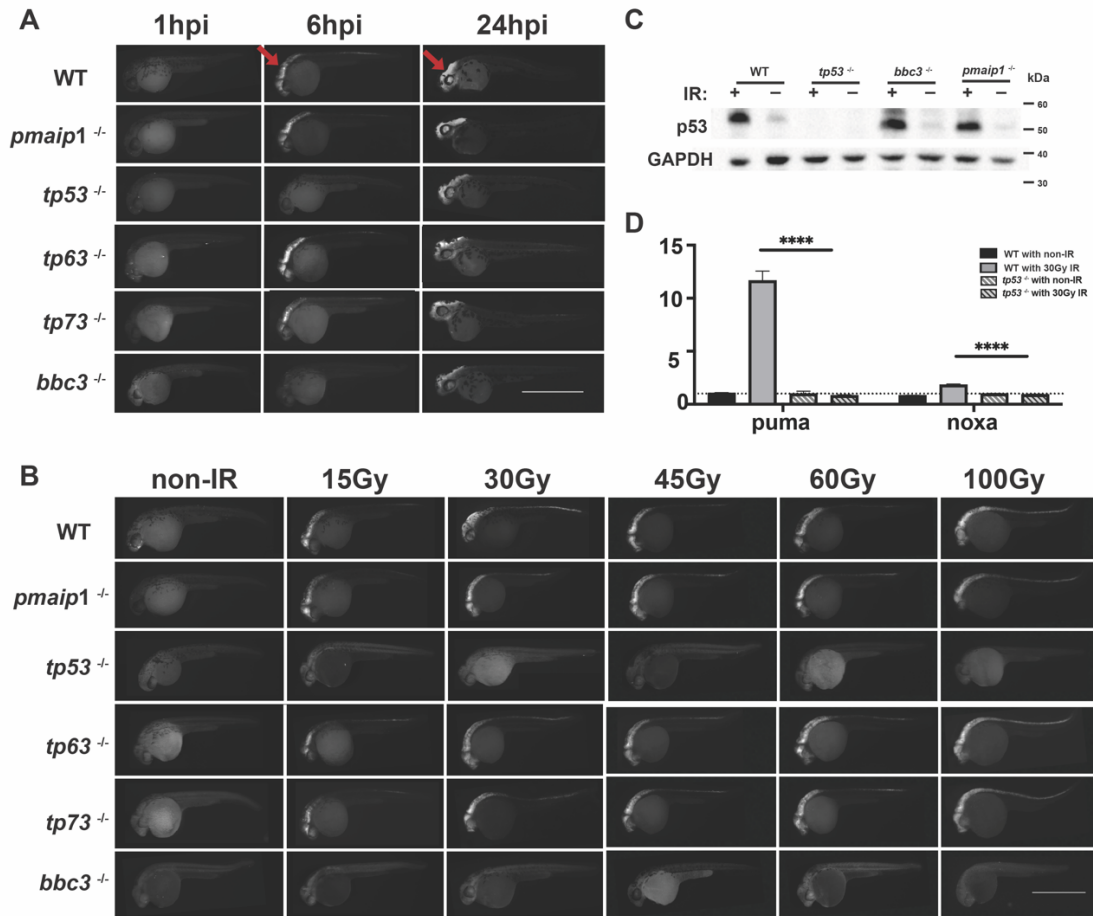


Figure 3. Loss of *puma* not *noxa* rescues IR-induced apoptosis in p53-dependent manner. **A.** anti-active Caspase-3 staining on 30hpf (1hpi and 6hpi panel) or 48hpf (24hpi panel) embryos. 29hpf wild-type, *pmaip1*^{-/-}, *tp53*^{-/-}, *tp63*^{-/-}, *tp73*^{-/-} and *bbc3*^{-/-} zebrafish embryos were treated with 30Gy IR-irradiation and fixed at 1h post treatment (1hpi panel); 24hpf embryos were treated with 30Gy IR-irradiation and fixed at 6h (6hpi panel) or 24h (24hpi panel) after treatment. Arrows in WT points out active apoptotic area in head region in WT embryos for 6hpi and 24hpi. Scale bar, 1000μM. **B.** anti-active Caspase-3 staining of 30hpf (6hpi) wild-type, *pmaip1*^{-/-}, *tp53*^{-/-}, *tp63*^{-/-}, *tp73*^{-/-} and *bbc3*^{-/-} zebrafish embryos treated w/o IR (non-IR) and with 15Gy, 30Gy, 45Gy, 60Gy and 100Gy IR. Scale bar, 1000μM. **C.** p53 protein expression level after IR-induction. Western blot analysis was performed using protein extracts from 30hpf (6hpi) wildtype, *tp53*^{-/-}, *bbc3*^{-/-} and *pmaip1*^{-/-} zebrafish embryos with (30Gy) or without IR treatment. **D.** qRT-PCR analysis of *puma* and *noxa* after IR-irradiation in zebrafish embryos. 24hpf wild-type or *tp53*^{-/-} zebrafish embryos were treated with 30Gy IR-irradiation and RNA samples for qRT-PCR were harvested at 6h after IR-irradiation. Expression levels were normalized to GAPDH. n=6 from ~30 pooled embryos per sample. Bars represent mean ± SEM. ****, p < 0.0001.

***puma*, but not *noxa*, is essential for *mdm2*-null induced *p53* dependent apoptosis**

There are a number of stresses, beyond genotoxic stress, that can activate a p53 dependent apoptosis. The role of Puma in these stresses is unclear and potentially mediated by other apoptotic regulators. To investigate if *puma* is the sole mediator of *p53* induced apoptosis we will employ the *mdm2* null zebrafish. Within this model, *mdm2* loss circumvents the need for signaling pathways involved in cellular stresses and induces a universal p53 activation response. Consistent with mouse, loss of *mdm2* in zebrafish results in an early embryonic lethality morphologically identifiable prior to 15hpf due to extensive apoptosis as early as 12 hpf (Figure S9E & 4A). Further, this lethality is completely rescued by loss of *p53* (Fig S9F & S9G). By qRT-PCR we determine that both *puma* and *noxa* are strongly induced in *mdm2* null embryos (Fig 4B), suggesting they are likely involved in the p53-dependent apoptotic response. To determine if *puma* and/or *noxa* are essential mediators of the p53 dependent apoptotic response, we generated double mutants, *mdm2*^{-/-}; *bbc3*^{-/-} and *mdm2*^{-/-}; *pmaip1*^{-/-} embryos and accessed their apoptotic and morphological phenotypes. Loss of *noxa* had no effect on the apoptosis or the morphological phenotype (data not shown). Loss of *puma* completely abrogated the apoptotic response and mildly rescued the phenotype (Figure 4C and 4D). The mild rescue of the phenotype suggests that other p53-induced biological outcomes (e.g., cell cycle arrest) are also influential in the phenotype. Importantly this indicates that *puma*, but not *noxa*, is the essential mediator of the *p53* dependent apoptotic response.

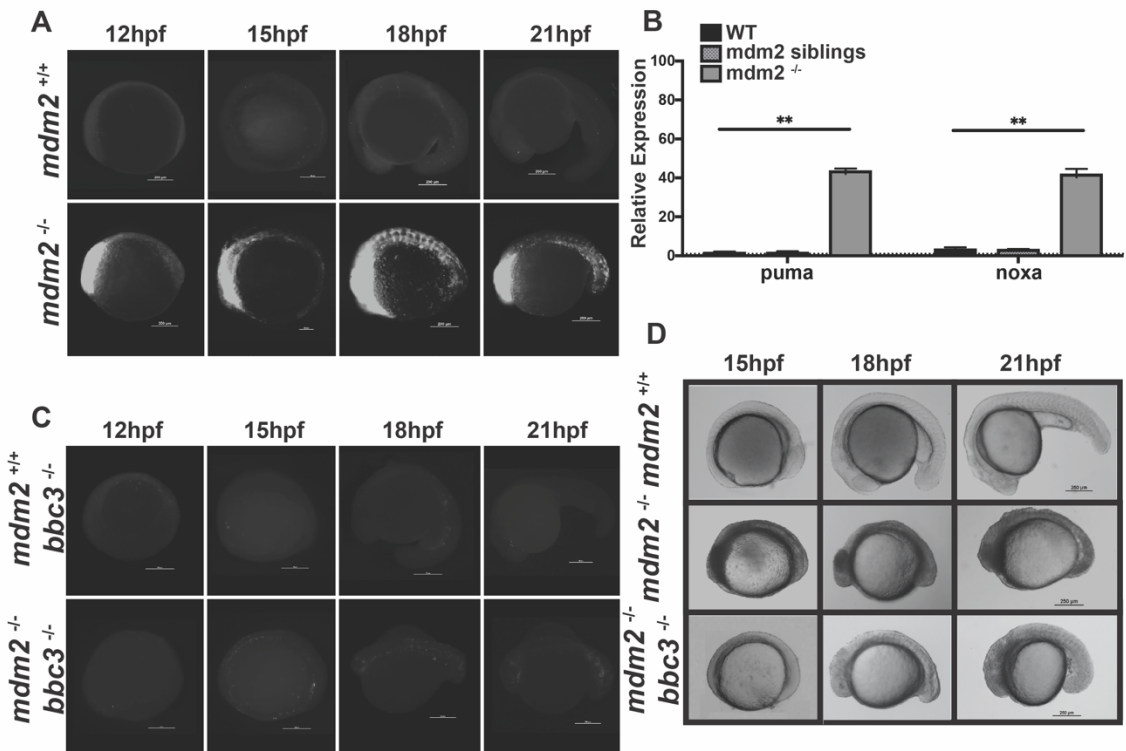


Figure 4. Loss of *puma* rescues *mdm2*-null induced apoptosis at early embryonic stage.

A. anti-active Caspase-3 staining on 12hpf, 15hpf, 18hpf and 21hpf *mdm2*^{+/+} and *mdm2*^{-/-} zebrafish embryos. **B.** qRT-PCR analysis of *puma* and *noxa* in 15hpf *mdm2*^{+/+}, *mdm2* siblings (*mdm2*^{+/+} and *mdm2*^{+/-}) and *mdm2*^{-/-} zebrafish embryos. n=3 from ~30 pooled embryos per sample. Bars represent mean \pm SEM. **, $p < 0.01$. **C.** anti-active Caspase-3 staining on 12hpf, 15hpf, 18hpf and 21hpf *mdm2*^{+/+} *bbc3*^{-/-} and *mdm2*^{-/-} *bbc3*^{-/-} zebrafish embryos. **D.** Gross images of 15hpf, 18hpf and 21hpf *mdm2*^{+/+}, *mdm2*^{-/-} and *mdm2*^{-/-} *bbc3*^{-/-} zebrafish embryos.

ER stress induced apoptosis response requires the involvement of *p63* and *puma* but not *noxa*, *p53* and *p73*

ER stress has been shown to be important in a number of disease states including but not limited to retinal degeneration, diabetes, obesity and neurological disorders (2). As with IR, ER stress has multiple outputs, one of them being apoptosis. Thapsigargin (Thaps.) is a well-studied ER stressor(64, 65). Previous studies in zebrafish indicated that ER stress, through IRE-1 and Perk but not Chop, activates p63 and Puma to induce an apoptotic response primarily in the epithelium (19). However, the validity of the Puma and p63 involvement are controversial due to the use of morpholinos that have potential off-target effects. Consistent with published data, we observe similar morphology changes in Thapsigargin treated embryos and elevated apoptosis by active Caspase 3 staining and TUNEL staining in the epithelial layer, particularly in the growing tail tip (Figure 5A). While all treated embryos have a morphological curved body phenotype, we did observe that about half have a mild apoptosis in the tail tip region (49.3%; lower mean florescent intensity Figure 5A-D) and half have a severe apoptosis (50.7%; higher mean florescent intensity; Figure 5A-D). By qRT-PCR we observed that *puma*, as well as *noxa*, are transcriptionally induced following treatment with Thaps. both at two and four hours post treatment (hpt) (Fig 5E); suggesting both of them are mediators of the apoptotic response. To define if *puma* and *noxa* are required for the ER stress induced apoptotic response, we performed the Thaps. treatment on *bbc3^{-/-}* and *pmaip1^{-/-}* embryos. While loss of *noxa* had no effect on apoptosis following Thaps. treatment (Figure 5C), *puma* loss significantly reduced apoptosis from 50.7% to 21.7%. It suggests that *puma*, but not *noxa*, is important in the ER stress induced apoptotic response at 24hpf embryos. It also suggests that other

factors are involved. Loss of either *noxa* or *puma* did not impact the overt morphological change (mild phenotype) which is likely due to ER stress induced non-apoptotic outcomes.

To further confirm these findings, we treated wild type and *bbc3*^{-/-} embryos with Brefeldin A (BFA), an additional ER stress inducing compound (19). Similar to Thapsigargin, BFA induced a similar morphological phenotype and a mild and severe apoptotic response (Fig S13A and S13B) with a longer treatment time (6hpt). It also induced *puma* and *noxa* transcriptionally at 6hpt (Figure S13C) and the apoptosis was suppressed in a *bbc3*^{-/-} background (88.3% to 2.3%, Fig S13D). The almost complete suppression of apoptosis could suggest that the ER stress response to Thaps. and BFA are slightly different, with BFA being more *puma* dependent. Together these data, supports that ER stress induces a *puma* dependent apoptotic response.

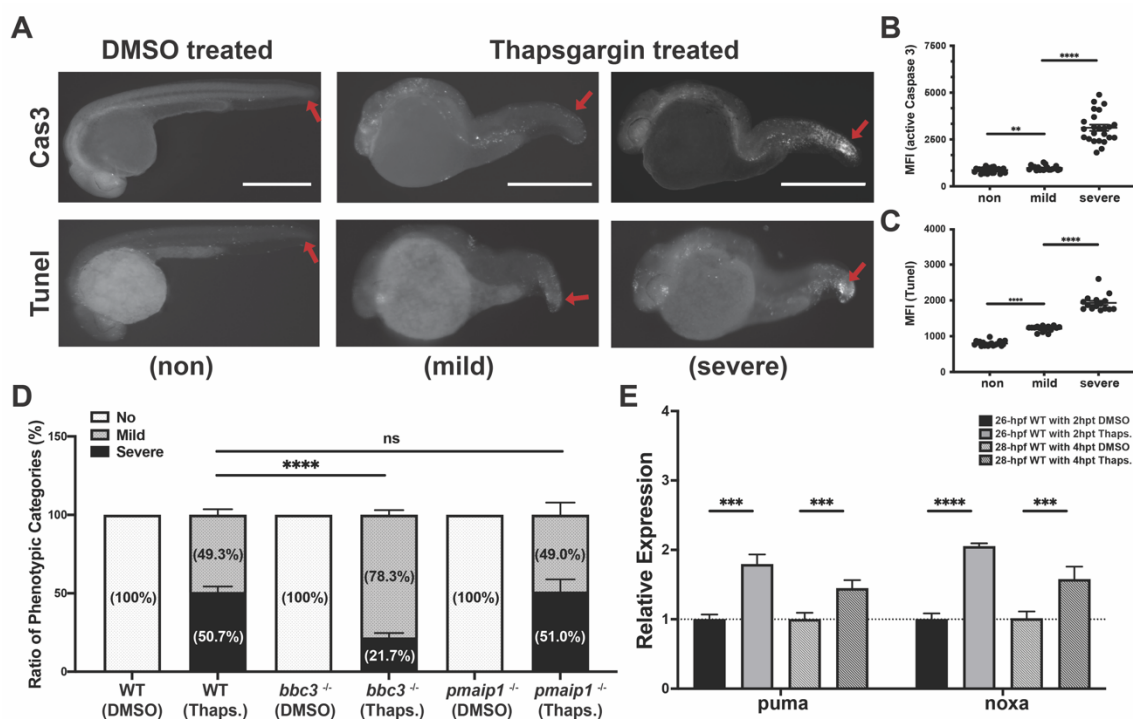


Figure 5. Loss of *puma* partially rescues Thapsigargin (Thaps.)-induced apoptosis at early embryonic stage. **A.** anti-active Caspase-3 (The Upper Panel) and TUNEL (The Lower Panel) staining on 28hpf (4 hours post treatment) wild-type zebrafish embryos with DMSO alone or with DMSO plus 5 μ M Thaps. Representative figures showing phenotypic categories of the apoptotic severity. Arrows points out apoptotic area in tail region in WT embryos with DMSO alone or with DMSO plus 5 μ M Thaps for 4 hours. Scale bar, 1000 μ M. **B.** Quantification of the fluorescence intensity of tail region of DMSO-treated and Thaps. treated embryos in mild and severe categories with anti-active Caspase-3 staining. **C.** Quantification of the fluorescence intensity of tail region of DMSO-treated and Thaps. treated embryos in mild and severe categories for TUNEL staining. Each dot represents mean fluorescence intensity (MFI) of the tail region of individual embryos from 2 independent experiments. Bars represent mean \pm SEM. ****, $p < 0.0001$. **D.** Loss of *puma* (not *nox*a) partially rescued Thaps. induced apoptosis at 24hpf. Ratio of phenotypic categories in wildtype, *bbc3*^{-/-} and *pmaip1*^{-/-} zebrafish embryos. n=7 (wildtype and *bbc3*^{-/-}) and n=4 (*pmaip1*^{-/-}) from pooled embryos per sample. The total number of Thaps. treated embryos: wildtype > 1000, *bbc3*^{-/-} > 900 and *pmaip1*^{-/-} > 550. Bars represent mean \pm SEM. ****, $p < 0.0001$. **E.** qRT-PCR analysis of *puma* and *nox*a after DMSO or 5 μ M Thapsigargin treatment in 24hpf zebrafish embryos across time (2hpt and 4hpt). Expression levels were normalized to GAPDH. n=5 (26-hpf WT with or w/o 2 hours post Thaps. treatment) and n=9 (28-hpf WT with or w/o 4h post Thaps. treatment) from approximately 30 pooled embryos per sample. Bars represent mean \pm SEM. ***, $p < 0.001$; ****, $p < 0.0001$.

To determine if p63 is involved in the ER stress response, we treated *tp63^{-/-}* embryos with Thaps. While *p63* null embryos display morphological phenotypes at 3.5dpf, we did not observe any difference in morphology or apoptosis in 24hpf *p63* homozygous null embryos versus wild type embryos (Figure S7F and S7G). However, we did observe a significant reduction in apoptosis in *p63* null embryos following Thaps. treatment (Figure 6A) when compared with wild type and sibling *tp63^{+/+}* (internal control). This reduction was similar to that observed in the *puma* null embryos (Fig 5D). To further test whether *p53* and *p73* are involved in the ER-induced apoptosis response, we treated double null embryos (*tp53^{-/-}; tp73^{-/-}*) with Thaps. and observed no significant change in apoptosis (51.9% to 54.9%, Figure 6B). Together these data indicate that the ER induced apoptotic response is partially through *p63/puma* axis, but is in a *p53*, *p73* or *noxa* dependent manner in 24hpf zebrafish embryos.

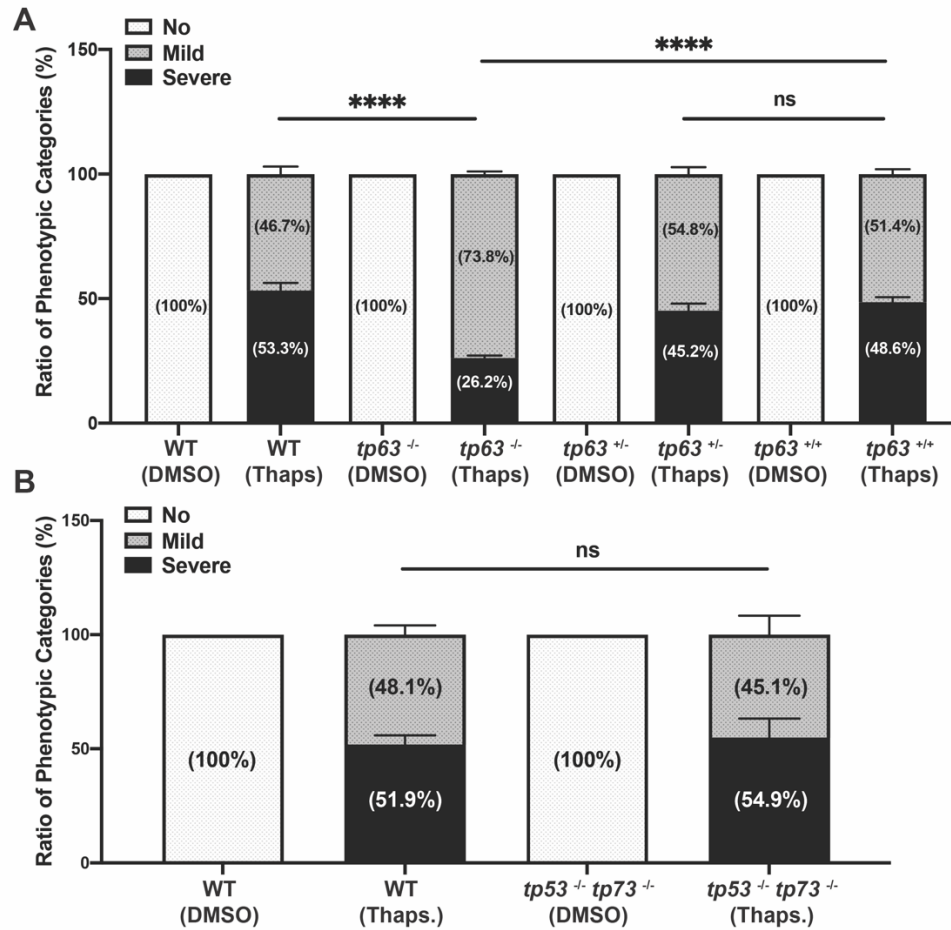


Figure 6. Loss of *p63* (not *p53* and *p73*) partially rescued Thaps. induced apoptosis at early embryonic stage. A. Loss of *p63* partially rescued Thaps. induced apoptosis at 24hpf. Ratio of phenotypic categories of the apoptotic severity in wildtype, *tp63*^{-/-}, sibling *tp63*^{+/-} and sibling *tp63*^{+/+} zebrafish embryos at 4h after DMSO or Thaps. treatment. Embryos from the intercross of heterozygous-mutant *tp63* adults were genotyped after sorted based on the apoptotic severity at tail region. **B.** Loss of *p53* and *p73* cannot rescue Thaps. induced apoptosis at 24hpf. Ratio of phenotypic categories in 24hpf wild-type and *tp53*^{-/-} *tp73*^{-/-} zebrafish embryos at 4h after DMSO or Thaps. treatment. n=6 (**A**) and n=4 (**B**) from pooled embryos per sample. Bars represent mean ± SEM. ****, p < 0.0001.

Oxidative stress induced *p63* mediated *puma/nox*a dependent apoptosis response that does not require the involvement of *p53* and *p73*

To decipher the oxidative stress induced apoptotic pathway we treated zebrafish embryos with PKC activator PMA. We observed a morphological change and elevated active Caspase 3 and TUNEL staining following PMA treatment of 24hpf embryos (Figure 7A). Like ER stress, the apoptosis is predominant in the embryonic epithelium, and we observe a mild and severe apoptotic phenotype at the tail tip region (Figure 7A-C). To investigate if *puma* or *nox*a are required for the oxidative stress induced apoptosis, we treated *bbc3^{-/-}* and *pmaip1^{-/-}* embryos with PMA and stained for activated Caspase 3. Interestingly, both *puma* and *nox*a are important for the PMA induced apoptotic response (64% vs 19.6% or 26.1% respectively, Figure 7D), suggesting that both *puma* and *nox*a are important in oxidative stress induced apoptosis response for 24hpf zebrafish embryos. While we observed both *puma* and *nox*a are transcriptionally induced following 4-hour PMA treatment, *puma* is induced earlier and can be observed following 2-hour PMA treatment (Figure 7E). However, loss of either *puma* or *nox*a did not rescue some non-apoptotic morphological outcomes induced by PMA treatment. Additionally, we observed a significant reduction in apoptosis in *tp63* null embryos treated with PMA treatment from 64.8% to 11.9% (Figure 8A) that is better than the rescue of loss of *puma* or *nox*a. We did not observe a significant reduction in apoptosis in *p53/p73* double null embryos after 4-hour PMA treatment (Figure 8B). These data suggest that PMA-induced apoptosis is *p63*, but not *p53* or *p73*, dependent; however, unlike ER stress, the apoptotic response requires the involvement of both *puma* and *nox*a.

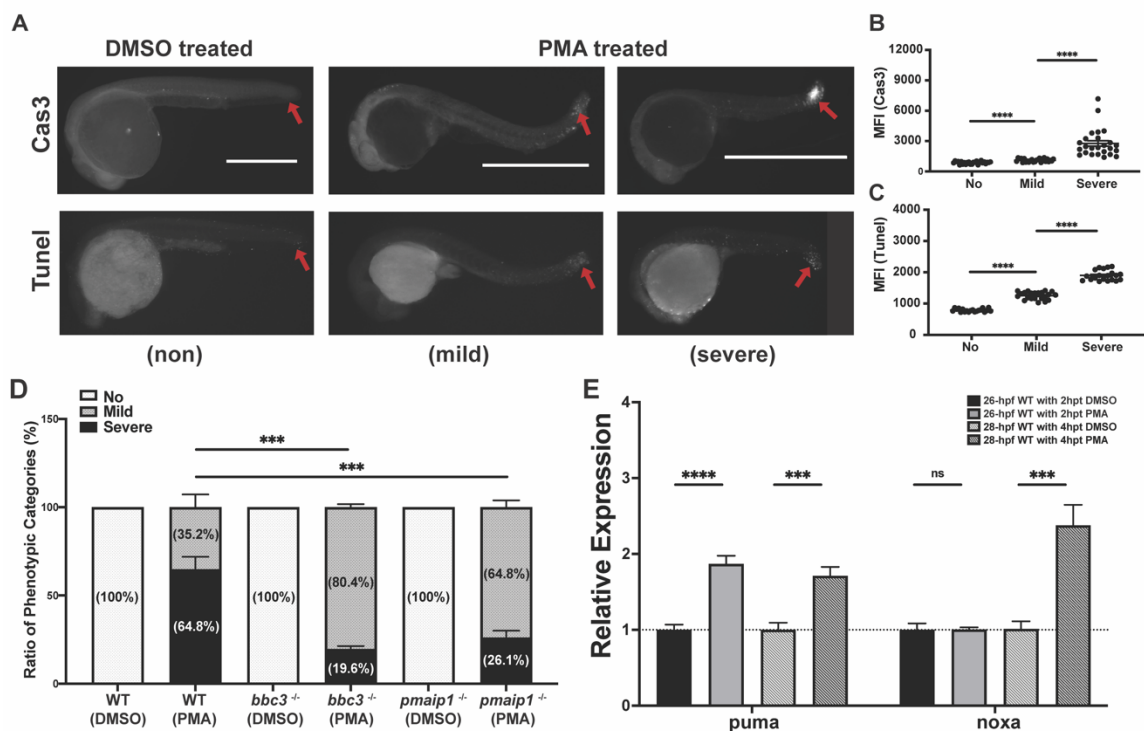


Figure 7. *puma* and *noxa* are required for PMA-induced apoptosis. **A.** anti-active Caspase-3 (The Upper Panel) and TUNEL (The Lower Panel) staining on 28hpf (4 hours post treatment) wild-type zebrafish embryos with DMSO or DMSO plus 3.3 μ M PMA. Representative figures showing phenotypic categories of the apoptotic degree. Arrows points out apoptotic area in tail region in WT embryos with DMSO alone or with DMSO plus 3.3 μ M PMA for 4 hours. Scale bar, 1000 μ M. **B.** Quantification of fluorescence intensity of tail region of DMSO-treated and PMA-treated embryos in mild and severe categories with anti-active Caspase-3. Each dot represents MFI of the tail region of individual embryos from three independent experiments. Bars represent mean \pm SEM. ****, $p < 0.0001$. **C.** Quantification of the fluorescence intensity of tail region of DMSO-treated and PMA treated embryos in mild and severe categories for TUNEL staining. Each dot represents mean fluorescence intensity (MFI) of the tail region of individual embryos from 2 independent experiments. Bars represent mean \pm SEM. ****, $p < 0.0001$. **D.** Loss

of both *puma* and *nox*a partially rescued PMA-induced apoptosis at 24hpf. Percentage of phenotypic categories in wildtype, *bbc3*^{-/-} and *pmaip1*^{-/-} zebrafish embryos. n=4 (wildtype and *bbc3*^{-/-}) and n=7 (*pmaip1*^{-/-}) from pooled embryos per sample. The total number of PMA-treated embryos: wildtype > 600, *bbc3*^{-/-} > 440 and *pmaip1*^{-/-} > 800. Bars represent mean ± SEM. ***, p < 0.001. E. qRT-PCR analysis of *puma* and *nox*a after DMSO or 3.3µM PMA treatment in 24hpf zebrafish embryos across time (2hpt and 4hpt). Expression levels were normalized to GAPDH. n=5 (26-hpf WT) and n=7 (28-hpf WT) from around 30 pooled embryos per sample. Bars represent mean ± SEM. ***, p < 0.001; ****, p < 0.0001.

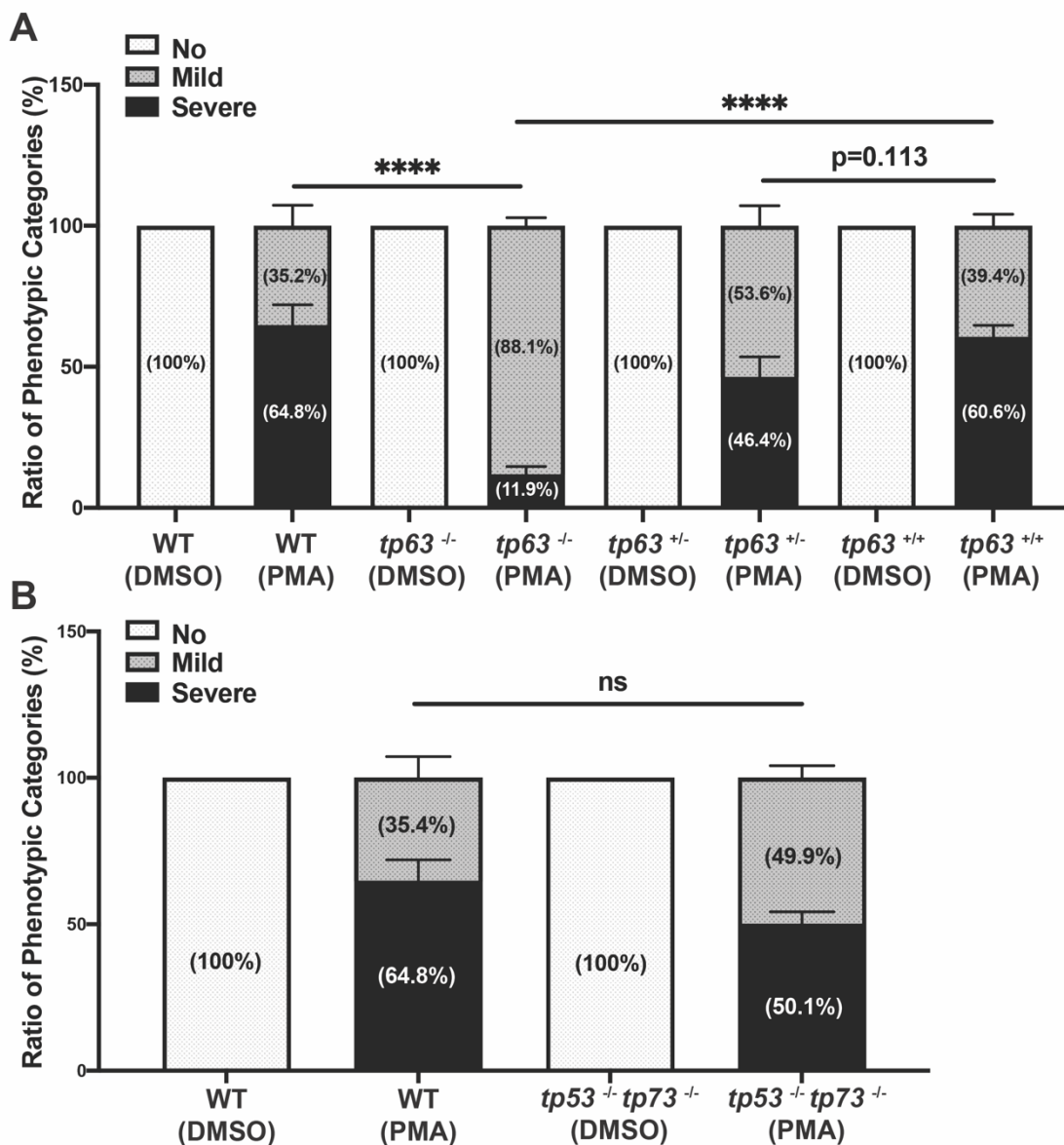


Figure 8. *p63*, but not *p53* and *p73*, are required for PMA-induced apoptosis. A. Percentage of phenotypic apoptotic categories in wild-type, *tp63*^{-/-}, sibling *tp63*^{+/-} and sibling *tp63*^{+/+} zebrafish embryos at 4h after treatment with DMSO or PMA. **B.** Percentage of phenotypic categories in 24hpf wildtype and *tp53*^{-/-} *tp73*^{-/-} zebrafish embryos at 4h after DMSO or PMA treatment. n=6 (A) and n=5 (B) from pooled embryos per sample. The total number of Thaps treated embryos: wildtype > 600, *tp63*^{-/-} > 140, *tp63*^{+/-} > 390, *tp63*^{+/+} > 180 and *tp53*^{-/-} *tp73*^{-/-} > 370. Bars represent mean ± SEM. ****, p < 0.0001.

DISCUSSION:

Genotoxic stress pathway: Consistent with previous reports, we have demonstrated that genotoxic stress induces a robust p53 dependent apoptosis in the neural tube of 24hpf zebrafish embryos (61, 62). This is consistent with mouse data demonstrating predominantly neural tube apoptosis in 13.5dpc embryos after irradiation (63). This suggests either that the neural tissues are poised for apoptosis or that there is a unique p53 transcriptional profile in the neural tissues that drives apoptosis preferentially. This could explain why so many DNA repair deficient or genomic instability associated diseases have neural associated defects, such as ataxia (66-69). Our data indicates that Puma is the key mediator of p53 dependent apoptosis due to genotoxic stress. Puma inhibitors could potentially be used to provide a neuro-protectant effect. Interestingly, we observed that there is a first wave of apoptosis that is *p53/puma* dependent, and a later wave 24hpi that is *p53/puma* independent. The molecular mechanism of this second wave is still unknown but could be a consequence of cells undergoing mitotic slippage while still containing broken chromosomes. The fact that Caspase 3 is activated indicates it is a programmed pathway which should be explored. The rescue of the *mdm2* null induced apoptosis, indicates Puma is the key mediator of p53 induced apoptosis. This brings into question of why is Noxa evolutionarily conserved and induced following genotoxic stress, and why does it alone not induce apoptosis when induced? While mammalian studies often refer to Puma and Noxa being essential for p53 dependent apoptosis, the data in mouse studies also strongly suggests that Puma is the key regulator of p53 dependent apoptosis (50, 51, 70). While we have focused on elevation of the noxa mRNA transcript, the post-translational

modifications of NOXA protein has been shown to influence its apoptotic function (71). Potentially under genotoxic stress noxa protein is not activated post-transcriptionally.

The response to ER stress: Many pathological studies have recently demonstrated that ER stress is central to many diseases. We have demonstrated that the full ER stress apoptotic response in the epidermis requires activation of *p63*, but not *p53* or *p73*. This is consistent with zebrafish morpholino data indicating the ER stress utilizes *p63* for apoptosis in the epidermis (19). Our data also indicates that *puma*, but not *noxa*, is required for ER stress induced apoptosis in the epidermis. The epidermal apoptosis is likely because *p63* has been described as important for maintenance of the epithelium and is predominantly expressed there (Figure S7E) allowing for *puma* induction preferentially in the epithelium. The loss of *p63* and *puma* did not completely abrogate the apoptotic response suggesting additional stress induced apoptotic pathways, not involving the *p53* family or *puma/noxa*. Genetic studies using mutants in other BH3 only proteins may help identify these other pathways. Interestingly, the ER stress response to BFA is almost completely mediated by *p63/Puma*, suggesting differences in drug induce ER stress responses. Future studies addressing the importance of IRF, ATF6 and PERK upstream of *p63*, would be useful to delineate this pathway as well as tissue specific differences in ER stress responses.

Reactive oxygen stress response: While reactive oxygen stress is often associated with genotoxic stress, it is unique. Towards this, we demonstrate that oxidative stress induced apoptosis is mediated by *p63* and not *p73* or the genotoxic stress mediator *p53*. Unlike ER stress, oxidative stress in the epithelium does involves both *puma* and *noxa*. What is unique about oxidative stress to require both factors are unknown? It is worth

noting that the actual outcomes of PMA treatment are quite prolific in response; for example, PMA does activate NF- κ B in some cell types (72, 73). This could confound if the pathway is purely oxidative stress involved. This does not take away for the unique apoptotic aspects in that *noxa* is induced in all stresses tested, but only with PMA is *noxa* required for the full apoptotic response.

Therapeutic application: while p53 has been most well studied in the context of cancer, p53 is also involved in many developmental and non-cancerous diseases. The potential for inhibition of p53 has been contemplated, however not pursued due to concerns over the impact on cancer predisposition. For example, Treacher Collins Syndrome (TCS) is a genetic disease associated with ribosomal stress inducing p53 dependent apoptosis predominantly in the neural crest cell resulting in craniofacial defects. Interestingly the TCS mouse phenotype is abrogated in a *p53* null background. While inhibition of p53 may have long term cancer implications, loss of Puma both in mouse and zebrafish do not form tumors and therefore inhibition of puma could be a very effective therapeutic to prevent stress induced apoptosis associated diseases.

Zebrafish to understand cellular stress associated diseases: while mouse is the dominant model in most disease research, zebrafish provides numerous advantages that have propagated its applications in biomedical research. The major limitation is genetic reagents since this is a relatively young model system. Within this study we provide 7 new zebrafish null alleles that can be used in the biomedical community. Toward monitoring the consequence of stress signals the transparency of zebrafish embryos and adults allows for single cell analysis of fluorescent reporter lines in real time in a live animal (74-77). Towards this, recently a zebrafish ER stress reporter line has been generated that allows

for in vivo visualization of ER stress (74). In conjunction with disease models this could assist in understanding the pathology of the disease. In addition, zebrafish are highly amenable to chemical treatments as well as drug screens for suppressor of stress induced phenotypes.

MATERIALS AND METHODS:

Zebrafish Lines and Maintenance

All zebrafish work was performed in the Zebrafish Research Facility (ZRF) of the University of Alabama at Birmingham (UAB). Adult fish and embryos are maintained as described by Westerfield et al (1995) by the ZRF Animal Resources Program which maintains full AAALAC accreditation and is assured with OLAW. All knock-out lines are generated on the AB strain. All animal studies have UAB IACUC approval.

Transcript IDs in Homology Analysis

For the homology analysis we used the following transcripts: hPUMA (ENST00000439096.3), hNOXA (ENST00000316660.7), hBMF (ENST00000397573.5), hBid (ENST00000622694.5), hBim (ENST00000308659.12), hHrk (ENST00000257572.5), hBik (ENST00000216115.3), hBad (ENST00000309032.8), zPuma (ENSDART00000137918.3), zNoxa (ENSDART00000123131.3), zBmf (ENSDART00000060713.5), zBid (ENSDART00000100716.7), zBim (ENSDART00000114318.3), zHrk (ENSDART00000132567.2), zBad (Bada: ENSDART00000125349.3 and Badb: ENSDART00000077219.5), *tp53* (ENSDART00000051549.5), *tp63* (TA: ENSDART00000163541.2 and Δ N: ENSDART00000065135.5), *tp73* (ENSDART00000124737.3).

Generation of New Knockout Alleles

Gene Knockouts were generated as described previously (75). Zinc Finger, TALEN, or gRNA target sites were identified using the ZiFiT Targeter software developed by the Zinc Finger Consortium (<http://zifit.partners.org/ZiFiT/>), TAL Effector Nucleotide Targeter 2.0 (<https://tale-nt.cac.cornell.edu/>), and the Zhang lab gRNA design tool (<http://crispr.mit.edu>); respectively (target sites listed in figures). OPEN Pool ZFN were assembled into the pH3U3-mcs plasmid and selected using the omega knockout bacterial hybrid selection strain USO hisB-pyrF-rpoZ (Addgene #18049) (78). TALENs were assembled using The Golden Gate TALEN and TAL effector kit (Addgene #1000000016) (79). The CRISPR gRNA sequences were clones into pDR274 (Addgene 42250). The cas9 mRNA was transcribed from pT3TS-nCas9n (Addgene 46757.) (80). After cloning specific target plasmids/guides into pCS2 variant vector, mRNA was generated by in vitro transcription off NotI linearized DNA using the Invitrogen mMMESSAGE mMACHINE™ SP6 Transcription Kit (Fisher Scientific AM1340) and purified with the MEGAclean™ Transcription Clean Up Kit (Fisher Scientific AM1908). Approximately 1-2nl of nuclease mRNA (or sgRNA/Cas9 mRNA) were microinjected into the yolk of one-cell-stage zebrafish embryos. For indel efficiency evaluation, genomic DNA was extracted from ~24 3dpf injected embryos and evaluated with HRM (see below). The remaining embryos (F0s) from the clutches were raised. Out of frame indels identified in F1 progeny were maintained and propagated. To “cleanup” genetic background all lines were breed at least 2 generation to the wildtype strain AB.

Identification of Mutated Alleles, Nonsense Mediated Decay and Alternative Splicing

To determine if the mutated allele is undergoing nonsense mediated decay or alternative splicing, a small piece of tail was cut from a single heterozygous fish (of each allele). RNA was extracted from each tail using Trizol Reagent (Life Technologies, 15596026), and cDNA was synthesized from each RNA sample using the High-Capacity cDNA Reverse Transcription Kit (Life Technologies, 4368814). The cDNA was PCR amplified using Takara Ex Taq DNA Polymerase (Takara Bio, RR001A), purified with the Promega Wizard SV Gel and PCR Cleanup System (Promega, A9282), and examined on a 1% agarose gel (for examining alternative splicing) and sequenced by the UAB Heflin Center for Genomic Sciences Sanger Sequencing Core. The mutated allele was determined to have undergone complete nonsense mediated decay if only the wild-type sequence was detected in the sequence chromatogram.

Genotyping with High Resolution Melt Analysis (HRMs)

To isolate genomic DNA from adults, tail clippings from each fish were incubated at 98°C for 20 min in 40µl 25mM NaOH in a 96-well plate; then neutralized with 40µl of 40mM Tris-HCl. Early-stage or stained embryos were incubated at 55°C 2h in 25µl ELB (10mM Tris pH 8.3, 50mM KCl, 0.3% Tween 20, 0.3% NP40, 1mg/ml Proteinase K) in 96-well plates; then incubated at 95°C for 15 min to inactivate the Proteinase K. PCR reactions contained 1ul of LC Green Plus Melting Dye (Biofire Defense, BCHM-ASY-0005), 1µl of 10x enzyme buffer, 0.2µl of dNTP Mixture (10mM each), 0.3µl of MgCl₂, 0.3µl of each primer (10µM), 1µl of genomic DNA, 0.05µl of Genscript Taq (E00101), and water up to 10µl. The PCR reaction protocol was 98°C for 30 sec, then 45 cycles of 98°C for 10 sec, 59°C for 20 sec, and 72° C for 15 sec, followed by 95°C for 30 sec and then rapid cooling to 4°C. Following PCR, melting curves were generated and analyzed

using the LightScanner instrument (Idaho Technology) over a 65-95°C range. Primers used for identifying zebrafish knockout lines are listed in supplementary table 1.

IR-irradiation and Apoptotic Detection

Embryos were placed at the closest position to the source of IR in a X-RAD 320 X-ray irradiator to expose the embryos to approximate 4.2 Gy/min. Apoptosis was assayed following IR treatment by Acridine Orange (AO) or active Caspase-3 staining. For AO staining (76), embryos were incubated in 50mg/ml of Acridine Orange (Sigma) for 45 min followed by 5 consecutive 5-min washes. Images were immediately taken using dissecting microscopy with 488nm wavelength filter.

Drug Treatment

1.5µl Thapsigargin (10mM stock in DMSO, Sigma), 3µl Brefeldin A (10mM stock in DMSO, Sigma) and 1µl Phorbol 12-myristate 13-acetate (10mM stock in DMSO, Sigma) were added into 3mL of sterile E3 egg water to prepare working solutions with a final concentration of 5µM Thapsigargin (19), 10µM Brefeldin A (BFA) or 3.3µM Phorbol 12-myristate 13-acetate (PMA). Approximate 30 24hpf embryos (\pm 15 min) were placed in each well of 6-well tissue culture plates (BD Falcon). For immediate apoptosis induction, embryos were left for 4h (Thapsigargin and PMA) or 6h (BFA) in the dark at 28.5°C, processed for active Caspase-3 whole-embryo staining and sorted based on phenotypic categories (described in figures) to define the degree of severity.

Whole-embryo Immunohistochemistry Staining

Embryos were fixed in 4% paraformaldehyde (PFA) overnight at 4°C and then permeabilized for at least 2h in methanol (for anti-active Caspase-3 staining) or for 7 min in acetone (for anti-p63 staining). After 1h blocking, embryos were incubated in primary

antibody overnight at 4°C. Anti-active Caspase-3 antibody (BD, 559565) was used at a dilution of 1:500 and anti-p63 primary antibody (Abcam, ab735) at 1:200. For Caspase-3 detection, the Alexa 488 goat anti-rabbit secondary antibody was used and for p63 detection, an Alexa 488 Donkey anti-mouse secondary antibody was used at a dilution of 1:200 for 2h at room temperature or overnight at 4°C. Subsequently, embryos were washed and stained in DAPI for 10 min (if nucleus measurement necessary) prior to imaging.

Light, Immunofluorescence and Confocal Imaging

Embryos were dechorionated at described stages with incubation in 0.03% pronase (Sigma P5147) for 6 min and anesthetized using 0.4% tricaine. In a 60 x 15 mm Falcon petri dish (light and immunofluorescence imaging) and glass-coverslip-bottomed dish (confocal imaging), embryos are mounted in 1% low melting agarose. Gross images and images with acridine orange or anti-active Caspase-3 staining were taken on a SMZ-18 Zoom Stereo Microscope. For quantification, all images were acquired at the same magnification, laser power, exposure time and gain. Images with anti-p63 staining were taken on a Nikon A1 inverted confocal microscope and approximate 100- μ m Z-stacks at 3.5- μ m intervals were obtained. After each embryo was imaged, embryos were removed from the agarose to generate genomic DNA for genotyping. Further figure processing and analysis was performed using Nikon NIS Element and ImageJ.

Quantitative Real-time PCR

RNA was isolated from at least 30 pooled whole embryos using the Qiagen RNeasy Mini Kit and subjected to cDNA preparation with High-Capacity cDNA Reverse Transcription Kit (Thermo Fisher, 4368814). Quantitative PCR (qPCR) was performed using the CFX Connect Real Time System (Bio-Rad) with TaqMan™ Gene Expression

Master Mix (Thermo Fisher, 4369016). Primers and probes are purchased from Thermo Fisher.

Western Blotting Analysis

Approximately 30 pooled embryos at 24-30 hpf were homogenized in 60 μ L protein cocktail (15 μ L 4X sample buffer, 10 μ L 6X protease inhibitor, 1.5 μ L β -Me and water up to 60 μ L). The quantity of the protein loaded onto the western blots was assessed by hybridizing with anti-GAPDH primary antibody (Cell Signaling Technology, 2118) at a dilution of 1:2000. Subsequent SFS-PAGE gels were adjusted based on anti-GAPDH results. p53 was detected by hybridization with anti-p53 primary antibody (GeneTex, 128135) at a dilution of 1:1000, washed and incubated with peroxidase goat anti-rabbit IgG (1:2000; Jackson ImmunoResearch, 111-035-003) and developed with Clarity Western ECL Substrate (Bio-Rad, 1705061). Signal was detected by Bio-Rad ChemiDoc MP system. Western blot images were processed and quantified with Image Lab.

Establishing Tumor Cohorts:

Our tumor cohorts were established by natural breeding of p53^{-/-} x p53^{-/-} parents. The cohort consisted of 96 fish and was derived from a single set of parents (a single male and female). At 4 months of age, all fish were separated into 4 tanks of 24 fish each. Adult fish were screened weekly or biweekly for tumors and/or missing/dead fish. Fish that were identified by eye to be tumor burdened were euthanized according to IACUC protocols. Kaplan-Meier analysis was performed using GraphPad Prism 8 software.

Fluorescence Quantification and Statistical Analysis:

GraphPad Prism 8 was used in generation of all graphs and statistical tests. For phenotypic categories and qRT-PCR quantification, overall statistical significance was

calculated using an unpaired t-test with error bars indicating SEM. Numbers of embryos and significance values are indicated in the figure legends.

Data availability:

The supplementary material available at <https://doi.org/10.1038/s41419-021-03902-6>.

ACKNOWLEDGEMENTS

The authors would like to acknowledge the members of the Parant lab for technical help and critical reading of the manuscript. We would like to thank Dr. Voytas, Dr. Joung, Dr. Chen, and Dr. Wolfe for providing reagents through Addgene. We would like to thank the Dr. Grunwald lab for providing the TALEN plasmids. This work is supported by an NIH grant NCI R01CA216108 and a UAB AMC21 award.

AUTHOR CONTRIBUTIONS

Author's contribution: J.M.P. oversaw study. J.W. performed the majority of experiments, statistical analysis and generated figures. H.R. T. generated all knock-out zebrafish lines and performed NMD and genomic identification of these knockout lines. Z.L. performed qRT-PCR and analyzed for PMA- and BFA-drug treatments. N.C.Y. and N.D. performed PCR amplification to examine alternative splicing for knockout lines.

COMPETING INTERESTS

The authors declare no competing interests.

REFERENCE:

1. Fulda S, Gorman AM, Hori O, Samali A. Cellular stress responses: cell survival and cell death. *Int J Cell Biol.* 2010;2010:214074.
2. Wang S, Kaufman RJ. The impact of the unfolded protein response on human disease. *J Cell Biol.* 2012;197(7):857-67.
3. Lindholm D, Korhonen L, Eriksson O, Koks S. Recent Insights into the Role of Unfolded Protein Response in ER Stress in Health and Disease. *Front Cell Dev Biol.* 2017;5:48.
4. Fisher SA, Langille BL, Srivastava D. Apoptosis during cardiovascular development. *Circ Res.* 2000;87(10):856-64.
5. Jackson SP, Bartek J. The DNA-damage response in human biology and disease. *Nature.* 2009;461(7267):1071-8.
6. Lowe SW, Lin AW. Apoptosis in cancer. *Carcinogenesis.* 2000;21(3):485-95.
7. O'Driscoll M. Diseases associated with defective responses to DNA damage. *Cold Spring Harb Perspect Biol.* 2012;4(12).
8. Vousden KH, Lane DP. p53 in health and disease. *Nat Rev Mol Cell Biol.* 2007;8(4):275-83.
9. Kultz D. Molecular and evolutionary basis of the cellular stress response. *Annu Rev Physiol.* 2005;67:225-57.
10. Harper JW, Elledge SJ. The DNA damage response: ten years after. *Mol Cell.* 2007;28(5):739-45.
11. Ciccia A, Elledge SJ. The DNA damage response: making it safe to play with knives. *Mol Cell.* 2010;40(2):179-204.

12. Malhotra JD, Kaufman RJ. ER stress and its functional link to mitochondria: role in cell survival and death. *Cold Spring Harb Perspect Biol.* 2011;3(9):a004424.
13. Haeri M, Knox BE. Endoplasmic Reticulum Stress and Unfolded Protein Response Pathways: Potential for Treating Age-related Retinal Degeneration. *J Ophthalmic Vis Res.* 2012;7(1):45-59.
14. Genestra M. Oxyl radicals, redox-sensitive signalling cascades and antioxidants. *Cell Signal.* 2007;19(9):1807-19.
15. Martindale JL, Holbrook NJ. Cellular response to oxidative stress: signaling for suicide and survival. *J Cell Physiol.* 2002;192(1):1-15.
16. Kasthuber ER, Lowe SW. Putting p53 in Context. *Cell.* 2017;170(6):1062-78.
17. Valente LJ, Gray DH, Michalak EM, Pinon-Hofbauer J, Egle A, Scott CL, et al. p53 efficiently suppresses tumor development in the complete absence of its cell-cycle inhibitory and proapoptotic effectors p21, Puma, and Noxa. *Cell Rep.* 2013;3(5):1339-45.
18. Gregg SQ, Robinson AR, Niedernhofer LJ. Physiological consequences of defects in ERCC1-XPF DNA repair endonuclease. *DNA Repair (Amst).* 2011;10(7):781-91.
19. Pyati UJ, Gjini E, Carbonneau S, Lee JS, Guo F, Jette CA, et al. p63 mediates an apoptotic response to pharmacological and disease-related ER stress in the developing epidermis. *Dev Cell.* 2011;21(3):492-505.
20. Maher P. How protein kinase C activation protects nerve cells from oxidative stress-induced cell death. *J Neurosci.* 2001;21(9):2929-38.

21. Baines CP, Zhang J, Wang GW, Zheng YT, Xiu JX, Cardwell EM, et al. Mitochondrial PKCepsilon and MAPK form signaling modules in the murine heart: enhanced mitochondrial PKCepsilon-MAPK interactions and differential MAPK activation in PKCepsilon-induced cardioprotection. *Circ Res.* 2002;90(4):390-7.
22. Hrubik J, Glisic B, Samardzija D, Stanic B, Pogrmic-Majkic K, Fa S, et al. Effect of PMA-induced protein kinase C activation on development and apoptosis in early zebrafish embryos. *Comp Biochem Physiol C Toxicol Pharmacol.* 2016;190:24-31.
23. Jackson JG, Post SM, Lozano G. Regulation of tissue- and stimulus-specific cell fate decisions by p53 in vivo. *J Pathol.* 2011;223(2):127-36.
24. Melino G, Lu X, Gasco M, Crook T, Knight RA. Functional regulation of p73 and p63: development and cancer. *Trends Biochem Sci.* 2003;28(12):663-70.
25. Levrero M, De Laurenzi V, Costanzo A, Gong J, Wang JY, Melino G. The p53/p63/p73 family of transcription factors: overlapping and distinct functions. *J Cell Sci.* 2000;113 (Pt 10):1661-70.
26. Botchkarev VA, Flores ER. p53/p63/p73 in the epidermis in health and disease. *Cold Spring Harb Perspect Med.* 2014;4(8).
27. Melino G, De Laurenzi V, Vousden KH. p73: Friend or foe in tumorigenesis. *Nat Rev Cancer.* 2002;2(8):605-15.
28. Belyi VA, Levine AJ. One billion years of p53/p63/p73 evolution. *Proc Natl Acad Sci U S A.* 2009;106(42):17609-10.
29. Pflaum J, Schlosser S, Muller M. p53 Family and Cellular Stress Responses in Cancer. *Front Oncol.* 2014;4:285.

30. Hofseth LJ, Saito S, Hussain SP, Espey MG, Miranda KM, Araki Y, et al. Nitric oxide-induced cellular stress and p53 activation in chronic inflammation. *Proc Natl Acad Sci U S A*. 2003;100(1):143-8.
31. Klibanov SA, O'Hagan HM, Ljungman M. Accumulation of soluble and nucleolar-associated p53 proteins following cellular stress. *J Cell Sci*. 2001;114(Pt 10):1867-73.
32. Brooks CL, Gu W. New insights into p53 activation. *Cell Res*. 2010;20(6):614-21.
33. Donehower LA, Harvey M, Slagle BL, McArthur MJ, Montgomery CA, Jr., Butel JS, et al. Mice deficient for p53 are developmentally normal but susceptible to spontaneous tumours. *Nature*. 1992;356(6366):215-21.
34. Jacks T, Remington L, Williams BO, Schmitt EM, Halachmi S, Bronson RT, et al. Tumor spectrum analysis in p53-mutant mice. *Curr Biol*. 1994;4(1):1-7.
35. Mello SS, Attardi LD. Deciphering p53 signaling in tumor suppression. *Curr Opin Cell Biol*. 2018;51:65-72.
36. Flores ER, Tsai KY, Crowley D, Sengupta S, Yang A, McKeon F, et al. p63 and p73 are required for p53-dependent apoptosis in response to DNA damage. *Nature*. 2002;416(6880):560-4.
37. Senoo M, Manis JP, Alt FW, McKeon F. p63 and p73 are not required for the development and p53-dependent apoptosis of T cells. *Cancer Cell*. 2004;6(1):85-9.
38. Yang A, Kaghad M, Wang Y, Gillett E, Fleming MD, Dotsch V, et al. p63, a p53 homolog at 3q27-29, encodes multiple products with transactivating, death-inducing, and dominant-negative activities. *Mol Cell*. 1998;2(3):305-16.

39. Reimertz C, Kogel D, Rami A, Chittenden T, Prehn JH. Gene expression during ER stress-induced apoptosis in neurons: induction of the BH3-only protein Bbc3/PUMA and activation of the mitochondrial apoptosis pathway. *J Cell Biol.* 2003;162(4):587-97.
40. Shao J, Li Y, Shen K, Lin B, Xu Y, Lu Y, et al. 7b, a novel amonafide analog, inhibited proliferation and phorbol 12-myristate 13-acetate/phytohemagglutinin-induced inflammatory responses of Jurkat T cells via p73-dependent pathway and decrease of nuclear factor-kappaB DNA-binding, respectively. *Leuk Lymphoma.* 2013;54(2):359-71.
41. Melino G, Bernassola F, Ranalli M, Yee K, Zong WX, Corazzari M, et al. p73 Induces apoptosis via PUMA transactivation and Bax mitochondrial translocation. *J Biol Chem.* 2004;279(9):8076-83.
42. Youle RJ, Strasser A. The BCL-2 protein family: opposing activities that mediate cell death. *Nat Rev Mol Cell Biol.* 2008;9(1):47-59.
43. Villunger A, Michalak EM, Coultas L, Mullauer F, Bock G, Ausserlechner MJ, et al. p53- and drug-induced apoptotic responses mediated by BH3-only proteins puma and noxa. *Science.* 2003;302(5647):1036-8.
44. Parant JM, George SA, Holden JA, Yost HJ. Genetic modeling of Li-Fraumeni syndrome in zebrafish. *Dis Model Mech.* 2010;3(1-2):45-56.
45. Stainier DY, Fouquet B, Chen JN, Warren KS, Weinstein BM, Meiler SE, et al. Mutations affecting the formation and function of the cardiovascular system in the zebrafish embryo. *Development.* 1996;123:285-92.

46. Xi Y, Noble S, Ekker M. Modeling neurodegeneration in zebrafish. *Curr Neurol Neurosci Rep.* 2011;11(3):274-82.
47. Patton EE, Widlund HR, Kutok JL, Kopani KR, Amatruda JF, Murphey RD, et al. BRAF mutations are sufficient to promote nevi formation and cooperate with p53 in the genesis of melanoma. *Curr Biol.* 2005;15(3):249-54.
48. Neiswender JV, Kortum RL, Bourque C, Kasheta M, Zon LI, Morrison DK, et al. KIT Suppresses BRAF(V600E)-Mutant Melanoma by Attenuating Oncogenic RAS/MAPK Signaling. *Cancer Res.* 2017;77(21):5820-30.
49. Langheinrich U. Zebrafish: a new model on the pharmaceutical catwalk. *Bioessays.* 2003;25(9):904-12.
50. Nakano K, Vousden KH. PUMA, a novel proapoptotic gene, is induced by p53. *Mol Cell.* 2001;7(3):683-94.
51. Yu J, Zhang L, Hwang PM, Kinzler KW, Vogelstein B. PUMA induces the rapid apoptosis of colorectal cancer cells. *Mol Cell.* 2001;7(3):673-82.
52. Taylor RC, Cullen SP, Martin SJ. Apoptosis: controlled demolition at the cellular level. *Nat Rev Mol Cell Biol.* 2008;9(3):231-41.
53. Brunelle JK, Letai A. Control of mitochondrial apoptosis by the Bcl-2 family. *J Cell Sci.* 2009;122(Pt 4):437-41.
54. Tait SW, Green DR. Mitochondria and cell death: outer membrane permeabilization and beyond. *Nat Rev Mol Cell Biol.* 2010;11(9):621-32.
55. Kubbutat MH, Jones SN, Vousden KH. Regulation of p53 stability by Mdm2. *Nature.* 1997;387(6630):299-303.

56. Haupt Y, Maya R, Kazaz A, Oren M. Mdm2 promotes the rapid degradation of p53. *Nature*. 1997;387(6630):296-9.
57. Chène P. Inhibiting the p53–MDM2 interaction: an important target for cancer therapy. *Nature Reviews Cancer*. 2003;3(2):102-9.
58. Montes de Oca Luna R, Wagner DS, Lozano G. Rescue of early embryonic lethality in mdm2-deficient mice by deletion of p53. *Nature*. 1995;378(6553):203-6.
59. Chua JS, Liew HP, Guo L, Lane DP. Tumor-specific signaling to p53 is mimicked by Mdm2 inactivation in zebrafish: insights from mdm2 and mdm4 mutant zebrafish. *Oncogene*. 2015;34(48):5933-41.
60. Sidi S, Sanda T, Kennedy RD, Hagen AT, Jette CA, Hoffmans R, et al. Chk1 suppresses a caspase-2 apoptotic response to DNA damage that bypasses p53, Bcl-2, and caspase-3. *Cell*. 2008;133(5):864-77.
61. Toruno C, Carbonneau S, Stewart RA, Jette C. Interdependence of Bad and Puma during ionizing-radiation-induced apoptosis. *PLoS One*. 2014;9(2):e88151.
62. Berghmans S, Murphey RD, Wienholds E, Neuberg D, Kutok JL, Fletcher CD, et al. tp53 mutant zebrafish develop malignant peripheral nerve sheath tumors. *Proc Natl Acad Sci U S A*. 2005;102(2):407-12.
63. Shimada M, Matsuzaki F, Kato A, Kobayashi J, Matsumoto T, Komatsu K. Induction of Excess Centrosomes in Neural Progenitor Cells during the Development of Radiation-Induced Microcephaly. *PLoS One*. 2016;11(7):e0158236.
64. Wali JA, Rondas D, McKenzie MD, Zhao Y, Elkerbout L, Fynch S, et al. The proapoptotic BH3-only proteins Bim and Puma are downstream of endoplasmic

- reticulum and mitochondrial oxidative stress in pancreatic islets in response to glucotoxicity. *Cell Death Dis.* 2014;5:e1124.
65. Luo X, He Q, Huang Y, Sheikh MS. Transcriptional upregulation of PUMA modulates endoplasmic reticulum calcium pool depletion-induced apoptosis via Bax activation. *Cell Death Differ.* 2005;12(10):1310-8.
 66. Teive HA, Moro A, Moscovich M, Arruda WO, Munhoz RP, Raskin S, et al. Ataxia-telangiectasia - A historical review and a proposal for a new designation: ATM syndrome. *J Neurol Sci.* 2015;355(1-2):3-6.
 67. Taylor AM, Groom A, Byrd PJ. Ataxia-telangiectasia-like disorder (ATLD)-its clinical presentation and molecular basis. *DNA Repair (Amst).* 2004;3(8-9):1219-25.
 68. Boder E, Sedgwick RP. Ataxia-telangiectasia; a familial syndrome of progressive cerebellar ataxia, oculocutaneous telangiectasia and frequent pulmonary infection. *Pediatrics.* 1958;21(4):526-54.
 69. Shiloh Y. Ataxia-telangiectasia and the Nijmegen breakage syndrome: related disorders but genes apart. *Annu Rev Genet.* 1997;31:635-62.
 70. Michalak EM, Villunger A, Adams JM, Strasser A. In several cell types tumour suppressor p53 induces apoptosis largely via Puma but Noxa can contribute. *Cell Death Differ.* 2008;15(6):1019-29.
 71. Albert MC, Brinkmann K, Kashkar H. Noxa and cancer therapy: Tuning up the mitochondrial death machinery in response to chemotherapy. *Mol Cell Oncol.* 2014;1(1):e29906.

72. Krappmann D, Patke A, Heissmeyer V, Scheidereit C. B-cell receptor- and phorbol ester-induced NF-kappaB and c-Jun N-terminal kinase activation in B cells requires novel protein kinase C's. *Mol Cell Biol.* 2001;21(19):6640-50.
73. Khalaf H, Jass J, Olsson PE. Differential cytokine regulation by NF-kappaB and AP-1 in Jurkat T-cells. *BMC Immunol.* 2010;11:26.
74. Clark EM, Nonarath HJT, Bostrom JR, Link BA. Establishment and validation of an endoplasmic reticulum stress reporter to monitor zebrafish ATF6 activity in development and disease. *Dis Model Mech.* 2020;13(1).
75. Thomas HR, Percival SM, Yoder BK, Parant JM. High-throughput genome editing and phenotyping facilitated by high resolution melting curve analysis. *PLoS One.* 2014;9(12):e114632.
76. Percival SM, Parant JM. Observing Mitotic Division and Dynamics in a Live Zebrafish Embryo. *J Vis Exp.* 2016(113).
77. White RM, Sessa A, Burke C, Bowman T, LeBlanc J, Ceol C, et al. Transparent adult zebrafish as a tool for in vivo transplantation analysis. *Cell Stem Cell.* 2008;2(2):183-9.
78. Maeder ML, Thibodeau-Beganny S, Sander JD, Voytas DF, Joung JK. Oligomerized pool engineering (OPEN): an 'open-source' protocol for making customized zinc-finger arrays. *Nat Protoc.* 2009;4(10):1471-501.
79. Cermak T, Doyle EL, Christian M, Wang L, Zhang Y, Schmidt C, et al. Efficient design and assembly of custom TALEN and other TAL effector-based constructs for DNA targeting. *Nucleic Acids Res.* 2011;39(12):e82.

80. Hwang WY, Fu Y, Reyon D, Maeder ML, Tsai SQ, Sander JD, et al. Efficient genome editing in zebrafish using a CRISPR-Cas system. *Nat Biotechnol.* 2013;31(3):227-9.

CHAPTER 3

p21, CCNG1, FOXO3B AND FBXW7 CONTRIBUTE TO
p53-DEPENDENT CELL-CYCLE ARREST

by

JUN WANG, ZHANG LI, HOLLY R. THOMAS, KE FAN, ROBERT G. THOMPSON,
YONGJIE MA, JOHN M. PARANT

In preparation for *Cell Death and Differentiation*

Format adapted for dissertation

ABSTRACT:

p53, a transcription factor, play a critical role in cancer prevention. However, the mechanisms by which p53 exerts its tumor-suppressive function is still unclear. While PUMA/BBC3 and NOXA/PMAIP1 are known to be important in p53-dependent apoptosis, and p21/CDKN1A is crucial for p53-dependent cell-cycle arrest, our study demonstrates that zebrafish lacking puma, noxa, and p21 do not show an increased predisposition to cancer. This suggests that additional p53 transcriptional targets are necessary for its tumor suppression function. Contrary to the prevailing belief that p21 is the key regulator of p53-dependent cell-cycle arrest, we provide evidence that p53 can still induce cell-cycle arrest in the absence of p21, following DNA damage or loss of mdm2 (p53 activation in the absence of stress). This implies the involvement of other p53 targets in mediating p53-dependent cell-cycle arrest. Since p53 tumor suppression is conserved across multiple vertebrate species, we conducted a cross-species comparative analysis of p53-dependent transcriptional profiles. This analysis allowed us to identify a conserved set of 132 p53-upregulated transcripts, providing insights into the common regulatory targets of p53 among different species. Additionally, we performed a CRISPR/Cas9 G0 “crisprant” screen in a genetic background lacking mdm2, puma, noxa, and p21 to identify key components involved in p53-dependent cell-cycle arrest. Our findings revealed that ccng1, fbw7, and foxo3b play important role in this process.

INTRODUCTION:

The p53 pathway plays an essential role in tumor suppression. Evidence from the Cancer Genome Atlas (TCGA) confirms that TP53 is the most frequently mutated gene in

various cancers, with an occurrence of approximately 50% [1]. For instance, p53 mutations have been found in up to 95% of ovarian cancer cases. In some cancers, although the TP53 gene remains wild-type, the p53 pathway is still repressed through alternative mechanisms, such as overexpression of mdm2 or mdm4 [2, 3]. This emphasizes the significance of p53 regulation in tumor suppression.

The importance of p53 in tumor suppression is further underscored by the Li-Fraumeni syndrome (LFS), an autosomal dominant cancer predisposition syndrome. LFS patients carry germline mutations in the TP53 gene, resulting in the loss of its functional activity. This syndrome is associated with a high penetrance of multiple cancer types, providing strong evidence for the critical role of p53 in preventing tumor development [4-9].

Furthermore, the tumor-suppressive activity of p53 is conserved across various vertebrate species. Studies in rats, mice, and zebrafish have demonstrated that animals with homozygous or heterozygous null p53 genotypes are prone to early onset of cancer [10-15]. This conservation of p53 function among different species highlights its fundamental role in tumor suppression.

Zebrafish are emerged as a powerful model organism for studying p53 and its related processes [16-18]. They offer several significant advantages over other vertebrate models. First, zebrafish have a high reproductive capacity. A mating pair can produce a large number of eggs (ranging from 50 to 300) in a single breeding event, with repeated breeding on average every week. This large brood size facilitates generation of complex genetic animal (such as quadruple null) within a few generations; it allows for high throughput genome editing; it enables for the generation of tumor cohorts (N=96 per

genotype) from a single mating pair; and external fertilization allows for ease of monitoring embryonic phenotypes in real time and enhanced sample number to achieve statistical significance. Additionally, transparent embryos and larvae allow for the imaging and visualization of cellular and molecular markers throughout the whole organism.

In “normal” cells, the levels of p53 protein are maintained at low levels primarily through the action of its negative regulator, MDM2. MDM2 functions as an E3 ubiquitin ligase, facilitating p53 degradation by tagging it with ubiquitin molecules [19-21]. However, p53 protein levels increase following a variety of cellular stresses, such as DNA damage and oncogene stress. This occurs because these stresses inhibit the MDM2-dependent degradation of p53 [22]. Upon p53 stabilization, p53 transcribes a variety of downstream targets and biological effector processes to promote either elimination or arrest of injured cells to prevent progression to a cancerous state [3, 23]. Among these biological processes, apoptosis (mediated by pro-apoptotic BCL-2 family members PUMA/BBC3 and NOXA/PMAIP1) and cell-cycle arrest (mediated by the CDK inhibitor p21/CDKN1A) are the most extensively studied and considered critical barriers against cancer development [24, 25]. However, a study by Valente et al. utilized mice deficient for Puma, Noxa and p21 ($puma^{-/-}$; $noxa^{-/-}$; $p21^{-/-}$) and found that these animals did not show an increased predisposition to cancer [26]. These findings indicate that p53 is capable of suppressing tumors even in the absence of Puma, Noxa and p21, suggesting the existence of other downstream targets and biological effector pathways that may be critical for p53-mediated tumor suppression.

Here, we investigated that the tumor suppressive function of p53 in zebrafish by generating $puma^{-/-}$; $noxa^{-/-}$; $p21^{-/-}$ (referred to as $pnp^{-/-}$) zebrafish. Similar to previous

findings in mice, these zebrafish remained tumor-free. However, when subjected to DNA damage and loss of mdm2, these animals exhibited p53-dependent cell-cycle arrest even in the absence of p21, suggesting the involvement of additional transcripts in this process. To define these additional transcripts involved in p53-mediated cell-cycle arrest and other noncanonical pathways, we employed a combination of cross-species comparative transcriptomics and identified 132 potential candidate genes that are conserved between mice and zebrafish and are upregulated by p53 activation. Subsequently, through a CRISPR/Cas9 "crisprant" screen that individually disrupt the top 24 cell cycle related candidate genes identified from the comparative analysis, we identified that in addition to p21, ccng1, fbxw7, and foxo3b are important components in p53-dependent cell-cycle arrest.

RESULTS:

p53 efficiently suppresses tumor predisposition in the complete absence of puma, noxa and p21

To further explore the conservation of the p53 tumor suppressive network across species, we generated zebrafish lacking puma/bbc3, noxa/pmaip1 [14], and p21/cdkn1a as shown in Figure S1. These puma^{-/-}; noxa^{-/-}; p21^{-/-} zebrafish, referred as to pnp^{-/-}, were then monitored for tumor predisposition (Fig. 1). Consistent with the findings in mice, none of the pnp^{-/-} zebrafish (N=43) developed tumors within 450 days after birth. In contrast, all of the p53^{-/-} zebrafish (N=96) have succumbed to tumors, as depicted in Figure 1. This observation suggests that additional p53 transcriptional targets and/or biological processes may regulate tumor suppression in the pnp^{-/-} background.

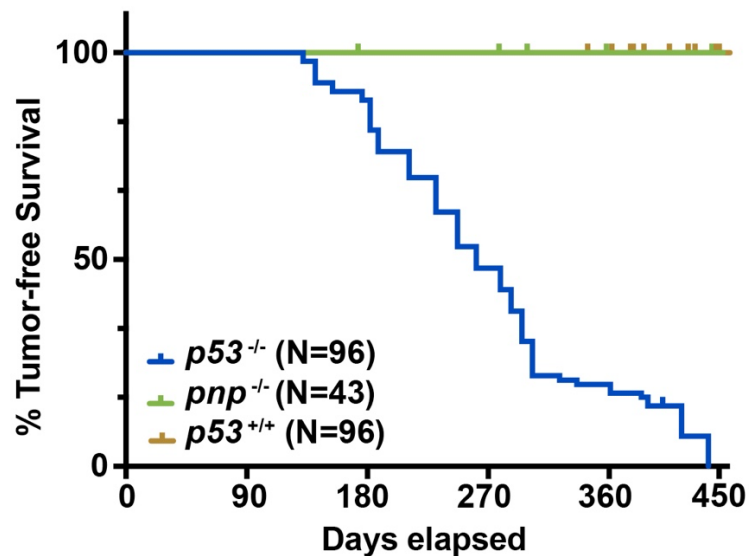


Figure 1. *puma*^{-/-}; *noxa*^{-/-}; *p21*^{-/-} zebrafish are not predisposed to spontaneous tumors. Kaplan-Meier tumor-free survival of *p53*^{-/-} (blue curve, N=96, T50=261 days) zebrafish compared with *puma*^{-/-}; *noxa*^{-/-}; *p21*^{-/-} (called *pnp*^{-/-}, N=43, green) and wildtype allele (N=96, orange). Long-rank statistic test was done. ****, p-value between *p53*^{-/-} and *pnp*^{-/-} < 0.0001 and p-value between *p53*^{-/-} and *p53*^{+/+} < 0.0001.

Loss of *puma*, *noxa* and *p21* are resistant to *p53*-dependent apoptosis

To assess the deficiency of *p53*-dependent apoptosis and cell-cycle arrest in our *pnp*^{-/-} zebrafish, we first conducted validation experiments. Previously, we had demonstrated a robust apoptotic response in the neural tube of 1-day post fertilization (dpf) zebrafish embryos 6 hours post irradiation (hpi) with 30Gy. We also observed that this apoptosis response was absent in *p53*^{-/-} or *puma*^{-/-} embryos [13, 14]. In this study, we performed cleavage caspase 3 staining on both irradiated and un-irradiated wildtype, *puma*^{-/-}; *noxa*^{-/-}, *pnp*^{-/-}, and *p53*^{-/-} zebrafish embryos at 1, 3 and 6 hpi (Fig. 2A,B). Comparing

these results to wildtype zebrafish embryos at 1 dpf, we observed that $p53^{-/-}$, $puma^{-/-}$; $noxa^{-/-}$ and $pnip^{-/-}$ embryos displayed resistance to p53-mediated apoptosis in response to irradiation. This indicated that puma and noxa are key mediators in p53-controlled apoptotic processes, and the $pnip^{-/-}$ zebrafish exhibit resistance to p53-dependent apoptosis.

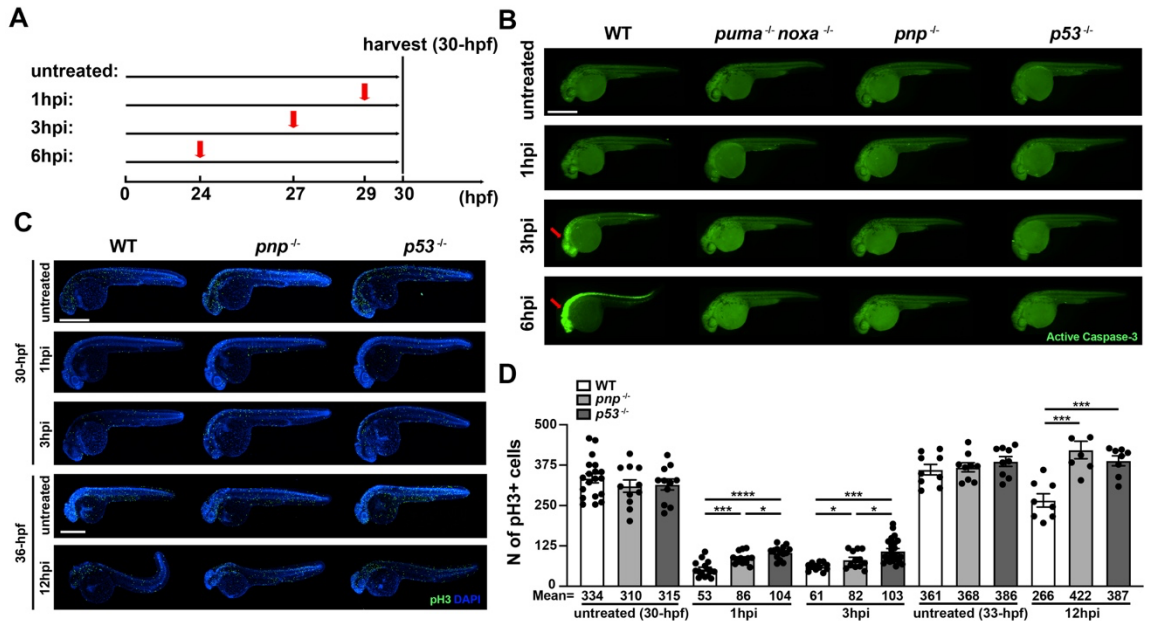


Figure 2. Loss of puma, noxa and p21 provide completely resistance to p53-mediated induction of apoptosis and partially resistant to p53-mediated cell-cycle arrest. A. Experimental workflow showing how to harvest samples. 29-, 27- and 24-hours post fertilization (hpf) wildtype, *puma*^{-/-}; *noxa*^{-/-}, *pnp*^{-/-} and *p53*^{-/-} zebrafish embryos were treated with 30Gy IR-irradiation and fixed at 1-, 3-, 6-, 9- and 12-hours post IR-treatment (hpi, 1hpi, 3hpi and 6hpi panels). B. Representative images of anti-active Caspase-3 staining on 30-hpf zebrafish embryos for each group. Arrows in WT points out active apoptotic area in head region at 3 and 6 hpi. Scale bar: 500 μ M. C. Representative images of phospho-histone H3 (pH3)-stained 30-hpf (1 and 3 hpi) or 36-hpf (12 hpi) zebrafish embryos for each group. Experimental design showing in Figure 2A and Figure S2A. Scale bar: 500 μ M. D. Quantification of pH3 positive cells in treated and untreated WT, *pnp*^{-/-} and *p53*^{-/-} embryos for each group. Each dot represents an individual. The average number of pH3+ cells (Mean) were indicated in each group. Bars represent mean \pm SEM. *, $p < 0.05$. ***, $p < 0.001$. ****, $p < 0.0001$.

Other p53 target genes are capable of inducing cell-cycle arrest in the absence of p21

To investigate p53-dependent cell-cycle arrest, we performed whole-embryo staining for Phospho-histone H3 (pH3), a marker for M phase cells, on embryos with and without IR-irradiation at different time points (Figs. 2A). We aimed to determine whether *pnp*^{-/-} embryos were resistant to p53-mediated cell-cycle arrest. At 30 hpf, embryos were fixed at 1- and 3-hours post 30Gy irradiation, followed by pH3 staining. Confocal imaging was then used to examine the number of pH3-positive cells in each embryo (Fig. 2C,D). A decrease in pH3 staining at 1 and 3-hour time points indicates cell-cycle arrest at the G2/M transition. We observed a substantial reduction in pH3-positive cells in wildtype (WT) control embryos after IR irradiation (53 and 61 pH3-positive cells at 1 and 3 hpi, respectively, compared to 334 in untreated embryos). However, the reduction in pH3-positive cells was less pronounced in both *pnp*^{-/-} (86 or 82 at 1 or 3 hpi, respectively) and *p53*^{-/-} zebrafish (104 or 102 at 1 or 3 hpi, respectively) (Fig. 2D). These findings suggest two important conclusions: Firstly, p53 is not the sole mediator of IR-induced cell-cycle arrest at the G2/M checkpoint, as evidenced by the presence of ~100 pH3-expressing cells in *p53*^{-/-} embryos following IR treatment. Secondly, amongst p53-dependent arrest mechanisms, puma, noxa and p21 are only partially functional in p53-dependent arrest, as indicated by the modest reduction in pH3-positive cells (~80 versus ~100) in the *pnp*^{-/-} embryos. This suggests that while p21 is an essential mediator for p53-mediated cell-cycle arrest, it is not the exclusive factor responsible for this process.

To access cell-cycle arrest at other phases of the cell cycle, we continued tracking the number of pH3-expressing cells at later timepoint (6, 9 and 12 hpi). Embryos at 24 hpf were exposed to 30Gy IR, and after 6, 9 and 12 hours, the number of pH3-positive cells

was examined (Figs. 2C,D&S2). Changes in pH3 staining at the 9 and 12-hour time points can reflect defects in various cell cycle phases, with changes at these time points predominantly indicating G1/S arrest. At 12 hpi, WT embryos exhibited significantly reduced pH3 staining compared to the untreated (266 vs 361). In contrast, both $p53^{-/-}$ and $pnp^{-/-}$ embryos showed pH3 staining levels similar to the untreated group (422 and 387 versus 368 and 386, respectively). This suggests the involvement of the p53-p21 axis in G1 arrest.

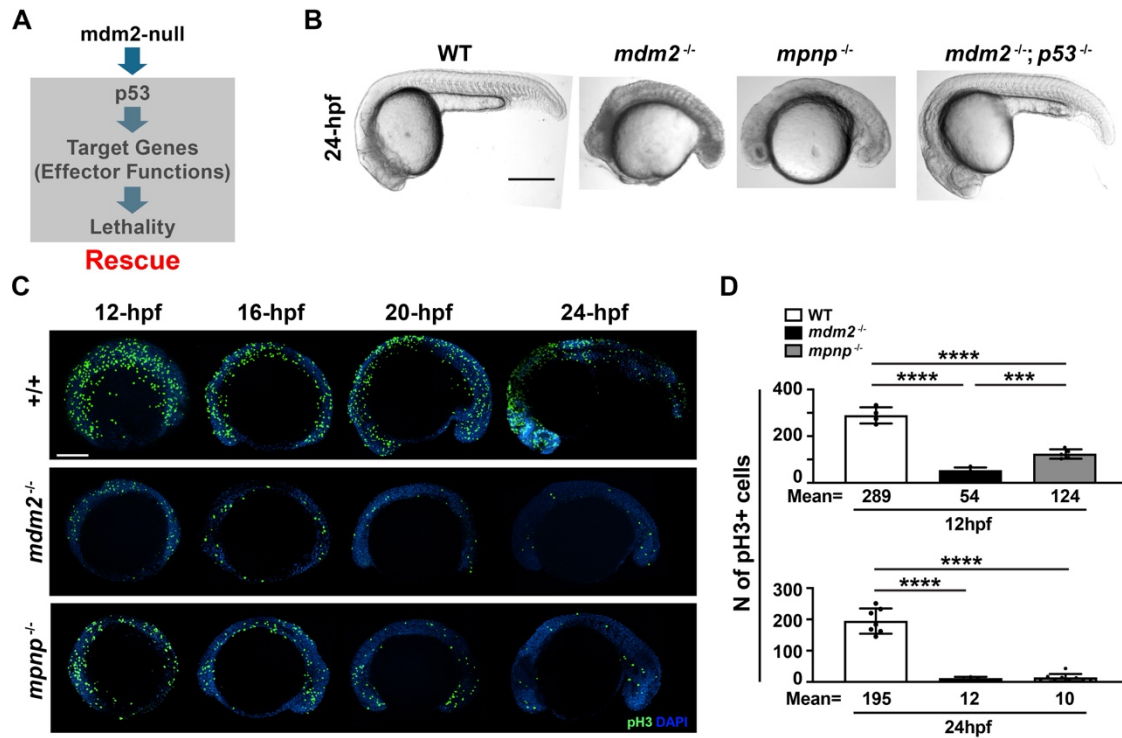


Figure 3. Loss of p21 partially rescues p53-dependent mdm2-null induced cell-cycle arrest. A. The conceptual diagram of mdm2-null induced embryonic lethality. Loss of mdm2 elevates p53 protein levels to induce downstream targets and effector functions to render the lethality. B. Representative gross images of 24-hpf *mdm2*^{+/+}, *mdm2*^{-/-}; *puma*^{-/-}; *noxa*^{-/-}; *p21*^{-/-} (*mpnp*^{-/-}) and *mdm2*^{-/-}; *p53*^{-/-} embryos. Scale bar: 500 μ M. C. pH3-stained *mdm2*^{+/+}, *mdm2*^{-/-}; *mpnp*^{-/-} embryos at 12-, 16-, 20- and 24-hpf. Scale bar: 500 μ M. D. Quantification of pH3 positive cells at 12 hpf (Top panel) and at 24 hpf (bottom panel). Each dot represents an individual. Bars represent mean \pm SEM. ***, $p < 0.001$. ****, $p < 0.0001$. Not statistical significance between *mdm2*^{-/-} and *mpnp*^{-/-} at 24 hpf.

To further investigate the role of p21 in p53-regulated cell-cycle arrest, we utilized *mdm2* knockout as a means to activate p53 in the absence of stress signaling pathways. MDM2 is an E3 ubiquitin ligase that targets p53 for degradation, and its loss results in p53 protein accumulation and activation of p53 target genes [19-21]. The simultaneous loss of p53 rescues the embryonic lethality caused by *mdm2* deletion in both mice and zebrafish (Fig. 3A & B) [14, 27-30], confirming that the lethality is p53-dependent.

Previously, we demonstrated that *mdm2*-null zebrafish embryos exhibit early morphological defects and extensive apoptosis, which can be partially rescued by the loss of *puma* [14]. However, the embryonic lethality persists, suggesting the potential involvement of p53-dependent cell-cycle arrest. To address this, we generated quadruple knockout embryos lacking *mdm2*, *puma*, *noxa*, and p21 (referred as to *mpnp*^{-/-}). Although these embryos showed improved morphological appearance compared to *mdm2*^{-/-} embryos, they were still developmentally delayed (Fig. 3B), indicating that the loss of *puma*, *noxa* and p21 only partially rescues the embryonic lethality in *mdm2*-null embryos.

We further stained mitotic cells in wild-type, *mdm2*^{-/-} and *mpnp*^{-/-} zebrafish embryos using a pH3 primary antibody at different time points (12, 16, 20, 24 hpf) to assess the effect of p21 loss on cell-cycle arrest in the absence of *mdm2* (Fig. 3C,D). We observed a significant reduction in the number of cells undergoing cell-cycle arrest in the absence of p21 at 12 hpf (Fig. 3D, 124 pH3-positive cells in *mpnp*^{-/-} vs. 54 in *mdm2*^{-/-}). However, compared to WT controls, a considerable number of cells were still arrested (124 in *mpnp*^{-/-} vs. 289 in +/+). This indicates that while p21 is important in the initial p53-dependent cell-cycle arrest, there are other p53 target genes capable of inducing cell-cycle arrest in the absence of p21. Furthermore, we quantified the number of pH3-positive cells in each

embryo at 24 hpf and found no significant difference between *mdm2*^{-/-} and *mpnp*^{-/-} embryos (Fig. 3D). These findings collectively suggest that while p21 is involved in the early p53-dependent cell-cycle arrest, there are additional p53 target genes capable of inducing cell-cycle arrest in the absence of p21.

Transcriptional analysis on a *pnp*^{-/-} background significantly reduced the number of p53 downstream genes

To define p53-dependent cell cycle regulatory transcripts, we first performed RNA-seq analysis of wild-type 30-hpf embryos 3 hours after 30Gy IR-irradiation and without IR (Fig. S3). We identified 449 differentially expressed genes (DEGs) with a fold change (FC) cutoff of ≥ 2 or ≤ -2 , $p\text{-value} \leq 0.05$ and $\text{baseMean} \geq 100$ (Fig. S3B). Considering that many of these DEGs may be secondary or tertiary to the primary p53 targets and/or apoptosis/cell-cycle arrest we again performed RNA-seq analysis of 30-hpf *pnp*^{-/-} embryos with and without IR at 3 hpi. With the same cutoff, we identified 162 DEGs (Fig. S3B). This suggested that ~72% of DEGs in the wild-type datasets were secondary to puma, noxa and p21 and/or apoptosis/partial cell-cycle arrest; and encouraged future analysis in the *pnp*^{-/-} background. We did identify 36 genes not shown in WT but in the *pnp*^{-/-} datasets (Fig. S3C), however we found most of these DEGs are just below the cutoff ($\text{FC} \geq 2$ or ≤ -2) in the wildtype dataset. Hence in the following analysis, we used a lower FC cutoff (>1.5) to define primary p53 targets. 261 p53 unregulated genes were defined in early response to IR-irradiation in zebrafish

Our pH3 staining results demonstrated that p21 is not the only mediator in p53-regulated cell-cycle arrest at 1 hpi (Fig. 2C&D). Therefore, to expand the timescale (1hpi

and 3hpi) and differentiate p53-dependent transcripts (*pnp*^{-/-} DEGs not induced in *p53*^{-/-}), we performed RNA-seq analysis on *pnp*^{-/-} and *p53*^{-/-} embryos at 1 and 3 hpi. To avoid identifying developmental DEGs, all embryos were harvested (~30-35 embryos per sample) at 30 hpf and irradiated at either 29-hpf (1 hpi) and 27-hpf (3 hpi). We set the cutoff for DEGs at fold change ≥ 1.5 (note the lower cutoff than above) and $q \leq 0.05$ for each comparison. Volcano plots of *pnp*^{-/-} treated versus untreated at 1 hpi and 3 hpi demonstrated well-established p53 targets such as *bbc3*, *cdnk1a*, and *mdm2* are significantly induced at both timepoints (Fig. 4A,B). We obtained 74 upregulated DEGs at 1 hpi and 321 at 3 hpi when compared *pnp*^{-/-} treated embryos with untreated embryos (Fig. 4C, Tables. S1,S2). To define whether those DEGs are p53-dependent, we again performed RNA-seq analysis of 30-hpf *p53*^{-/-} embryos with and without IR at 1 and 3 hpi and subtracted fold change in *pnp*^{-/-} treated versus untreated at 1 and 3 hpi to that in *p53*^{-/-}, respectively. If the value ≥ 1.5 , the gene was defined as p53-upregulated DEGs in response to IR-irradiation. With this algorithm, we defined 58 p53-induced genes in *pnp*^{-/-} treated vs untreated at 1 hpi and 239 at 3 hpi (Fig. 4C, Tables. S1,S2). We combined them to obtain 261 p53-induced genes after IR-irradiation in zebrafish (Fig. 4D). Some of well-established p53 targets, such as *gadd45aa*, *mdm2*, and *ccng1*, are among the list and showed a progressive increase level in *pnp*^{-/-} but not in *p53*^{-/-} datasets in response to IR-treatment (Fig. 4E). 203 were only in the 3-hpi timepoint and either represent p53-dependent late-induced genes or potentially secondary targets downstream the true p53 transcribed genes.

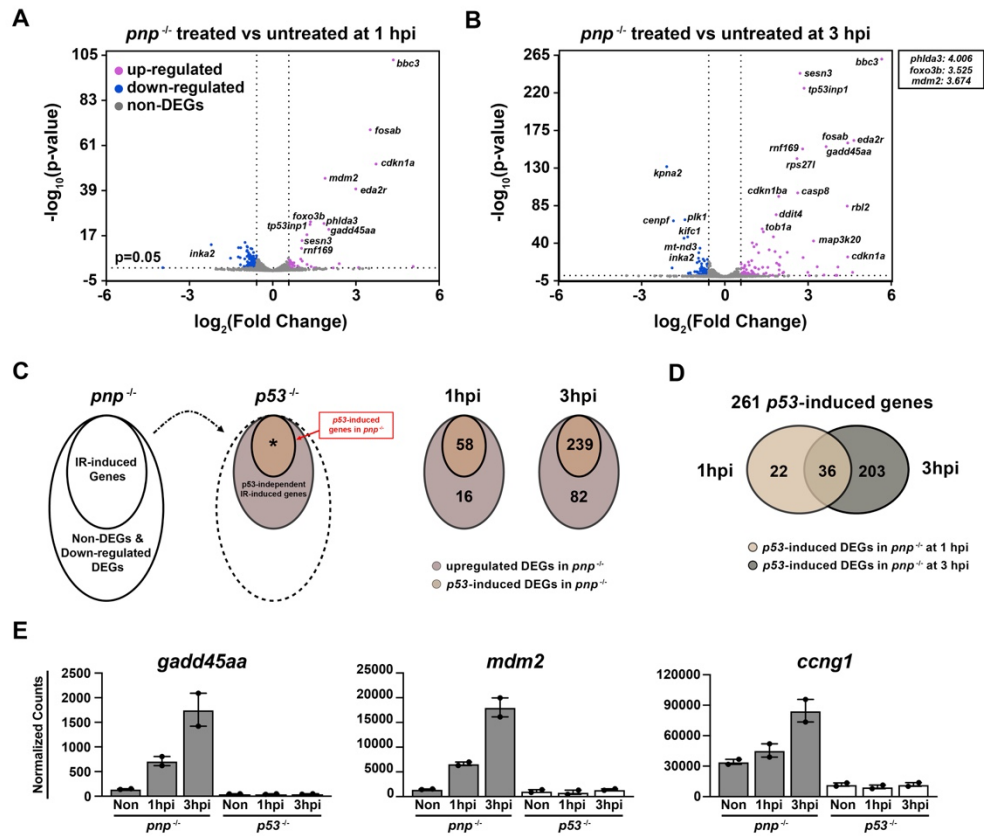


Figure 4. Defining early-responsive p53-upregulated genes in response to IR-irradiation in zebrafish. Volcano plots showing 30-hpf zebrafish *pnp*^{-/-} embryos with the treated versus untreated at 1 (A) and 3 hpi (B). The cutoff was set as fold change ≥ 2 or ≤ -2 and p value ≤ 0.05 . Upregulated DEGs were color-labelled with magenta and the down-regulated were labelled with blue. The gene symbol of some TOP DEGs was indicated on the plot. The p-value of *phlda3*, *foxo3b* and *mdm2* treated versus untreated at 3 hpi is 0. Their $\log_2(\text{Fold change})$ values were pointed out (top right square). C. Venn graphs representing p53-upregulated DEGs in *pnp*^{-/-} at 1 and 3 hpi. The cut-off is fold change ≥ 1.5 and $q \leq 0.05$. D. Venn graph showing 261 p53-induced genes in *pnp*^{-/-} between 1 and 3 hpi. E. Representative plots showing well-established p53 targets in *pnp*^{-/-} but not *p53*^{-/-} datasets in response to IR-treatment.

2,377 p53 upregulated genes were defined in early response to IR-irradiation in mouse

Loss of p53 in both mice and zebrafish resulted in spontaneous tumor formation with 100% penetrance [10, 13, 14, 31], which indicates that the p53-regulated transcriptional networks that prevents tumor formation is conserved among these species. To reduce the number of p53 target gene candidates, we conducted a cross-species comparative transcriptomic analysis between zebrafish and mouse datasets. We performed RNA-seq analysis on E9.5 dpc p53^{+/+} and p53^{-/-} mouse embryos, roughly equivalent developmental stage as zebrafish 30-hpf embryos based on organ development, with and without 30Gy IR-irradiation (Fig. S4A,B). Consistence with zebrafish data, the volcano plots indicated that Bbc3, Cdkn1a and Mdm2 were all induced within 1 hour and accumulated at the 3-hpi timepoint (Fig. S4C,D). Compared with the untreated, we identified 122 upregulated DEGs at 1 hpi and 2,729 at 3 hpi in mouse, with 65 at 1 hpi and 2,416 at 3 hpi being p53-dependent (Fig. 5A, Tables S3, S4), with a combine of p53-induced genes count at 2,442 (Fig. 5B). Conceptually like zebrafish, there were 39 DEGs that span both the 1-hpi and 3-hpi timepoints, while 26 DEGs only in the 1hpi timepoint, and 2,377 only in the 3hpi timepoint (Fig. 5B). Many of the latter likely represent secondary transcripts of p53 transcripts or biological outcomes. Unfortunately, unlike zebrafish, we did not have the Puma^{-/-}; Noxa^{-/-}; p21^{-/-} mice to remove the secondary targets after p53 activation.

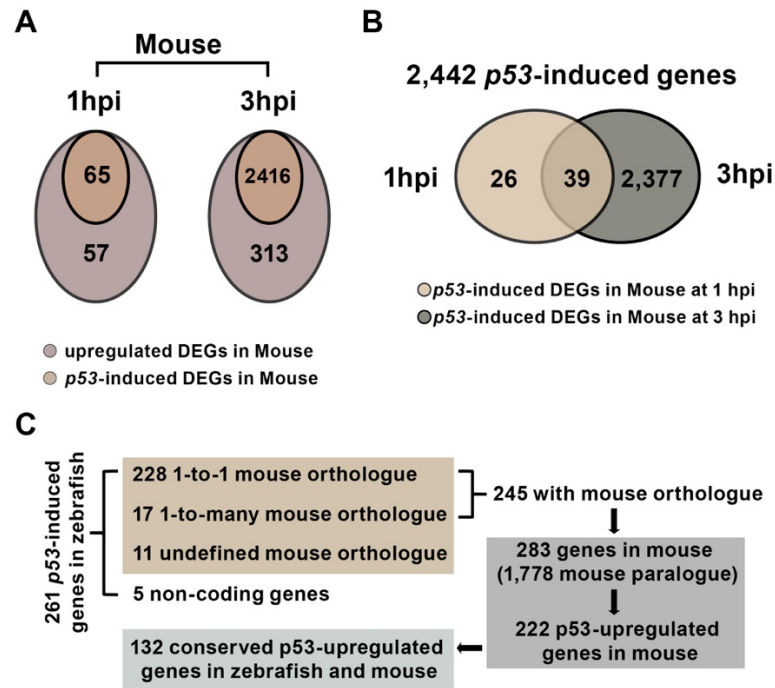


Figure 5. Defining conserved p53-upregulated genes in zebrafish and mouse. A. Venn graphs representing p53-upregulated DEGs in mouse $p53^{+/+}$ at 1 and 3 hpi. The cut-off is fold change ≥ 1.5 and $q \leq 0.05$. B. Venn graph showing 2,442 p53-induced genes in mouse $p53^{+/+}$ between 1 and 3 hpi. C. The diagram showing the analysis on mouse orthologues of p53-upregulated DEGs in $pnp^{-/-}$ zebrafish embryos at 1 and 3 hpi. For 261 p53-upregulated DEGs defined in zebrafish at 1 or 3 hpi, 245 of them are with mouse orthologues. Among them 228 genes have one orthologue and 17 of them are with multiple orthologues. 11 did not define orthologues in mouse. Five of them are non-coding genes. And 245 zebrafish upregulated DEGs are corresponding to 283 mouse orthologues and 1,778 mouse paralogues. Among them 222 genes are upregulated in mouse WT but not in $p53^{-/-}$ treated versus untreated. Finally, defining 132 zebrafish p53-induced DEGs are also conserved upregulated by p53 in mouse.

132 conserved p53-upregulated genes were identified in mouse and zebrafish

To define conserved p53-upregulated DEGs across these two species, we utilized the Alliance of Genome Resources database (<https://www.alliancegenome.org/>) and found that among 261 p53-upregulated DEGs in zebrafish, 245 have one or multiple mouse orthologues which correspond to 283 mouse genes (Fig. 5C, Table. S5). Interestingly, based in manual analysis in some cases the mouse paralogue but not orthologue of some zebrafish DEGs are upregulated by p53. For example, *sesn1*, *sesn3* and *sesn4* (si:zfos-80g12.1) were amongst the top upregulated DEGs in zebrafish, however only *Sesn2* was significantly induced in mice (Fig. S5). Therefore, to analyze the conservation more comprehensively, we also defined 1,778 paralogues of these 283 mouse orthologues (Fig. 5C, Table. S6) and examined whether these ortholog/paralogs are p53-induced genes in mice. Among them 222 are p53-upregulated in mice which correspond to 132 zebrafish DEGs (Fig. 5C, Tables. S7,S8). This represents the 132 conserved p53-unregulated genes in both zebrafish and mouse that potentially providing p53 tumor suppressing activity. From this dataset we have made several unique observations: 1) 31 conserved zebrafish DEGs only possess p53-upregulated mouse orthologues, such as *phlda3*, *atf3*, *tp53inp1* and *mdm2*. 2) 22 conserved zebrafish DEGs have both induced orthologues and paralogues by p53 in mice, e.g., *ptp4a3a* is p53-induced genes in zebrafish and correspond to three upregulated genes *Ptp4a3* (orthologue gene), *Ptp4a1* and *Ptpdc1* by p53 in mice. These 53 gene can be defined by conservation analysis even without going through paralogues. 3) 79 conserved DEGs are with one or multiple p53-upregulated paralogues, but not the orthologue in mouse. For example, with zebrafish p53-dependent *isg20* gene, the mouse paralogue *Aen* (29.33% sequence similarity) was induced but not the orthologue *Isg20*.

Fischer et al found AEN is a p53-upregulated target gene shown in 11 of 16 human genome-wide datasets [32]. Importantly in the absence of the inclusion of mouse paralogues we would not identify these 79 DEGs as conserved, which may include important p53-mediated genes. We are also curious about the expression of the zebrafish orthologues for these p53 induced mouse paralogues. All of zebrafish orthologues were non-DEGs regulated by p53 except one gene *Txnip*. The zebrafish orthologue *Txnipa* was just below the FC cutoff (Fold change=1.48 and q-value=1.37E-14).

Furthermore, GO analysis on these 132 conserved p53-regulated DEGs defined multiple significant biological process and KEGG pathways with cell cycle and cell proliferation being near the top (Fig. 6A). To further expand our time-course analysis, we collected *pnp*^{-/-} 30Gy treated versus untreated zebrafish embryos at 2 hpi (Fig. 6B), Hierarchical clustering accurately depicted the change of gene expression at 1, 2 and 3 hpi (Fig. 6B) and grouped these 132 conserved gene candidates into two main clusters. 1) Cluster I: the expression level of the genes in the cluster labeled with orange sidebar increased from 1 to 3 hpi; and 2) Cluster II: the expression level of the genes in the cluster labeled with green sidebar significantly increased initially but then dropped (Fig. 6B). To further investigate the dynamics of gene expression, we divided them into eight sub-clusters (Fig. S6). Cluster I consist of six sub-clusters (Fig. S6A) and Cluster II have two-subclusters (Fig. S6B). For example, the expression level of the genes, such as *tp53inp1*, *fbxw7* and *foxo3b*, gradually increased across time after IR; the expression level of the genes, such as *atf3*, *ddit4* and *sesn1*, significantly increased before 1 hpi, kept relatively flat 1-2 hpi, then dramatically increased 2-3 hpi; and the expression level of the genes,

including *ccng1*, *rb12*, *rps271* and others, slightly increased before 3 hpi but dramatically rise at 3 hpi (Fig. S6A).

We next defined 24 of the 132 DEGs that were either identified by gene ontology terms (Fig. 6A), or manually curated based on literature to be related to regulation of cell cycle or proliferation. Many of these 24 p53-induced genes also participate in different downstream effector processes beyond cell cycle regulation (Fig. 6C); e.g., *gadd45aa* is involved in p53 signaling pathway, regulation of cell cycle, FoxO signaling pathways, apoptotic process, MAPK signaling pathways and mitotic cell cycle. These 24 genes were labeled on the heatmap on Figure 5B, and their mRNA expression level are continuously increased across time and fall into the Cluster I (Fig. 5C) and sub-clusters No.1-6 (Fig. S6A).

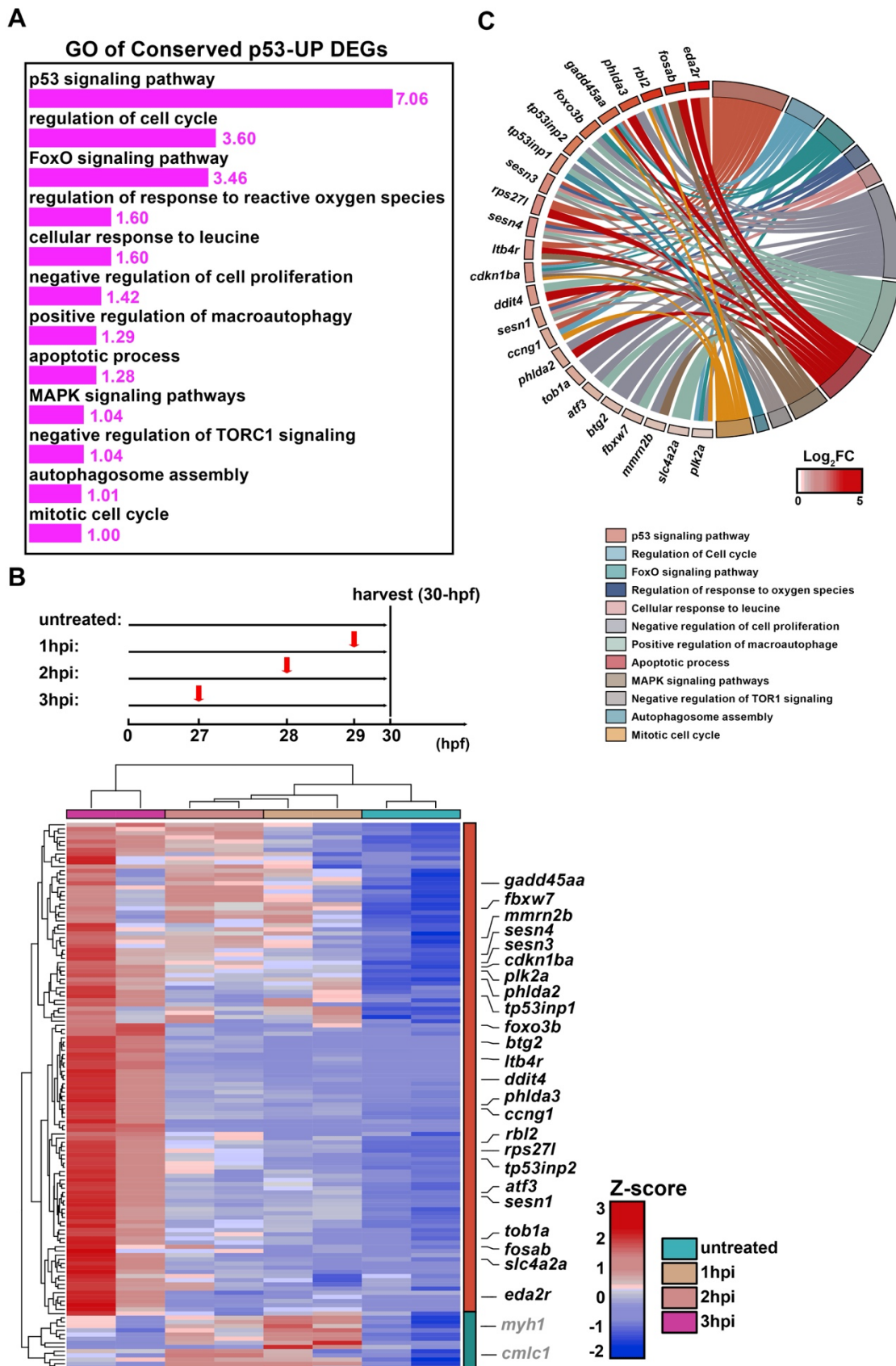


Figure 6. The functional enrichment analysis for conserved p53-induced genes in zebrafish and mouse. A. The histogram showing top significantly enriched GO terms. The $-\log_{10}$ (q-value) of each term was pointed out. B. Heatmap showing transcriptional changes for 132 conserved genes after IR-irradiation. Experimental workflow about how to harvest samples shown in top panel. Colored bars represent different experimental groups. All 132 genes were clustered into two groups (orange and green sidebar). Representative genes in each cluster were pointed out. 24 genes of interest (GOIs) were labeled in black word. C. The chord diagram of TOP significantly enriched GO terms including biological processes and KEGG pathways. The left semicircle represents the 24 GOIs and the right shows these GO terms.

Investigating 24 GOIs in *mpnp*-null induced cell-cycle arrest

We next aimed to examine the importance of these 24 genes of interest (GOIs) with regard to the *mpnp*^{-/-} cell-cycle arrest. This system provides multiple advantages: 1) the activation of p53 is in the absence of extensive stresses; 2) embryo lethality is in a p53-dependent manner; and 3) *mdm2*-null induced cell-cycle arrest is in a p53-dependent manner as well. To further define which of these conserved p53 target genes are involved in the *mdm2*-null induced cell cycle arrest and/or embryonic lethality, we analyzed bulk RNA-seq data between *mpnp*^{-/-} and its sibling controls (called *mpnp*^{+/+}) at 18 hpf. 18 hpf is the earliest time point we can distinguish *mpnp*^{-/-} from *mpnp*^{+/+} embryos by morphological differences. We defined 2,582 upregulated (DEGs) in *mpnp*^{-/-} versus *mpnp*^{+/+} group (Fig. 7A, Table. S9). This large number of DEGs includes p53-direct targets but also contain many secondary and downstream induced genes which are the

consequence of using morphology to define *mdm2*-null animals many hours after molecular changes (cell cycle defects were observed at 12hpf). Amongst the 132 conserved p53-dependent IR-induced DEGs, 108 were also in the DEGs *mpnp*^{-/-} versus *mpnp*^{+/+} at 18 hpf. The 24 GOIs are contained in the overlapped 108 DEGs.

We next performed RNA-seq analysis on pools (N≈30-35) of un-genotyped progeny from *mdm2*^{+/-}; *puma*^{-/-}; *noxa*^{-/-}; *p21*^{-/-} intercrosses at 8, 10, 12, 14, 16 hpf (Fig. 7B). While this generated a dilution of the RNA transcripts since ¾ of embryos are not *mpnp*^{-/-}, we were able to glimpse at the dynamics of p53 target gene induction in *mpnp*^{-/-} animals. We first used average normalized counts (without consideration of dilution effects) to generate heatmap for overlapped 108 genes across time (Figs. 7B). Eight clusters were defined, and Clusters 3 and 4 were the major ones. For Cluster 3, the expression level of the genes, such as *foxo3b*, *gadd45aa* and *rbl2*, gradually increased across time. For Cluster 4, the expression level of the genes, such as *sesn1*, *tp53inp1* and *cdkn1ba* smoothly grew from 8 to 14 hpf but dramatically rise at 16 hpf (Fig. 7B). Next, we generated plots for the individual 24 GOI (Figs. 7C,S7) to identify the fold change of the genes across time. We used an equation to compensate for the dilution and to more accurately monitor the changes in gene expression, and the equation is based on two conditions: one is that ¼ embryos in mutant samples are *mpnp*^{-/-} embryos; the other one is that the expression level of the genes in *mdm2*^{+/-}; *puma*^{-/-}; *noxa*^{-/-}; *p21*^{-/-} (referred as to *mpnp*^{+/-}) and in *mdm2*^{+/-}; *puma*^{-/-}; *noxa*^{-/-}; *p21*^{-/-} (referred as to *mpnp*^{+/+}) equals to that in *pnp*^{-/-}. While the trend for many of these genes are unique, as a generalization they all continue to increase expression from 8 hpf into 16 hpf timepoints (Figs. 7C&S7), well before the morphological differences. Most importantly, the induction of these 24 genes is early (the fold change reached or passed 2

before 12 hpf), suggesting they may influence cell-cycle arrest in the *mpnp*^{-/-} embryos as well.

We have previously demonstrated the use of CRISPR/Cas9 F0 “crispant” analysis to rapidly define genes responsible for ciliopathies in zebrafish [33]. To test whether this technique can be applied to rescue *mdm2*-null embryonic lethality, we first assessed if the crispants in which p53 is targeted could rescue *mdm2*-null phenotypes. Cas9 protein co-injected with a four p53 specific guides (p53 crispants) into *mdm2*-null embryos rescued the lethal phenotype (Fig. S8A). Approximately 25% of injected *mdm2* null embryos were morphologically normal-looking similar to zygotic wildtype or *mdm2*^{-/-}; *p53*^{-/-} embryos at 24 hpf. The rest of the injected embryos were significantly rescued with some minor deformities that can be distinguished under the microscope (Fig. S8A). We next stained for mitotic cells in p53 crispants and un-injected embryos with pH3 antibody (Fig. S8B) at 21 hpf. We observed that p53-injected F0 crispants did not undergo cell-cycle arrest, similar to the un-injected wildtype embryos (18 pH3-expressing cells in un-injected *mdm2*^{-/-} versus 263 in p53-injected *mdm2*^{-/-} and 266 in p53-injected *mdm2*^{+/+} sibling controls). To help define the level of rescue of cell-cycle arrest, we introduced a concept, Rescue/resistance Ratio (RR), that is the percentage of the average number of pH3-expressing cells in mutant embryos versus that in their sibling controls. A RR value closer to 100 represents a more complete rescue of cell cycle arrest. We calculated RR for p53-injected group and the value equals to 99.21, suggesting complete rescues of cell-cycle arrest in *mdm2*^{-/-} embryos. Together these data suggest that four-guide injected CRISPR/Cas9 crispants can be used to rescue the cell-cycle arrest and/or lethal phenotype associated with *mdm2* loss.

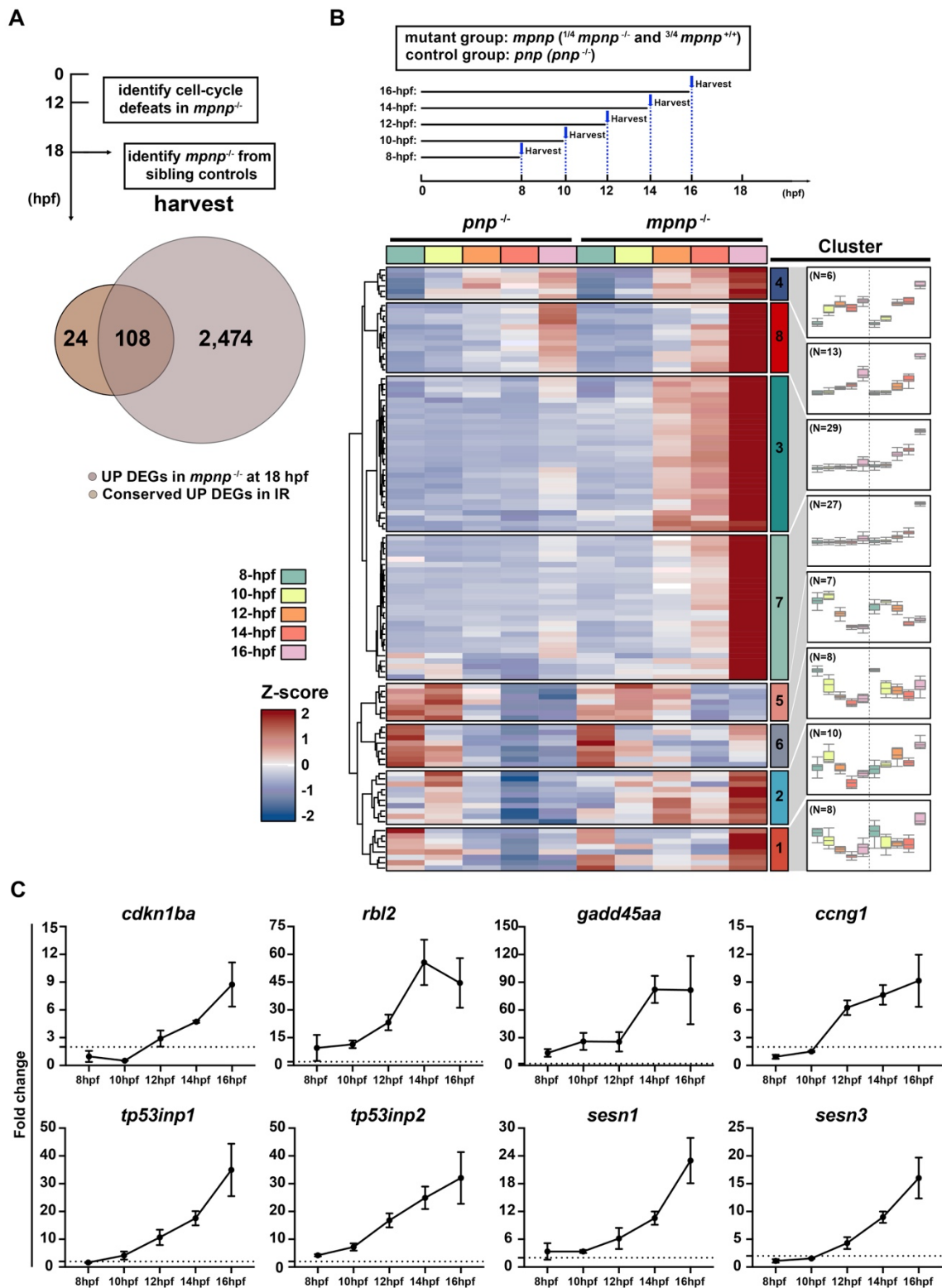


Figure 7. Comparing 132 conserved genes with DEGs in *mpnp*^{-/-} datasets. A. Venn graph displaying the overlapping genes between upregulated (UP) DEGs in *mpnp*^{-/-} versus sibling controls (*mpnp*^{+/+}) and conserved UP DEGs in both zebrafish and mouse with IR-irradiation. Experimental timeline showing the timepoint that distinguish *mpnp*^{-/-} embryos from sibling controls and how to harvest RNA samples at the time (Top panel). B. Heatmap showing transcriptional changes for 108 overlapped genes over time in early *mpnp*^{-/-} datasets (8, 10, 12, 14 and 16 hpf). Each timepoint was measured in duplicate. The experimental workflow about how to harvest samples shown in top panel. Note mutant samples in each timepoint are four-time diluted by their sibling controls ($\frac{1}{4}$ *mpnp*^{-/-} and $\frac{3}{4}$ sibling controls). Genes behaving similarly over time were clustered together and broken into eight groups. Gene trend and size for each cluster were shown on right panel. C. Line graphs showing the kinetics of 8 of 24 GOIs in early *mpnp* datasets. Line graphs for the rest 16 of 24 GOIs are in Figure S7.

fbxw7, foxo3b, and ccng1 partially rescue p53-dependent cell cycle arrest

With the success of the pilot crispant experiments, we next investigated if injection of a four-guide cocktails against any one of the 24 selected p53-induced genes would rescue the morphological abnormality in the *mpnp*^{-/-} embryos. None of the 24 GOIs crispants rescued the embryonic lethality of the *mpnp*^{-/-} embryos (Fig. S9). We next tested if any of the 24 GOI crispants would alter the number of pH3 positive cells in the *mpnp*^{-/-} embryos. Amongst them only *fbxw7*, *foxo3b*, and *ccng1* increased the number of pH3 positive cells (from the control 18 pH3 positive cells to 53, 40, and 41 respectively; Fig. 8). Representative images for injected embryos of each gene were present in Figure S10, and Rescue/resistance ratio (RR) were ranked to show the effect of these genes on cell-cycle arrest (Fig. S11). Note, *si:dkey-204l11.1* (corresponding to mouse *Eda2r* or *Tnfrsf19* gene, regarded as *eda2r* in figures), *fosab*, *tob1a* and *slc4a2a* had less pH3⁺ cells when compared to uninjected controls, suggesting these genes may play an important role during development in *mpnp*^{-/-} background (Fig. 8B). Interesting, more developed embryos in which the eye has begun to form, and more somites exist were observed in the *mnrn2b*- and *tp53inp1*-guides injected, suggesting they may play a role in the lethality independent of the cell-cycle defeat (Fig. S10).

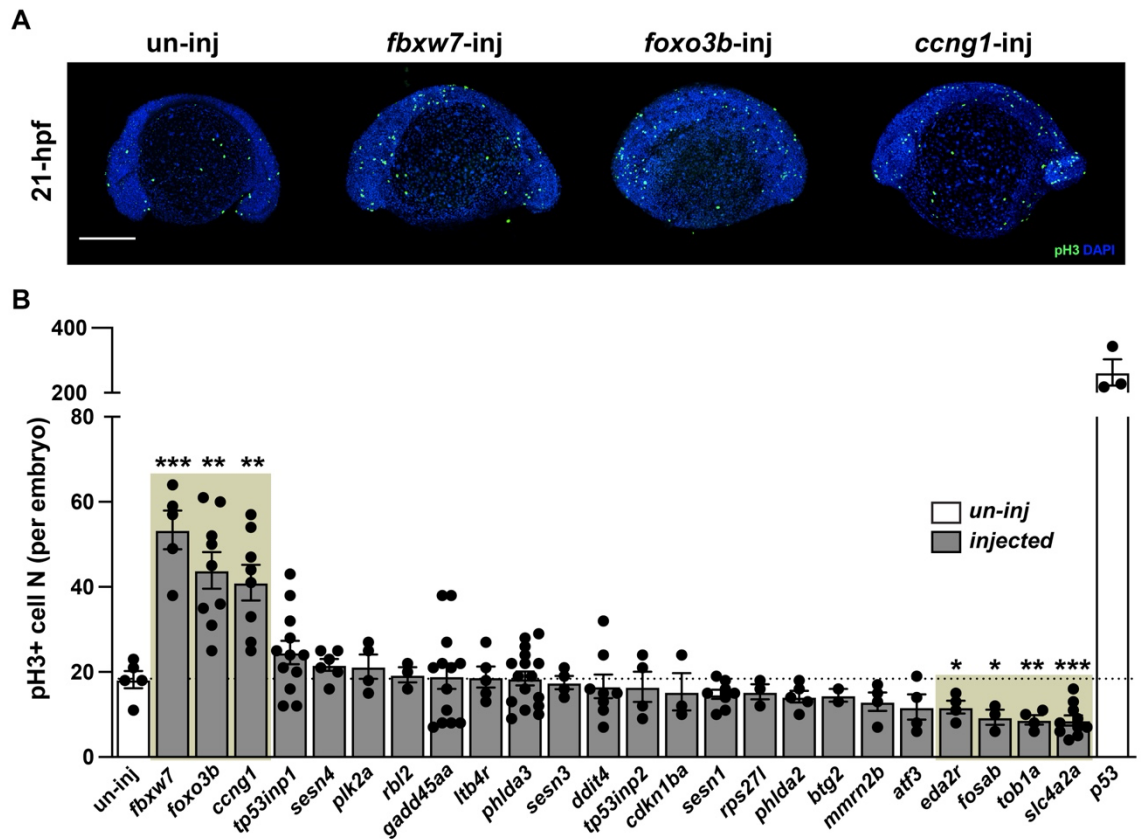


Figure 8. *fbxw7*, *foxo3b* and *ccng1* G0 crispants partially rescued *mnpn*-null induced cell-cycle arrest. A. Representative images showing pH3-stained un-injected (control, un-inj) and injected embryos at 21 hpf. Scale bar: 500 μ M. B. Quantification of pH3 positive cells in injected *mnpn*^{-/-} G0 chimera for 24 GOIs. un-inj group (negative control); p53 (positive control). Each dot represents an individual. Bars represent mean \pm SEM. *, $p < 0.05$. **, $p < 0.01$. ***, $p < 0.001$.

DISCUSSION:

p53 tumor suppression is highly conserved across species. Consistent with the observation in mice [26], we showed that zebrafish deficient for puma, noxa and p21 do not form spontaneous tumors, suggesting that p53-mediated apoptosis and cell-cycle arrest may be dispensable for tumor prevention, and more importantly, other p53 downstream biological processes may be critical. However, an important caveat is that in the mouse studies the ablation of p53-mediated cell-cycle arrest was only examined in several types of cells, such as MEF and thymocytes [26, 34, 35], but not in the whole organism. Therefore, it remains unclear whether p53-dependent cell-cycle arrest is truly absent in multiple cell types or tissues in the *pnp*^{-/-} mouse. To address this, we took advantage of transparent zebrafish embryos to visualize apoptosis and cell-cycle arrest throughout the whole organism. We demonstrate that puma and noxa are essential mediators in p53-mediated apoptosis and *puma*^{-/-}; *noxa*^{-/-}; *p21*^{-/-} zebrafish are resistant to apoptosis in a p53-dependent manner. However, through whole-embryo pH3 staining, we found *p21* loss does not disable p53-mediated cell-cycle arrest. This does not exclude the importance of other effector pathways but emphasizes further understanding of p53 cell-cycle arrests are needed.

The only relevant metric to determine which genes and effector pathways are involved in tumor suppression, is to look at how a gene affects tumor formation in vivo [26]. In this regard, the idea is to ablate the p53 target gene and monitor the tumor cohort. If the ablation renders tumor formation equivalent to p53 loss, then the underlying process is crucial for p53 tumor suppression. If not, it is viewed as being unnecessary or there are redundancies. However, these experiments can require 2-3 years to investigate a single gene, requiring a large space to maintain the animals. To reduce experimental time

associated with true tumor cohort analysis, we took advantages of our *mpnp*^{-/-} zebrafish which is morphological lethality with cell-cycle defeats that are both p53-dependent. In our opinion this is an ideal model for studying p53 tumor suppression in that there is no true oncogenic or stress signal, but mis-regulation of p53 to induce transcription and effector pathways. The lethality occurs due to systemic tumor suppressive effects and therefore emulates how p53 prevents tumor initiation/progression. Undoubtedly, there are several limitations in our *mpnp*^{-/-} models. Kon et al, generated p53-5KR mice that form early-onset spontaneous tumors [42]. But the kinetics of tumor formation is still slower than p53-null mice, suggesting p53-5KR mice still possessed some tumor-suppressive function. However, the embryonic lethality is fully rescue in *p53*^{5KR/5KR}; *mdm2*^{-/-} mice. The data indicates there are slight differences between p53 tumor suppression and its activity to rescue *mdm2*^{-/-} during embryogenesis. While *ccng1*, *fbxw7* and *foxo3b* partially rescued cell-cycle defeats, but none of them rescued morphological abnormality, suggesting the rescue of *mpnp*^{-/-} induced lethality may be required multiple p53 downstream targets and effector pathways involved (not only the ones in cell-cycle regulation).

While numerous human and mouse gene expression datasets were generated to define thousands of p53 direct target genes, many of these analyses are not in agreement. One concern is that these sequencing data were acquired with a few limited in-vitro cell lines, lacking the diversity of cell or tissue types. To further define other p53 targets, especially those functioning in the regulation of cell cycle, we performed a cross-species comparative transcriptional analysis, and identified 132 conserved p53-upregulated transcripts between zebrafish and mice. There are several merits in our approach: 1) We utilized *puma*^{-/-}; *noxa*^{-/-}; *p21*^{-/-} zebrafish, which help exclude many (~72%) of secondary

and tertiary targets in response to p53 activation. 2) We studied DEGs induced only 1- and 3-hours post IR, conducive to p53 early responsive genes and not secondary transcripts. 3) We analyzed both mouse orthologues and paralogues of zebrafish p53-upregulated DEGs which prevent omission of important target genes (79 of the 132). 4) Our analysis used whole mouse or zebrafish embryos which includes cellular complexity of tissues and normal physiology of the organism.

With the *mpnp*^{-/-} model, we quantified pH3 staining results on 24 p53 regulated GOIs. Amongst them *fbxw7* (RR=19.21), *foxo3b* (RR=15.77), and *ccng1* (RR=16.18) showed an increase in the number of pH3 positive cells. FBXW7 is part of E3 ubiquitin ligase complex that results in proteasome-mediated degradation of different cell cycle related molecules, including cyclin E and KLF5. This suggests that p53 controls the cell cycle through FBXW7 mediated degradation of cell cycle regulators. The Forkhead box O3 (FOXO3) transcription factor is an important transcription regulator that modulates cell-cycle arrest, cell death, DNA repair, autophagy, aging and longevity [36-39]. Toward cell cycle control FOXO3 induces certain cell-cycle related molecules, such as CDKN1A/p21, CDKN1B/p21, and Gadd45, which are involved in DNA repair and cell cycle checkpoints activation in response to DNA damage. In addition, Cyclin G1, encoded by CCNG1, is one of the earliest p53 targets to be identified. Previous studies demonstrate that cyclin G1 plays an important role in the cell cycle machinery and are involved in the activation of cyclin-dependent kinases (CDKs) that control cell progression through different phases of the cell cycle. However, since the mouse KO and MEFs did not display a cell cycle defect little attention has been given to cyclin G1. While none of these genes provide a complete cell cycle rescue, the fact the three independent genes were identified

may argue all three plus p21 may have overlapping or compensatory role in p53-dependent cell-cycle arrest. It will be interesting to know if in the absence of these three genes in a *pnp^{-/-}* background will tumor onset be equivalent to the p53 nulls. While this experiment appears challenging (6 gene knockout), with the advantages of zebrafish genetics it is achievable.

Other p53 transcriptional targets have been reported in regulation of cell cycle, such as 14-3-3 σ , PCNA, PP2A, LATS2, BubR1 and GADD45 α [3]. The genes that encode 14-3-3 σ , PCNA, PP2A are not induced by p53 in both mice and zebrafish at 1 or 3 hpi (may be a late-responsive genes after IR-irradiation). The gene that encodes LATS2 is not induced by IR at 1 and 3 hpi but is at 6 hpi in zebrafish and upregulated by p53 in mice at 3 hpi as well. Therefore, this may be a late-responsive gene, or more likely secondary downstream transcript of the puma, noxa and p21 effector pathway. Bub1b encoding BubR1 is inhibited (not induced) by p53 in both species (likely a secondary indirect p53 target). The Gadd45 family encodes three genes GADD45a, GADD45b, and GADD45g, of which GADD45 α is a well-known p53 target gene, which has been shown to arrest cells in both G1/S and G2/M phase [10, 40, 41]. However, loss of *gadd45aa* did not increase the pH3⁺ cell numbers in *mpnp^{-/-}* embryos (RR=5.97), suggesting *gadd45aa* might not be the p53 downstream mediator in arresting cell cycle in *mpnp^{-/-}* embryos. However, our data indicates, unlike in mouse, in zebrafish *gadd45aa*, *gadd45bb* and *gadd45ga* are p53-upregulated genes leaving the possibility of redundancies in the *gadd45* family.

When comparing IR DEGs and *mpnp* DEGs we found the IR early-responsive genes are not represented in the *mpnp* data. For example, *myl7* and *myh7* are conserved p53-upregulated genes after IR-irradiation but they are undetected in our time-cross *mpnp^{-/-}*

^{-/-} data. Myl7 and myh7 encode myosin regulatory heavy chain proteins, primarily expressed in the heart, however mpnp^{-/-} data were harvest from 8 to 18 hpf, a timepoint when the heart is not formed. Suggesting they maybe tissue specific p53 regulated genes. Sec14l8 is induced in mpnp^{-/-} data detected as early as 8 hpf (Fold change= 6.31 and p-value= 3.32E-05) but not in IR data, again this might be attributed to the gene being involved in very early Wnt signaling and axis elongation. This emphasizes the importance of studying tissue specific differences that exist in the p53 network.

MATERIALS AND METHODS:

Zebrafish Lines and Maintenance:

All zebrafish work was performed in the Zebrafish Research Facility (ZRF) of the University of Alabama at Birmingham (UAB). Adult fish and embryos are maintained as described by Westerfield et al (1995) by the ZRF Animal Resources Program which maintains full American Association for Accreditation of Laboratory Animal Care (AAALAC) accreditation and is assured with the Office of Laboratory Animal Welfare (OLAW). All animal studies have UAB Institutional Animal Care and Use Committee (IACUC) approval. All knock-out alleles were generated and maintained on the AB strain.

Mouse Lines and Maintenance:

All mouse studies were conducted in compliance with the National Institutes of Health Guide for the Care and Use of Laboratory Animals and approved by the IACUC at UAB. The p53 KO allele was obtained from Jackson Labs (Strain #002101). The p53 allele was maintained on a C57BL6/J genetic background.

Generation and Validation of a New p21/cdkn1a Knockout Allele in Zebrafish:

Gene Knockouts were generated as described previously [43]. gRNA target sites were identified using the Zhang lab gRNA design tool (<http://crispr.mit.edu>). The target site and PAM motif were listed in figures S1. The procedures to prepare the gRNA and Cas9 mRNA for microinjection as described previously [14]. Approximately 1-2nl of nuclease mRNA (or sgRNA/Cas9 mRNA) were microinjected into the yolk of one-cell-stage zebrafish embryos. For indel efficiency evaluation, genomic DNA was extracted from ~24 3-5 dpf injected F0 embryos and evaluated with HRM curve (see below). The remaining embryos (F0s) from the examined clutches were raised. Multiple out of frame alleles were identified in F1 progeny. The $\Delta 2$ allele was sequenced by the UAB Heflin Center for Genomic Sciences Sanger Sequencing Core and maintained and propagated. To “cleanup” genetic background F1s were breed at least two generations to the wildtype strain AB.

Genotyping with High Resolution Melt Analysis (HRMs):

Adult genomic DNA were isolate as described[33]. Genomic DNA from stained zebrafish embryos were incubated at 55°C 2h in 30 μ l ELB (10mM Tris pH 8.3, 50mM KCl, 0.3% Tween 20, 0.3% NP40, 1mg/ml Proteinase K); then incubated at 95°C for 15 min to inactivate Proteinase K and store at 4°C. PCR reactions were performed as described [33].

Establishing Tumor Cohorts:

Our tumor cohorts were derived by natural breeding of a single set of parents (one male and one female). The cohort size (N number) was indicated in figure legends. At 4 months of age, all fish were separated into 4 tanks of 24 fish each. Adult fish were screened weekly or biweekly for tumors and/or missing/dead fish. Fish that were identified by eye

to be tumor burdened were euthanized according to IACUC protocols. Kaplan-Meier analysis was performed using GraphPad Prism 9 software.

Ionizing Radiation Irradiation:

Zebrafish Embryos or Mouse female with E9.5-stage embryos were placed at the closest position to the source of ionizing radiation (IR)-irradiation in a X-RAD 320 X-ray irradiator to expose the embryos to approximate 4-5 Gy/min. 30Gy IR-irradiation were given.

Whole-Mount Immunohistochemistry:

Embryos were fixed in 4% paraformaldehyde (PFA) overnight at 4°C. Dehydrate and rehydrate with series of methanol solution (PBST, 25%, 50%, 75% and 100% methanol in PBST for dehydration and reverse order for rehydration) is necessary for pH3 staining on embryos older than 24 hpf. Next, embryos were permeabilized for at least 2h in methanol (for anti-active Caspase-3 staining) or for 7 min in acetone (for anti-pH3 staining). After 1h blocking, embryos were incubated in primary antibody overnight at 4°C. Anti-active Caspase-3 antibody (BD, 559565) was used at a dilution of 1:500 and anti-pH3 primary antibody (Cell Signaling, 9701) at 1:200. For anti-active Caspase-3 staining, 1h blocking is necessary before adding secondary antibody. For secondary antibody, the Alexa 488 goat anti-rabbit secondary antibody was used and at a dilution of 1:200 for 2h at room temperature or overnight at 4°C. Subsequently, embryos were washed and stained in 4',6-diamidino-2-phenylindole (DAPI) for 10 min (if nucleus measurement necessary) prior to imaging.

Light, Immunofluorescence and Confocal Imaging:

Embryos were dechorionated at described stages with incubation in 0.03% pronase (Sigma P5147) for 6 min and anesthetized using 0.4% tricaine. In a 60 x 15 mm Falcon petri dish (light and immunofluorescence imaging) and glass-coverslip-bottomed dish (confocal imaging), embryos are mounted in 1% low melting agarose if needed. Images with anti-active Caspase-3 staining were taken on a SMZ-18 Zoom Stereo Microscope with at the same magnification, laser power, exposure time and gain. Images with anti-pH3 staining in Figure 3 were taken on a Nikon A1 inverted confocal microscope and approximate 100- μ m Z-stacks at 3.5- μ m intervals were obtained. Images with anti-pH3 staining in other figures were taken on Nikon AX-R Confocal Microscope and whole embryos were scanned with variable Z-stacks. Same laser power and gain for GFP channel was set up for quantification. After each embryo was imaged, embryos that did not know the genotype were removed from the agarose to generate genomic DNA for genotyping. Further figure processing and analysis was performed using Nikon NIS Element and ImageJ.

Quantification of pH3-positive Cells and Rescue/resistant Ratio Calculation:

Image J was used to quantify pH3-expressing cells in each embryo. “Freehand selections” Tool is applied to circle the shape of the embryo body without yolk. Quantification of mitotically active cells was performed by counting the number of pH3-stained cells inside the circled area in individuals. Each dot in the plots represents each individual embryo. All animals were harvested from at least two independent experiments.

Fluorescence Quantification and Statistical Analysis:

GraphPad Prism 9 was used in generation of all graphs and statistical tests. For the quantification, overall statistical significance was calculated using an unpaired t-test with

error bars indicating SEM. Numbers of embryos and significance values are indicated in the figure legends.

Bulk RNA Sequencing and Analysis:

RNA samples were prepared with Qiagen RNeasy Plus Mini Kit. RNA library was prepared with Illumina RNA with PolyA selection package and sequenced with Illumina HiSeq 2x150bp, single index by Genewiz, or 2x75bp, single index by UAB Heflin Center for Genomic Core. Raw sequencing reads were aligned with to *Danio rerio* GRCz11 or *Mus musculus* GRCm39. Differentially expressed genes (DEGs) were calculated with DESeq2 (the cutoff for DEGs was indicated in each figure) in R. The gene expression was quantified via RSEM with the default setting and the normalized count was used to generate heatmaps with pheatmap and Mfuzz in R. Gene ontology analysis were performed with DAVID Bioinformatics Resources 6.8 [44] and were plotted with GOplot in R. For early *mpnp*^{-/-} datasets, mutant samples were un-genotyped, including ¼ *mpnp*^{-/-}, ½ *mpnp*^{+/-} and ¼ *mpnp*^{+/+} embryos in theory. To compensate for the effects of dilution at early timepoint, we generated an equation to calculate fold change. It is based on that the expression level of the genes in *mpnp*^{+/-} and in *mpnp*^{+/+} equals to that in *pnnp*^{-/-} in Figure 7C & Supplementary Figure S7.

$$\text{Fold change} = \frac{(4 * (\text{count}^{mpnp} - \text{count}^{pnnp}) + \text{count}^{pnnp})}{\text{count}^{pnnp}}$$

Cas9 Ribonucleoprotein (RNP) Preparation and Microinjection for G0 Knockouts Screening:

Alt-R crRNA were designed with Integrated DNA technologies (IDT) predesigned CRISPR-Cas9 guide RNA tool (https://www.idtdna.com/site/order/designtool/index/CRISPR_PREDESIGN). Alt-R CRISPR-Cas9 crRNA, tracrRNA (IDT, 1072532) and Alt-R S.p. Cas9 Nuclease V3 (IDT, 1081058) was prepared following manufacturer's instruction. Detailed procedures for RNA complex preparation were performed as described[33]. Final concentration of each guide is 1.5 μ M. Microinjection was performed by injecting \sim 1nL of RNP complex into the yolk of 1-cell stage embryos. RNP complex was freshly prepared and left on ice until microinjection[45]. IDT crRNA used for multiple guide RNA injections are listed in Table S3.

Identification of Cleavage Efficiency of G0 Crispants with NGS:

DNA was extracted from 5-dpf F1 progeny generated by two pairs of p53-injected $mdm2^{-/-}$ parents (one male and one female in each breeder) with proteinase K (details above). $mdm2^{-/-}$ embryos were selected for the following step through HRM curves. 1ul genomic DNA was used to obtain the HRM curve. For PCR amplicon, 1ul of genomic DNA from each $mdm2^{-/-}$ sample was amplified with HS PhusionTM High-Fidelity DNA polymerase (ThermoFisher Scientific, F530S) for each cleavage site. PCR cycling conditions are 98°C for 30 sec, followed by 25 cycles of 98 °C for 10 sec, 60 °C for 30 sec, 72 °C for 15 sec, and then followed by 72 °C for 10 min. The products of all first round PCR reactions were then gel purified. We used 25 ng of the purified PCR products for sample indexing in preparation for next-generation sequencing (NGS) using Illumina TruSeq indexing primers. PCR cycling conditions are 98°C for 30 sec, then 8 cycles of 98°C for 10 sec, 60°C for 30 sec, 72 °C for 15 sec, and followed by 72°C for 10 min. The

final PCR products were gel purified and run on the Illumina MiSeq platform using 2 × 150bp paired end reads. For each mutant sample, the percentage of NGS reads containing wild-type or mutant sequences were analyzed using Cas-Analyze.

ACKNOWLEDGEMENTS:

The authors would like to acknowledge the members of the Parant lab for technical help and critical reading of the manuscript. We use the following core facilities: UAB Zebrafish Research Facility, UAB Heflin Center for Genomic Science, UAB High Resolution Imaging Facility.

AUTHOR CONTRIBUTIONS:

HRT generated zebrafish mutants, determined Mendelian inheritance, and validated alleles. JW monitored tumor cohorts. JW and RGT performed cleavage-caspase 3 staining and imaging. JW and ZL performed pH3 staining, imaging and quantification. JW, ZL and KF performed bulk-RNA sequencing and analysis. JW and YM performed the CRISPR G0 screen and phenotypic analysis. JW, with consultation from JMP, made all figures and performed statistical analysis. JMP and JW wrote the manuscript with revision by all authors.

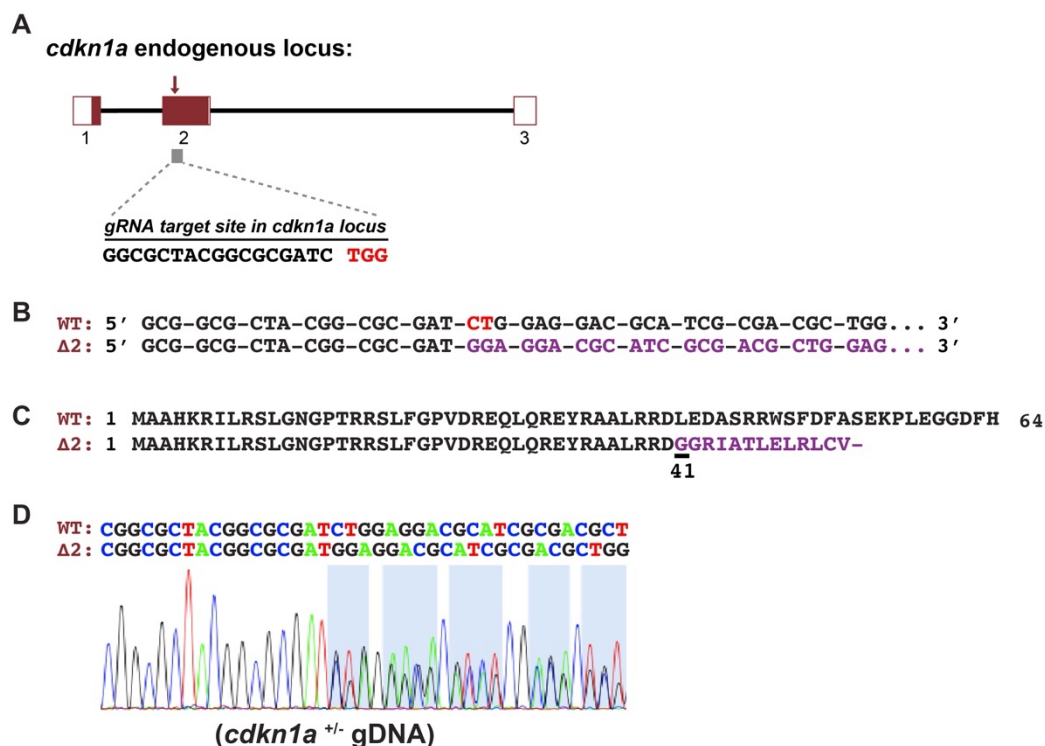


Figure S1. Generation and validation of a stable *cdkn1a/p21* mutant in zebrafish. A.

Diagram of the target site in zebrafish *cdkn1a* endogenous locus, gRNA target site in exon 2 of the *cdkn1a* gene (red arrow), PAM motif (red) and gRNA sequence shown. The propagated out-of-frame allele has a deletion of 2bp ($\Delta 2$) resulting in a truncated *p21* protein (mentioned as *p21*^{-/-}). **B.** Sequence alignment between *cdkn1a* wildtype (WT) and stable mutant ($\Delta 2$). The two nucleotides (CT) deleted are red-color labelled and purple indicates the out-of-frame nucleotides. **C.** The wild-type and truncated p21 protein sequence. Purple indicates the out-of-frame amino acid sequence in mutant allele and '-' indicates stop codon. **D.** Genomic DNA (gRNA) sequence of *cdkn1ba* from the heterozygous (+/-) adult zebrafish tail. The homozygous null zebrafish are viable and fertile.

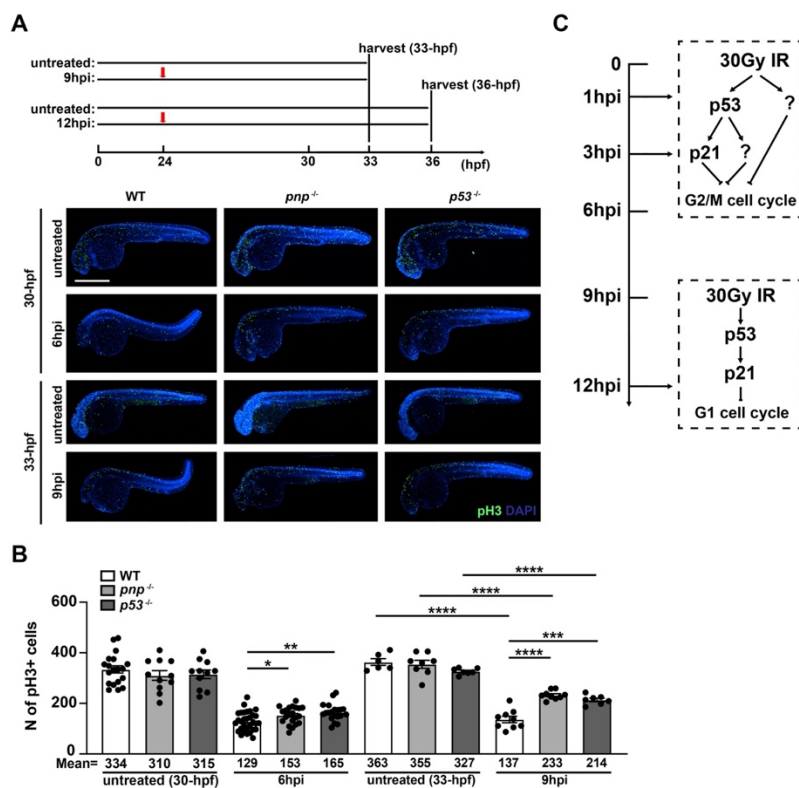


Figure S2. IR-induced cell-cycle arrest at 6 and 9 hpi. **A.** pH3 staining on 30- and 33-hpf zebrafish embryos 6- and 9-hours post 30Gy IR respectively. Experimental workflow for IR-irradiation at 9 hpi and 12 hpi (for Figure 2) was shown in top panel. 24-hpf wildtype, *pnp*^{-/-} and *p53*^{-/-} zebrafish embryos were treated with 30Gy IR-irradiation and fixed embryos 9 and 12 hours later. Scale bar: 500μM. **B.** Quantification of pH3 positive cells in treated and untreated WT, *pnp*^{-/-} and *p53*^{-/-} embryos at 6 and 9 hpi. Each dot represents an individual. Average values (Avg.) were indicated in each group. Bars represent mean ± SEM. *, $p < 0.05$. **, $p < 0.01$ ***, $p < 0.001$.****, $p < 0.0001$. **C.** A diagram showing conceptual pathways of IR-induced cell-cycle arrest across time. Other genes downstream *p53* and/or cooperating with *p53* respond to G2/M cell-cycle arrest at early time points after IR-irradiation. *p53*-mediated *p21* contributes G1 cell cycle arrest at late time point.

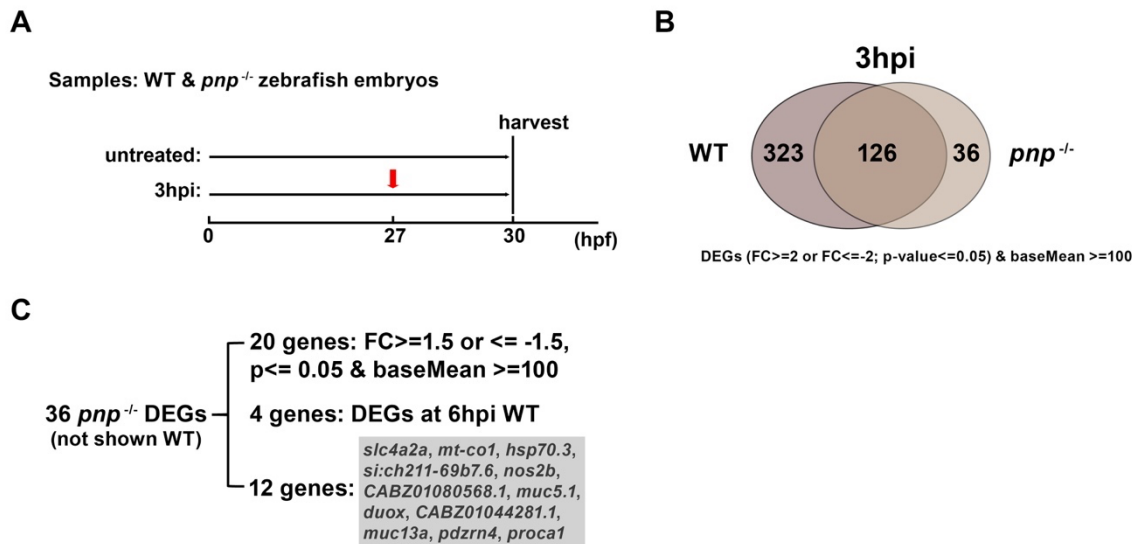


Figure S3. Loss of *puma*, *nox*a and *p21* getting rid of their downstream p53 indirectly regulated differentially expressed genes (DEGs). **A.** Experimental workflow about how to harvest whole-embryo RNA samples from each group. **B.** Venn graph showing DEGs between WT and *pnp*^{-/-} at 3 hpi. The cut-off is fold change >=2 or <=-2; p <=0.05 and baseMean >= 100. **C.** Detailed classification chart of 36 DEGs only shown in *pnp*^{-/-} but not in WT.

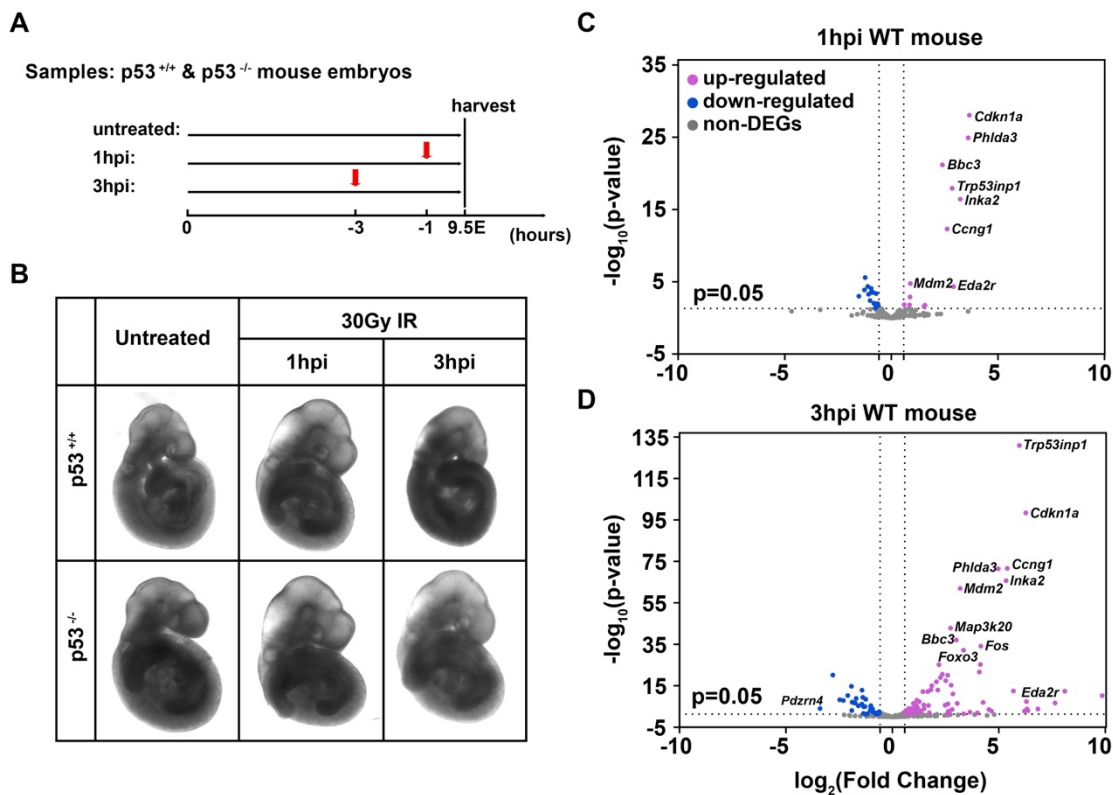


Figure S4. Transcriptional analysis on IR-treated mouse embryos. **A.** Experimental workflow showing how to harvest whole-embryo RNA samples from each mouse group. Treated and untreated mouse embryos were harvested at E9.5 and 30Gy IR-irradiation were done 1 or 3 hours before harvest (1 or 3 hpi). **B.** Representative gross images showing mouse embryos were homogenized to extract total RNA. Volcano plots showing WT mouse embryos with the treated versus untreated at 1 hpi (**Figure C**) and 3 hpi (**Figure D**). The cutoff was set as fold change ≥ 2 or ≤ -2 and p value ≤ 0.05 . Upregulated DEGs were color-labelled with magenta and the down-regulated DEGs labelled with blue. The gene symbol of some TOP DEGs was indicated on the plot.

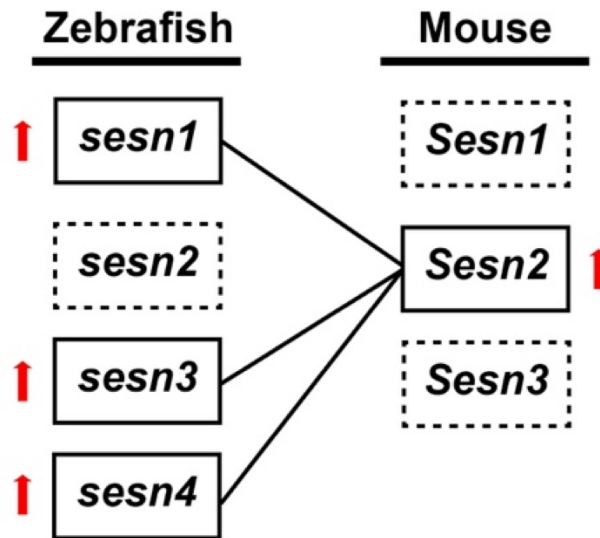


Figure S5. One example of not orthologue but paralogues of zebrafish DEGs upregulated in mice. Sestrins family proteins in zebrafish and mouse. Solid square and red arrow pointed out the genes were upregulated by p53 in zebrafish or mouse after IR-irradiation.

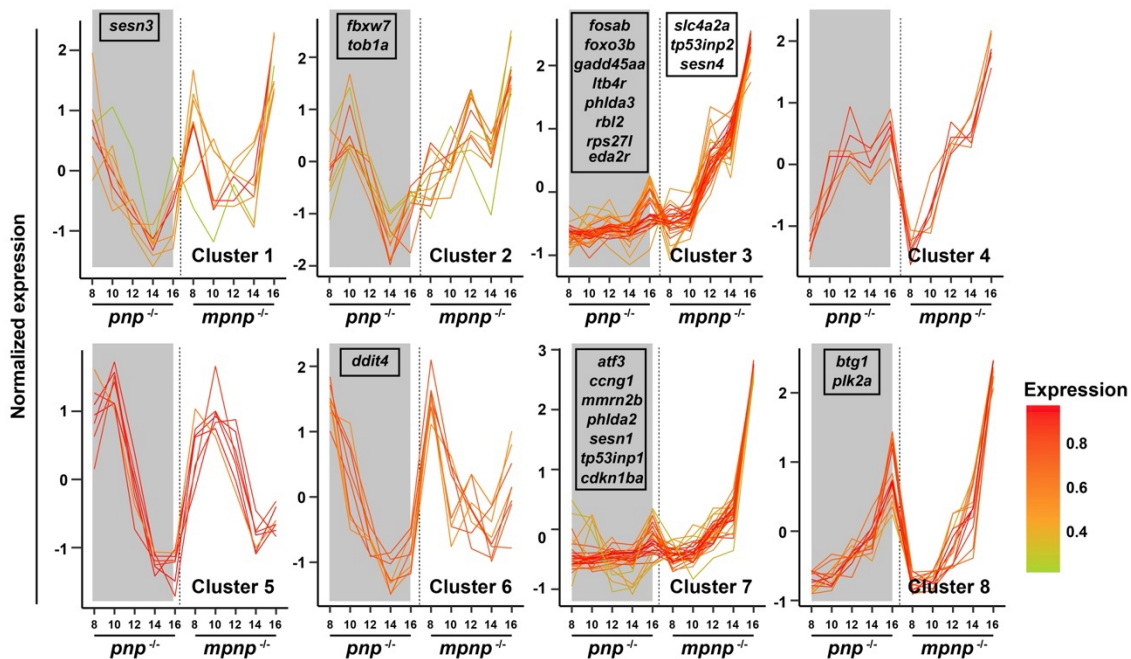


Figure S7. Line graphs showing the kinetics for 108 overlapped p53-upregulated genes from 8 to 16 hpf in MPNP and PNP group. All of them were clustered into eight groups. 24 GOIs were indicated in each plot. Grey rectangle masked the changes in PNP dataset, not p53-dependent, related to development.

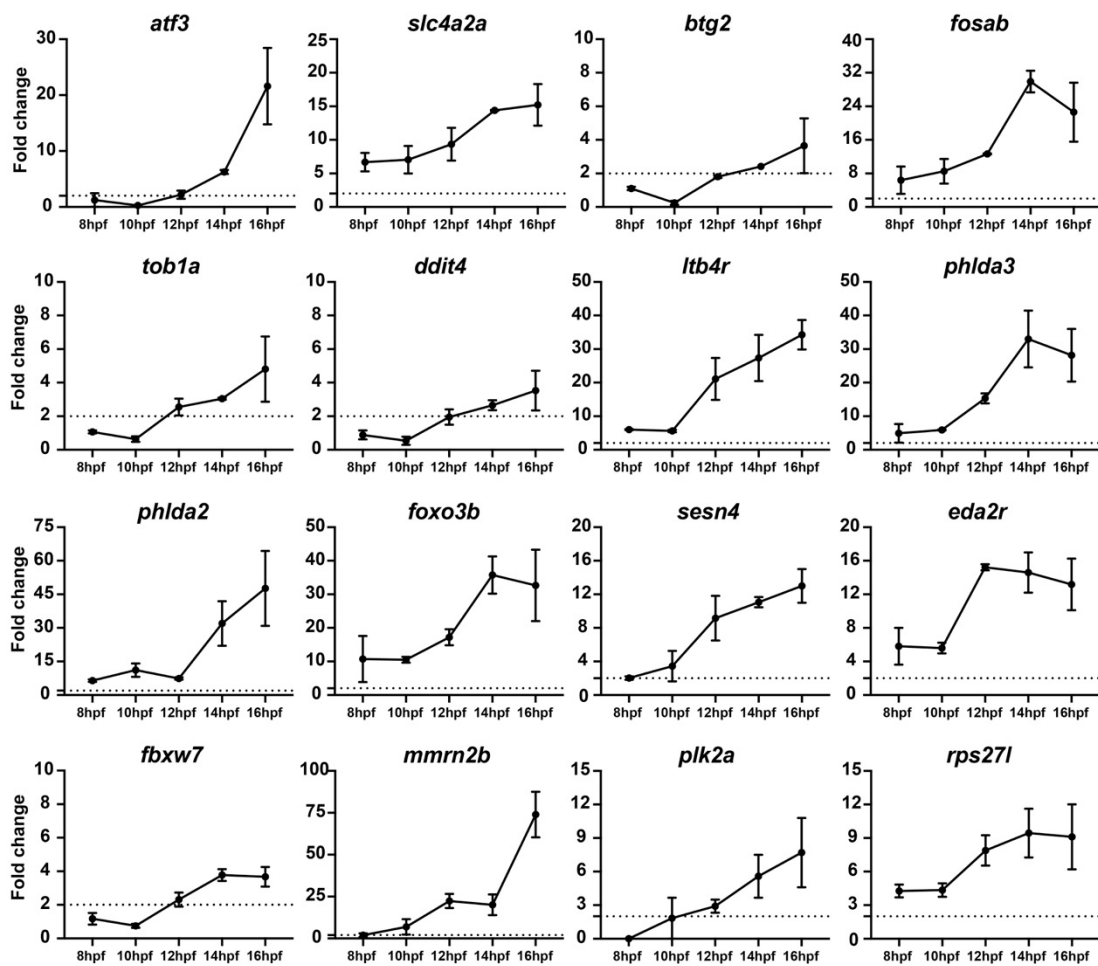


Figure S8. Line graphs showing the kinetics of the rest 24 GOs in MPNP datasets.

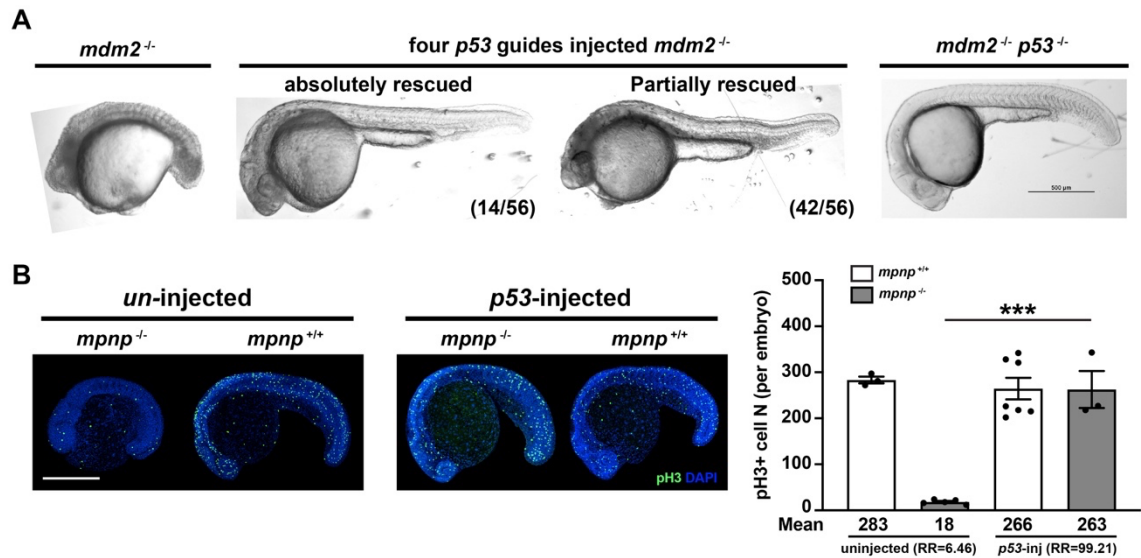


Figure S9. Recapitulation of Null phenotypes in G0 embryos by four-guide targeting p53. **A.** Lateral view images of 1-dpf zygotic wildtype, *mdm2*^{-/-}; *p53*^{-/-} embryos and p53 *mdm2*^{-/-} G0 chimera (partially rescue, right; completely rescue, left). The number of complete and partially rescued embryos was indicated. Scale bar: 500 μ M. **B.** Representative images showing pH3-stained un-injected (control, un-inj) and p53-injected G0 chimera at 21 hpf. Scale bar: 500 μ M. **B.** Quantification of pH3 positive cells in un-injected and p53-injected G0 chimera for *mpnp*^{-/-} and sibling controls. Each dot represents an individual. Bars represent mean \pm SEM. ***, $p < 0.001$. Rescue/resistance ratio (RR) and the average of pH3+ cell for each group were pointed out.

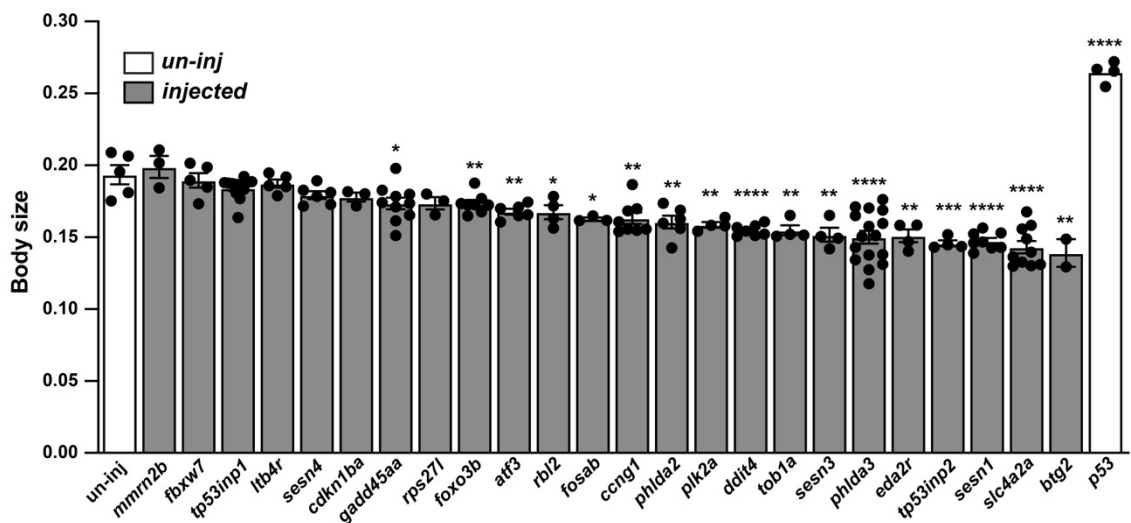


Figure S10. None crispants of 24 GOIs rescue morphological abnormality for *mpnp*^{-/-} embryos. Quantification of body size for each injected *mpnp*^{-/-} embryos. un-inj group (negative control); p53 (positive control). Each dot represents an individual. Bars represent mean \pm SEM. *, $p < 0.05$. **, $p < 0.01$. ***, $p < 0.001$. ****, $p < 0.0001$.

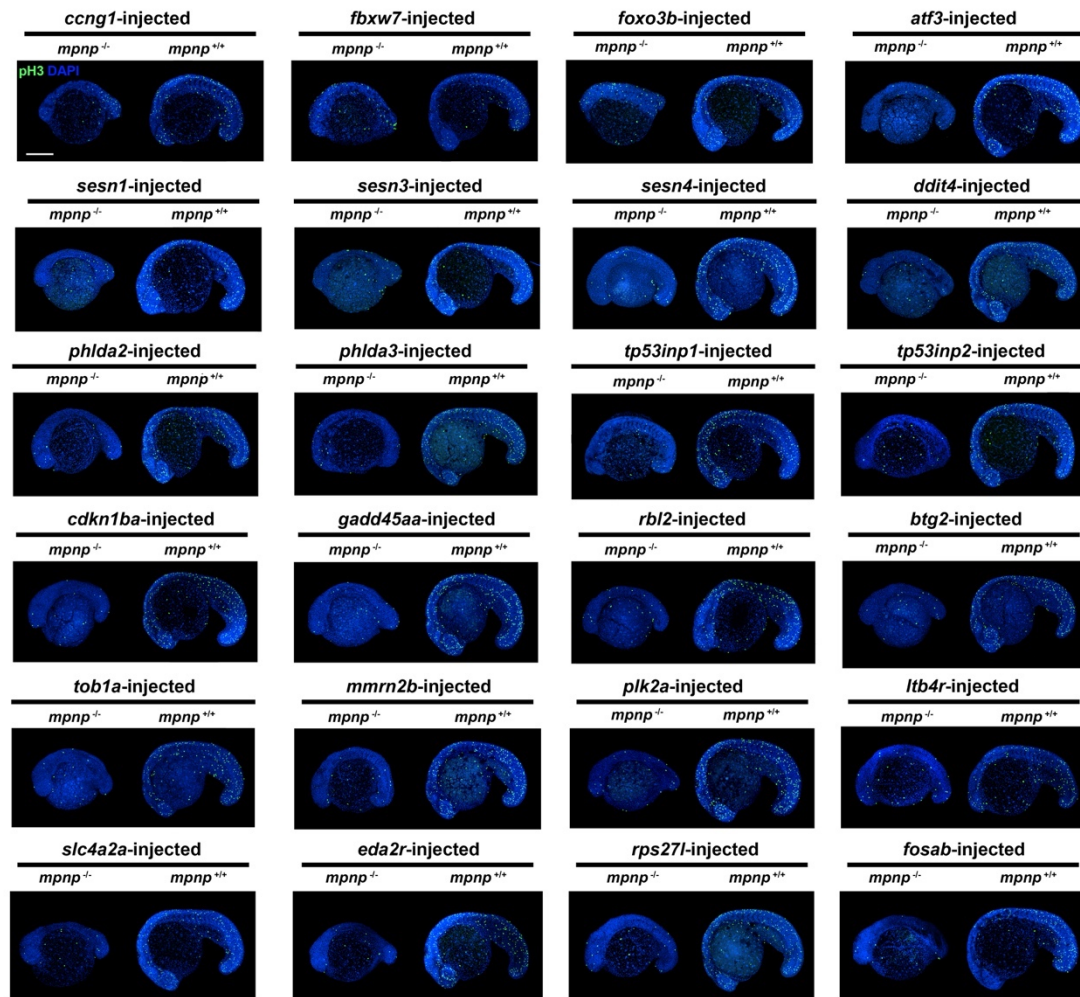


Figure S11. Representative pH3-stained images for injected *mpnp*^{-/-} and sibling controls for all 24 GOIs. Scale bar: 500 μM.

$$RR = \frac{\text{Average N of pH3+ cells in mutant embryos}}{\text{Average N of pH3+ cells in control embryos}} \times 100\%$$

Group	RR
<i>fbxw7</i>	19.21
<i>ccng1</i>	16.18
<i>foxo3b</i>	15.77
<i>plk2a</i>	12.71
<i>tp53inp1</i>	9.53
<i>sesn4</i>	7.32
<i>phlda3</i>	7.09
<i>ltb4r</i>	6.99
<i>rbl2</i>	6.78
<i>phlda2</i>	6.24
<i>sesn3</i>	6.07
<i>gadd45aa</i>	5.97
<i>cdkn1ba</i>	5.96
<i>ddit4</i>	5.79
<i>tp53inp2</i>	5.74
<i>atf3</i>	5.42
<i>rps27l</i>	5.35
<i>btg2</i>	5.22
<i>sesn1</i>	5.21
<i>mvrn2b</i>	5.00
<i>eda2r</i>	4.22
<i>fosab</i>	3.53
<i>tob1a</i>	3.50
<i>slc4a2a</i>	2.98

Figure S12. Rescue/resistance ratio (RR) for all 24 GOIs. The formula to define RR on the top panel.

REFERENCES:

1. Bailey, M.H., et al., Comprehensive Characterization of Cancer Driver Genes and Mutations. *Cell*, 2018. 174(4): p. 1034-1035.
2. Donehower, L.A., et al., Integrated Analysis of TP53 Gene and Pathway Alterations in The Cancer Genome Atlas. *Cell Rep*, 2019. 28(11): p. 3010.
3. Kasthuber, E.R. and S.W. Lowe, Putting p53 in Context. *Cell*, 2017. 170(6): p. 1062-1078.
4. Schneider, K., et al., Li-Fraumeni Syndrome, in *GeneReviews*((R)), M.P. Adam, et al., Editors. 1993: Seattle (WA).
5. Chompret, A., et al., P53 germline mutations in childhood cancers and cancer risk for carrier individuals. *Br J Cancer*, 2000. 82(12): p. 1932-7.
6. Kleihues, P., et al., Tumors associated with p53 germline mutations: a synopsis of 91 families. *Am J Pathol*, 1997. 150(1): p. 1-13.
7. Varley, J.M., D.G. Evans, and J.M. Birch, Li-Fraumeni syndrome--a molecular and clinical review. *Br J Cancer*, 1997. 76(1): p. 1-14.
8. Varley, J.M., et al., Germ-line mutations of TP53 in Li-Fraumeni families: an extended study of 39 families. *Cancer Res*, 1997. 57(15): p. 3245-52.
9. Varley, J.M., Germline TP53 mutations and Li-Fraumeni syndrome. *Hum Mutat*, 2003. 21(3): p. 313-20.
10. Donehower, L.A., et al., Mice deficient for p53 are developmentally normal but susceptible to spontaneous tumours. *Nature*, 1992. 356(6366): p. 215-21.
11. Donehower, L.A., The p53-deficient mouse: a model for basic and applied cancer studies. *Semin Cancer Biol*, 1996. 7(5): p. 269-78.

12. Berghmans, S., et al., tp53 mutant zebrafish develop malignant peripheral nerve sheath tumors. *Proc Natl Acad Sci U S A*, 2005. 102(2): p. 407-12.
13. Parant, J.M., et al., Genetic modeling of Li-Fraumeni syndrome in zebrafish. *Dis Model Mech*, 2010. 3(1-2): p. 45-56.
14. Wang, J., et al., Puma, noxa, p53, and p63 differentially mediate stress pathway induced apoptosis. *Cell Death Dis*, 2021. 12(7): p. 659.
15. van Boxtel, R., et al., Homozygous and heterozygous p53 knockout rats develop metastasizing sarcomas with high frequency. *Am J Pathol*, 2011. 179(4): p. 1616-22.
16. Goessling, W., T.E. North, and L.I. Zon, New waves of discovery: modeling cancer in zebrafish. *J Clin Oncol*, 2007. 25(17): p. 2473-9.
17. Feitsma, H. and E. Cuppen, Zebrafish as a cancer model. *Mol Cancer Res*, 2008. 6(5): p. 685-94.
18. White, R., K. Rose, and L. Zon, Zebrafish cancer: the state of the art and the path forward. *Nat Rev Cancer*, 2013. 13(9): p. 624-36.
19. Haupt, Y., et al., Mdm2 promotes the rapid degradation of p53. *Nature*, 1997. 387(6630): p. 296-9.
20. Honda, R., H. Tanaka, and H. Yasuda, Oncoprotein MDM2 is a ubiquitin ligase E3 for tumor suppressor p53. *FEBS Lett*, 1997. 420(1): p. 25-7.
21. Kubbutat, M.H., S.N. Jones, and K.H. Vousden, Regulation of p53 stability by Mdm2. *Nature*, 1997. 387(6630): p. 299-303.
22. Shieh, S.Y., et al., DNA damage-induced phosphorylation of p53 alleviates inhibition by MDM2. *Cell*, 1997. 91(3): p. 325-34.

23. Kaiser, A.M. and L.D. Attardi, Deconstructing networks of p53-mediated tumor suppression in vivo. *Cell Death & Differentiation*, 2017. 25(1): p. 93-103.
24. Williams, A.B. and B. Schumacher, p53 in the DNA-Damage-Repair Process. *Cold Spring Harb Perspect Med*, 2016. 6(5).
25. Sammons, M.A., et al., Tumor suppressor p53: from engaging DNA to target gene regulation. *Nucleic Acids Res*, 2020. 48(16): p. 8848-8869.
26. Valente, L.J., et al., p53 efficiently suppresses tumor development in the complete absence of its cell-cycle inhibitory and proapoptotic effectors p21, Puma, and Noxa. *Cell Rep*, 2013. 3(5): p. 1339-45.
27. Chua, J.S., et al., Tumor-specific signaling to p53 is mimicked by Mdm2 inactivation in zebrafish: insights from mdm2 and mdm4 mutant zebrafish. *Oncogene*, 2015. 34(48): p. 5933-41.
28. Montes de Oca Luna, R., D.S. Wagner, and G. Lozano, Rescue of early embryonic lethality in mdm2-deficient mice by deletion of p53. *Nature*, 1995. 378(6553): p. 203-6.
29. Jones, S.N., et al., Rescue of embryonic lethality in Mdm2-deficient mice by absence of p53. *Nature*, 1995. 378(6553): p. 206-8.
30. Langheinrich, U., et al., Zebrafish as a model organism for the identification and characterization of drugs and genes affecting p53 signaling. *Curr Biol*, 2002. 12(23): p. 2023-8.
31. Lowe, S.W., et al., p53 is required for radiation-induced apoptosis in mouse thymocytes. *Nature*, 1993. 362(6423): p. 847-9.

32. Fischer, M., Census and evaluation of p53 target genes. *Oncogene*, 2017. 36(28): p. 3943-3956.
33. Wang, J., et al., Variable phenotypes and penetrance between and within different zebrafish ciliary transition zone mutants. *Dis Model Mech*, 2022. 15(12).
34. Li, T., et al., Tumor suppression in the absence of p53-mediated cell-cycle arrest, apoptosis, and senescence. *Cell*, 2012. 149(6): p. 1269-83.
35. Brady, C.A., et al., Distinct p53 transcriptional programs dictate acute DNA-damage responses and tumor suppression. *Cell*, 2011. 145(4): p. 571-83.
36. Alvarez, B., et al., Forkhead transcription factors contribute to execution of the mitotic programme in mammals. *Nature*, 2001. 413(6857): p. 744-7.
37. Tran, H., et al., DNA repair pathway stimulated by the forkhead transcription factor FOXO3a through the Gadd45 protein. *Science*, 2002. 296(5567): p. 530-4.
38. Furukawa-Hibi, Y., et al., FOXO transcription factors in cell-cycle regulation and the response to oxidative stress. *Antioxid Redox Signal*, 2005. 7(5-6): p. 752-60.
39. Flachsbart, F., et al., Association of FOXO3A variation with human longevity confirmed in German centenarians. *Proc Natl Acad Sci U S A*, 2009. 106(8): p. 2700-5.
40. Kastan, M.B., et al., A mammalian cell cycle checkpoint pathway utilizing p53 and GADD45 is defective in ataxia-telangiectasia. *Cell*, 1992. 71(4): p. 587-97.
41. Jin, S., et al., GADD45-induced cell cycle G2-M arrest associates with altered subcellular distribution of cyclin B1 and is independent of p38 kinase activity. *Oncogene*, 2002. 21(57): p. 8696-704.

42. Kon, N., et al., mTOR inhibition acts as an unexpected checkpoint in p53-mediated tumor suppression. *Genes Dev*, 2021. 35(1-2): p. 59-64.
43. Thomas, H.R., et al., High-throughput genome editing and phenotyping facilitated by high resolution melting curve analysis. *PLoS One*, 2014. 9(12): p. e114632.
44. Sherman, B.T., et al., DAVID: a web server for functional enrichment analysis and functional annotation of gene lists (2021 update). *Nucleic Acids Res*, 2022. 50(W1): p. W216-W221.
45. Wu, R.S., et al., A Rapid Method for Directed Gene Knockout for Screening in G0 Zebrafish. *Dev Cell*, 2018. 46(1): p. 112-125 e4.

CHAPTER 4

REDUCED SISTER CHROMATID COHESION ACTS AS
A TUMOR PENETRANCE MODIFIER

by

JUN WANG, HOLLY R. THOMAS, YU CHEN, STEFANIE M. PERCIVAL,
STEPHANIE C. WALDREP, RYNE C. RAMAKER, SARA J. COOPER,
ZECHEN CHONG, JOHN M. PARANT*PLOS Genetics*Wang, J., Thomas, H. R., Chen, Y. et al. Reduced sister chromatid cohesion acts as a
tumor penetrance modifier. *PLoS genetics*, 18(8), e1010341 (2022).
<https://doi.org/10.1371/journal.pgen.1010341>Copyright
2022
by
PLOS

Used by permission

Format adapted for dissertation

ABSTRACT

Sister chromatid cohesion (SCC) is an important process in chromosome segregation. ESCO2 is essential for establishment of SCC and is often deleted/alterd in human cancers. We demonstrate that *esco2* haploinsufficiency results in reduced SCC and accelerates the timing of tumor onset in both zebrafish and mouse p53 heterozygous null models, but not in p53 homozygous mutant or wild-type animals. These data indicate that *esco2* haploinsufficiency accelerates tumor onset in a loss of heterozygosity (LOH) sensitive background. Analysis of The Cancer Genome Atlas (TCGA) confirmed ESCO2 deficient tumors have elevated number of LOH events throughout the genome. Further, we demonstrated heterozygous loss of *sgo1*, important in maintaining SCC, also results in reduced SCC and accelerated tumor formation in a p53 heterozygous background. Surprisingly, while we did observe elevated levels of chromosome missegregation and micronuclei formation in *esco2* heterozygous mutant animals, this chromosomal instability did not contribute to the accelerated tumor onset in a p53 heterozygous background. Interestingly, SCC also plays a role in homologous recombination, and we did observe elevated levels of mitotic recombination derived p53 LOH in tumors from *esco2* haploinsufficient animals; as well as elevated levels of mitotic recombination throughout the genome of human ESCO2 deficient tumors. Together these data suggest that reduced SCC contributes to accelerated tumor penetrance through elevated mitotic recombination.

Author Summary: Tumorigenesis often involves the inactivation of tumor suppressor genes. This often encompasses an inactivation mutation in one allele and loss of the other wild-type allele, referred to as loss of heterozygosity (LOH). The rate at which the cells lose the wild-type allele can influence the timing of tumor onset, and therefore an

indicator of a patient's risk of cancer. Factors that influence this process could be used as a predictive indicator of cancer risk, however these factors are still unclear. We demonstrate that partial impairment of sister chromatid cohesion (SCC), a fundamental component of the chromosome segregation in mitosis and homologous recombination repair, enhanced tumorigenesis. Our data suggest this is through elevated levels of mitotic recombination derived p53 LOH. This study emphasizes the importance of understanding how impaired SCC, mitotic recombination rates, and LOH rates influence cancer risk.

INTRODUCTION

Genomic alterations including missegregation, aneuploidy and micronuclei formation, are hallmarks of cancers and associated with poor patient outcomes(1). These genomic alterations often occur due to mitotic error; however mutational drivers of these genomic instabilities in tumors are unclear(2-4). Defects in microtubule attachment and spindle assembly checkpoint have been demonstrated to contribute to genomic instability and cancer predisposition(5, 6). Sister chromatid cohesion (SCC) is another essential process required for equal segregation of chromatids into daughter cells during mitosis and is a probable target for mutations that induce these genomic instabilities. At the core of mitotic SCC, is the cohesin ring, made up of a multiprotein complex that includes SMC1a, SMC3, RAD21, and SA1/2, which lasso the sister chromatids together. ESCO2 establishes SCC around the sister chromatids as they are synthesized during S-phase, whereas Sororin and SGOL1 protect the established SCC until mitosis(7, 8). During metaphase of mitosis the microtubule tension on the kinetochore aligns the sister chromatid into a metaphase plate. During the transition from metaphase to anaphase, the cohesin ring is cleaved by

Separase, allowing equal segregation of the sister chromatids to each daughter cell. While SCC is most well-studied with regard to chromosome segregation, it also influences several other biological processes, including DNA repair/homologous recombination(9-13). The involvement of compromised SCC in cancer has been less well studied since complete loss of SCC triggers cell cycle arrest, apoptosis and/or cellular senescence, which is not conducive to cellular viability, and therefore viewed as disadvantageous to a tumor(14). Further, mild SCC dysfunction is also suggested to be toxic to the cell due to the need for centromeric cohesion to establish bi-orientation of kinetochores(15). Hence, SCC is considered an all or none process regarding cellular viability. That said, missense mutations in some components of the SCC have been identified in human tumors, however the mechanistic importance of these mutations remains unknown(16, 17).

Li Fraumeni Syndrome (LFS) is an autosomal dominant cancer predisposition syndrome, due to germline heterozygous mutations in p53, in which 50% of patients will succumb to a tumor by age 30(18). Part of the etiology of tumor formation in LFS, as well as sporadic tumors, is that the first allele has a p53 mutation, and the second undergoes loss of wild-type allele (Loss Of Heterozygosity, LOH) often through whole chromosome deletion/duplication or mitotic recombination(19). Mouse and zebrafish heterozygous p53 null models have recapitulated this early tumor susceptibility, as well as the LOH of the wild-type allele in tumors (20-24). Further, murine LFS models suggest that within a cohort of p53 heterozygous animals the timing of tumor onset correlates with the prevalence of p53 LOH in tumors(25); i.e. the trend is that early-onset tumors often have p53 LOH while late tumors often do not. This suggests that the rate of p53 LOH or prevalence of LOH events influences tumor penetrance. Further, the frequency of tumors with p53 LOH in p53

heterozygous null mice is strain-dependent, in that p53 LOH in a mixed C57/129 strain is ~50%, while in a BALB/c background it is ~96%, suggesting there are undefined genetic factors that can impact the rate of p53 LOH. Note tumor onset was earlier in the BALB/c mice, and the overall higher frequency of mitotic recombination, suggesting difference in DNA repair influence the frequency of p53 LOH and timing of tumor onset(26). While not explicitly examined with respect to p53 LOH, inactivation of RecQ helicases, such as WRN or BLM, have been shown to increase the rate of mitotic recombination and therefore act as a LOH modifier(27-29).

Our data indicate that reduced SCC, resulting from haploinsufficient loss of *esco2* or *sgo1*, can be tolerated at an organismal level; but leads to accelerated tumor onset in a *p53* heterozygous null LOH sensitive background. Further, the reduced SCC contributes to low-level chromosomal instability in somatic tissues. However, it is elevated mitotic recombination, not chromosomal instability, derived LOH that drives early tumor formation in the *p53* heterozygous null background. TCGA analysis of human cancer corroborates these findings.

RESULTS

ESCO2 is frequently deleted/altered in a variety of cancer types.

We surveyed The Cancer Genome Atlas (TCGA) database for prevalence of genetic alterations in key sister chromatid cohesion (SCC) factors and found that ESCO2 was most frequently deleted or mutated gene in many cancers (**Figure 1A**). Further patients with ESCO2 alterations have significantly lower probabilities of survival (**Figure 1B**). We observed that approximately 5-8% of patients within nine of the most common cancers

show alterations in ESCO2 and that these alterations are predominantly deletions and a few protein-altering mutations (**Figure 1C**). The deletions are defined as at least 50% reduction of gene copy number, suggesting that ESCO2 may be a haploinsufficient tumor suppressor gene. However, ESCO2 resides on chromosome 8p21, and in many human cancers, including liver, breast, prostate, ovarian, uterine, colorectal, bladder and lung cancers, recurrent deletion of genes on the p arm of chromosome 8 is observed (**Figure 1D & 1E**). This recurring deletion has been associated with advanced tumor progression and poor patient survival(30-32). This region appears rich in tumor suppressor genes(33). For example, in breast cancer, genes between 8p21-23 represent five of the top ten most deleted genes(34). Within this region, there are established tumor suppressors (DLC1, DOK2 and LZTS1), as well as potential tumor suppressor genes (CSMD1, MTUS1, and MSR1), and many other genes not established in cancers(35-40). Some of these genes, including ESCO2, may be passengers, deleted purely based on their proximity to tumor suppressors, while others may represent novel genes with a role in cancer formation and progression. ESCO2 is important for the establishment of SCC following new synthesis of the sister strand during S-phase of the cell cycle (7). ESCO2 has not previously been implicated in human cancers, but its function certainly suggests it could be important, and it appears to be at one of the sub-peaks of this deletion region (**Figure 1D, 1E & S1**). In further support of ESCO2 playing a role in tumorigenesis, some Roberts Syndrome patients (RBS) who carry autosomal recessive germline inactivating mutations in ESCO2, display early-onset cancer predisposition(41-43).

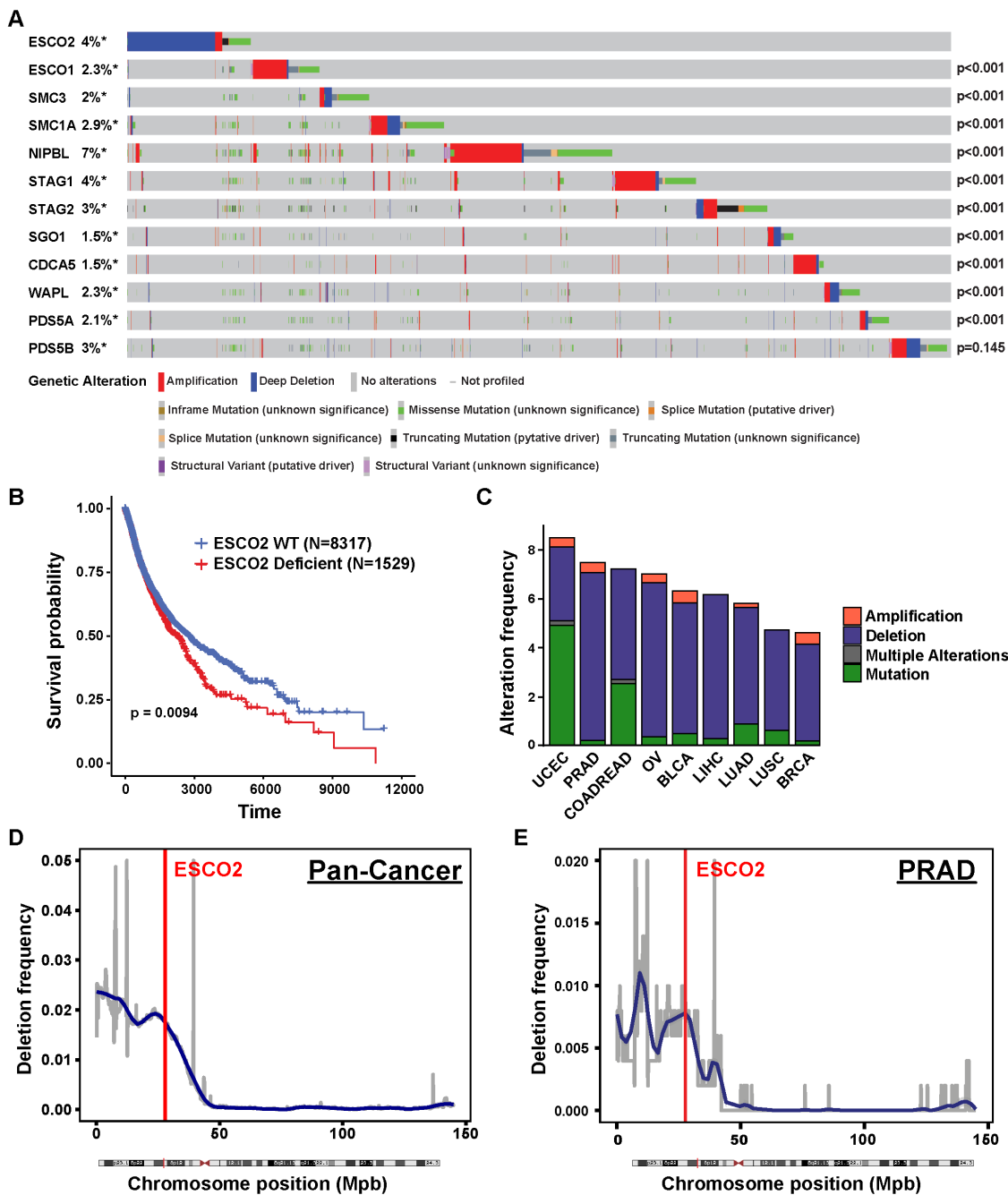


Figure 1. Esco2 deficiencies are common in multiple tumor types and associated with poor patient survival. (A) Oncoprint plot of genetic alterations in ESCO2 and other SCC-associated genes in TCGA dataset. N=10950. Number of samples with each mutation: $N_{(ESCO2)}=404$, $N_{(ESCO1)}=252$, $N_{(SMC3)}=216$, $N_{(SMC1A)}=322$, $N_{(NIPBL)}=743$, $N_{(STAG1)}=429$, $N_{(STAG2)}=374$, $N_{(SGO1)}=165$, $N_{(CDCA5)}=159$, $N_{(WAPL)}=248$, $N_{(PDS5A)}=227$ and $N_{(PDS5B)}=375$. P-values shown in the figure indicate significance of co-occurrence with ESCO2 from one-sided Fisher Exact test. (B) Kaplan-Meier survival analysis of patients with ESCO2 deficient (N=1529) versus ESCO2 WT (N=8317) tumors within TCGA dataset samples. P-value was determined by log-rank test. (C) Stacked bar plot indicating the percentage of patients with an ESCO2 deletion (blue), amplification (red) or mutation (green) and multiple alterations (grey) in uterine corpus endometrioid (UCEC), prostate (PRAD), colorectal (COADREAD), ovarian (OV), bladder (BLCA), liver (LIHC), lung adenocarcinoma (LUAD), lung squamous (LUSC), and breast cancer (BRCA) in the TCGA dataset. Cancer type is ordered based on the genetic alteration frequency. Number of samples with mutation/ total samples in each cancer type: 45/529 UCEC, 37/494 PRAD, 43/594 COADREAD, 41/584 OV, 26/411 BLCA, 23/372 LIHC, 33/566 LUAD, 23/487 LUSC, 50/1084 BRCA. The frequency of deletion in 100 kbp windows throughout Chromosome 8 in 1,111 pan-cancer type (Figure D, N=11203) and prostate adenocarcinoma (PRAD, Figure E, N=502) cancer patients. A region is considered as deleted if $\text{Log}^2(\text{Copy Number}/2) < -1$. Blue line shows smoothed deletion frequency. Red vertical line indicates the locus of ESCO2 gene.

ESCO2 deficiency results in accelerated tumor onset in LOH-sensitive animal models and elevated LOH in human tumors.

To decipher if ESCO2 loss is a driver of tumorigenesis, we wanted to determine if ESCO2-deficient animals are tumor predisposed. Both mouse and zebrafish homozygous ESCO2 null animals are embryonic lethal(44, 45), therefore to determine if reduction in ESCO2 specifically contributes to tumorigenesis, we generated and monitored tumor formation in cohorts (N=96/cohort) of *esco2*^{+/+} and *esco2*^{hi2865/+} (hi2865 allele is an intron 1 gene trap that results in >95% knockdown of transcript) zebrafish in a tumor sensitized *p53* mutant background, *p53*^{zy7/+} (*zy7* allele is a thymine to cytosine transition in codon 164 in the p53 DNA binding domain that results in the inability of DNA binding)(22, 44). Within all zebrafish tumor cohort studies to reduce the influence of background genetic variability, zebrafish cohorts to be compared, were generated from a single pair of zebrafish. Therefore, these two cohorts were generated from an *esco2*^{hi2865/+}; *p53*^{zy7/zy7} crossed to a wild-type AB strain zebrafish. We observed statistically significant acceleration of tumor onset (**Figure 2A**) in the *esco2* heterozygous mutant cohort (T₅₀=467 days in *esco2*^{hi2865/+}; *p53*^{zy7/+} cohort vs. 561 days in the *p53*^{zy7/+} cohort; p<0.0001 based on log-rank test) suggesting loss of *esco2* is a tumor driving event. However, these experiments were performed in a tumor-sensitized background and did not indicate if *esco2* haploinsufficiency acts as an autonomous tumor suppressor gene. Therefore, we also monitored cohorts of *esco2*^{+/+} and *esco2*^{hi2865/+} zebrafish in a *p53* wild-type background, derived from a single pair of *esco2*^{hi2865/+} crossed to wild-type AB. However, over a 2-year period only 2 of 96 *esco2*^{hi2865/+} animals developed a tumor compared to 0 of 96 wild-type animals (**Figure 2A**), suggesting that if *esco2* does act as an autonomous tumor suppressor

gene it has low penetrance. These data indicate that haploinsufficiency for *esco2* enhances tumorigenesis only in a p53 heterozygous background. Loss of the wild-type *p53* allele (loss of heterozygosity (LOH); $p53^{m/+} \rightarrow p53^m$ or m/m) is an important step during tumorigenesis in *p53* heterozygous mutant humans (Li Fraumeni Syndrome) and animals (zebrafish and mouse *p53* knockouts)(20, 22, 46-51); therefore we postulated that *esco2* heterozygosity may enhance tumor formation in a *p53* heterozygous animal by accelerating *p53* LOH. If true, *esco2* heterozygosity would not enhance tumor formation in a *p53* homozygous background (insensitive to *p53* LOH). Therefore, we monitored a cohort of $p53^{zy7/zy7}$ and $esco2^{hi2865/+}; p53^{zy7/zy7}$ zebrafish and found a non-significant difference in tumor enhancement in the $p53 p53^{zy7/zy7}; esco2^{hi2865/+}$ cohort compared to $p53^{zy7/zy7}$ cohorts created from single pair of $esco2^{hi2865/+}; p53^{zy7/zy7} \times p53^{zy7/zy7}$ (**Figure 2A**; T_{50} =330 days in the $esco2^{hi2865/+}; p53^{zy7/zy7}$ cohort vs. 320 days in the $p53^{zy7/zy7}$ cohort; $p = 0.526$ based on Log-rank test). This finding suggests that *esco2* heterozygosity influences tumor onset only in a LOH sensitive (*p53* heterozygous) background. To determine if these observations were also true in mice, we generated similar cohorts of mice using a *p53* null allele and a *Esco2* null allele (deletion of exon 4)(49, 52). The mouse cohort data is consistent with the zebrafish data, in that *Esco2* haploinsufficient loss accelerates tumor onset only in a LOH sensitive background (**Figure 2B**; T_{50} =516 days in the $Esco2^{+/-}; p53^{+/-}$ cohort vs. 563 days in the $p53^{+/-}$ cohort; $p=0.0377$ based on Log-rank test). To determine if a higher proportion of the *esco2* deficient derived zebrafish tumors have *p53* LOH, we genotyped paired normal and tumor genomic DNA for the *p53* allele. The percentage of tumors in the $p53^{zy7/+}$ cohort having LOH of the wild-type *p53* allele was 85%, while tumors from the $p53^{zy7/+}; esco2^{hi2865/+}$ cohort was ~92% (**Figure 2C**). While this is trending, it is a non-significant

change in the frequency of LOH-containing tumors. However, measuring LOH in a tumor which is the end-product of tumorigenesis may not reflect the process or rate of LOH in somatic precancerous tissues in these animals. We also determined that the *esco2* gene did not undergo LOH in any of these tumors, suggesting the phenotype is a consequence of a gene dose haploinsufficient state (**Figure 2C**). Further, we did not observe a change in tumor spectrum, in that 19 of 20 *p53^{zy7/+}* tumors were malignant peripheral nerve sheath tumors (MPNSTs), and 23 of 23 *p53^{zy7/+}; esco2^{hi2865/+}* tumors were also MPNSTs (**Figure 2C**). We also evaluated if there was a change in the physical location of the MPNSTs (Figure S2), but we did not observe a statistical difference between the populations. We did observe more undifferentiated sarcomas (Figure 2D) in the *Esco2^{+/-}; p53^{+/-}* mice cohort, however the timing of this tumor type was not statistically different suggesting this is not the driving force for the accelerated tumor onset. Evaluation of human tumors in the TCGA dataset, indicates that there is statistically significant increase in p53 LOH in Liver hepatocellular carcinoma (LIHC), while there is a trend for increased p53 LOH in ESCO2 deficient tumors compared to ESCO2 proficient tumors (**Figure 2E**). Further, analysis of other tumor suppressor genes in TCGA data indicated that there are statistically significant increases in LOH of BRCA1, PTEN and NF1 genes in ESCO2 deficient tumors. (**Figure 2F**). To determine if the increased LOH frequency was only associated with tumor suppressor gene or genes under a selective pressure for LOH, we surveyed the entire genome for LOH frequencies in ESCO2 wild-type and deficient tumors (Table S1 & S2). In multiple tumor types we observed significant elevated LOH rates throughout the genome (**Figure 2G**). Together this indicates that haploinsufficiency in ESCO2 results in a globally higher LOH frequency in tumors.

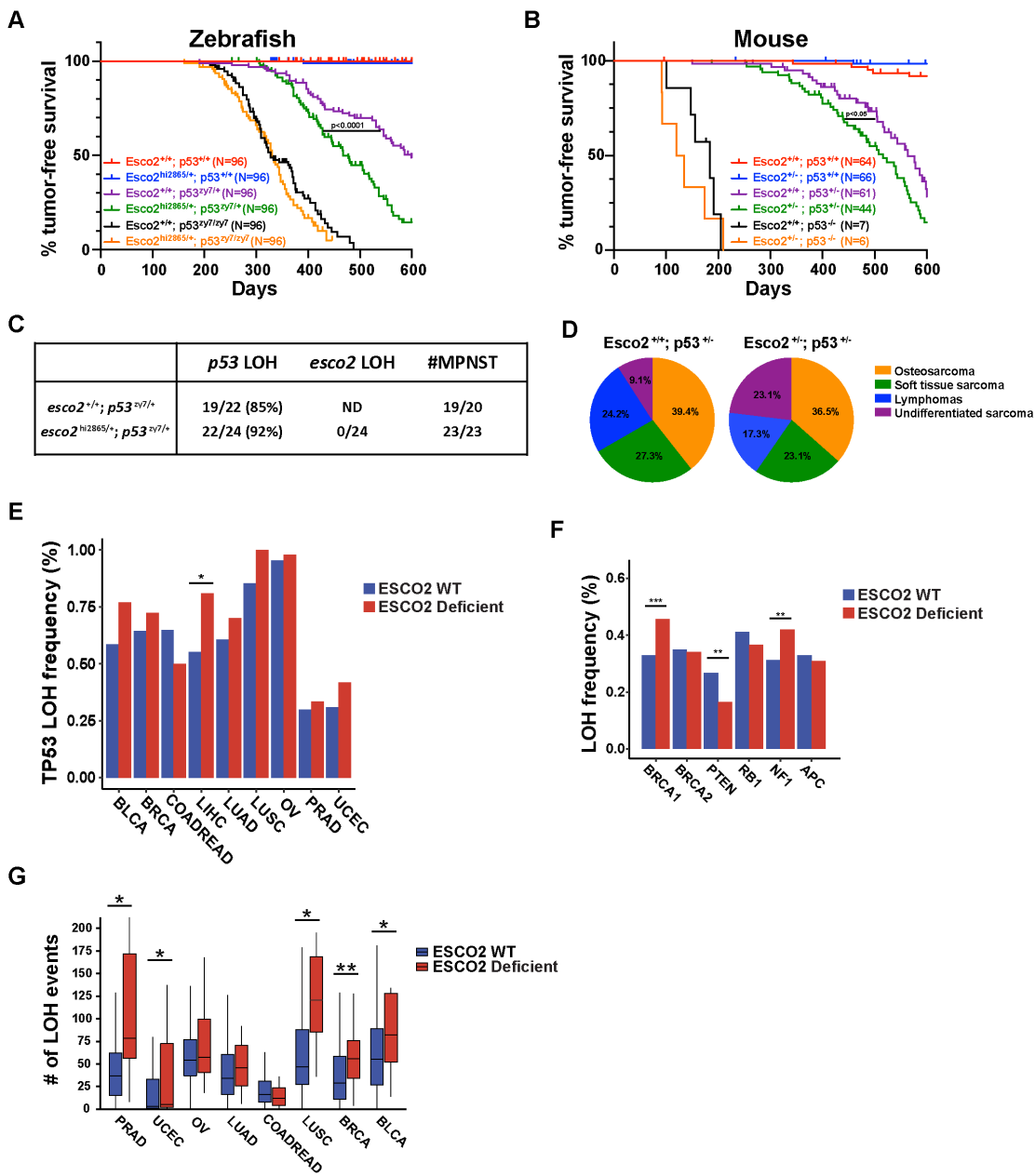


Figure 2. Esco2 deficiencies accelerate tumor onset in a LOH-sensitive background.

(A) Zebrafish Kaplan-Meier curves for tumor-free survival for wild-type, *esco2*^{2865/+}, *p53*^{J19/+}, *esco2*^{2865/+}; *p53*^{J19/+}, *p53*^{J19/J19}, and *esco2*^{2865/+}; *p53*^{J19/J19} cohorts. Compared cohorts were established by natural single pair breeding of *esco2*^{m/+} x AB (wild-type strain), *esco2*^{m/+}; *p53*^{m/m} x AB, or *esco2*^{m/+}; *p53*^{m/m} x *p53*^{m/m} parents (all cohorts were n=96). The p-value = <0.0001 when comparing *p53*^{J19/+} with *esco2*^{2865/+}; *p53*^{J19/+} cohorts based on Log-rank (Mantel-Cox) test. (B) Mouse Kaplan-Meier curves for tumor-free survival for wild-type, *Esco2*^{+/-}, *p53*^{+/-}, *Esco2*^{+/-}; *p53*^{+/-} and *p53*^{-/-} cohorts (cohorts with *p53*^{+/+} and *p53*^{+/-} background were n>60 and cohorts with *p53*^{-/-} background were n>6). The p-value = <0.05 when comparing *p53*^{+/-} with *esco2*^{+/-}; *p53*^{+/-} curves based on Log-rank (Mantel-Cox) test. (C) Frequency of *p53* wild-type loss of heterozygosity (LOH) and *esco2* wild-type LOH in zebrafish tumors; as well as the frequency of tumors being Malignant Peripheral Nerve sheath tumors (MPNST). (D) Pie charts showing tumor spectrum in *Esco2*^{+/+}; *p53*^{+/-} (left panel) and *Esco2*^{+/-}; *p53*^{+/-} (right panel) mice. No statistically significant in tumor spectrum with Chi-square test. (E) Percentage of patients with LOH on TP53 in TCGA cancer samples with or w/o ESCO2 mutation/deletion. The number of WT and deficient samples in each tumor were indicated. BLCA: 393 WT + 13 Deficient; BRCA: 935 WT + 29 Deficient; COADREAD: 482 WT + 38 Deficient; LIHC: 333 WT + 21 Deficient; LUND: 495 WT + 10 Deficient; LUSC: 478 WT + 8 Deficient; OV: 383 WT + 46 Deficient; PRAD: 481 WT + 6 Deficient; UCEC: 479 WT + 43 Deficient. * indicates p<0.05 from Fisher's exact test. (F) Percentage of patients with LOH covering in tumor suppressor gene PTEN, BRCA1, BRCA2, , RB1, NF1 and APC in the TCGA dataset. N= 4,126 for ESCO2-WT cohort and N=193 for ESCO2-deficiency cohort. ** and ***

indicate $p < 0.01$ and $p < 0.001$ with Fisher's Exact test. (G) The number of LOH events per tumor sample in TCGA cancer samples with or w/o ESCO2 mutation/deletion. The number of WT and deficient samples in each tumor were indicated: PRAD: 481 WT + 6 Deficient; UCEC: 479 WT + 43 Deficient; OV: 383 WT + 46 Deficient; LUAD: 495 WT + 10 Deficient; COADREAD: 482 WT + 38 Deficient; LUSC: 478 WT + 8 Deficient; BRCA: 935 WT + 29 Deficient; BLCA: 393 WT + 13 Deficient. * and ** indicate $p < 0.05$ and $p < 0.01$ from Mann-Whitney test.

Reduced sister chromatid cohesion drives early tumor onset.

The most striking observation was that amongst the zebrafish *esco2* heterozygous metaphase spreads, 8.3% displayed a "railroad" (RR) phenotype not observed in the wild-type sibling spreads (**Figure 3A& 3B**). While similar phenotypes have been described in cell culture, it has never been observed in a live organism(16). It has been presumed that this phenotype would result in embryonic lethality in a live organism due to the inability to properly orient the kinetochore required for microtubule attachment(15). However, in this case potentially the viability is associated with the low proportion of cells that have RR. These observations indicate that there is a gene dose-dependent reduction in cohesion establishment in *esco2* heterozygous animals. To address if accelerated tumor onset is specific to *esco2* or reduced SCC, we also generated a zebrafish *sgo1* null allele using CRISPR/Cas9 technique. SGO1 plays an important role in maintaining SCC after establishment by ESCO2. Homozygous null *sgo1* are lethal (**Figure S3**), however *sgo1* heterozygous mutant animals are viable and display low-level RR (13.4%) in metaphase spreads similar to *esco2* heterozygous mutants (**Figure 3C**). This led us to ask would the

reduced SCC in *sgo1* mutants also predisposes to early tumor onset in a *p53* heterozygous background. Consistent with the *esco2* haploinsufficient results, heterozygous loss of *sgo1* resulted in statistically significant accelerated tumor onset in a *p53* heterozygous background (**Figure 3D**, $T_{50}=422$ days in the *sgo1*^{Δ8/+}; *p53*^{+2/+} cohort vs. 478 days in the *p53*^{+2/+} cohort; $p < 0.0001$ based on Log-rank test). Together this provides two independent genetic models of reduced SCC that are associated with accelerated tumors in a LOH sensitive background.

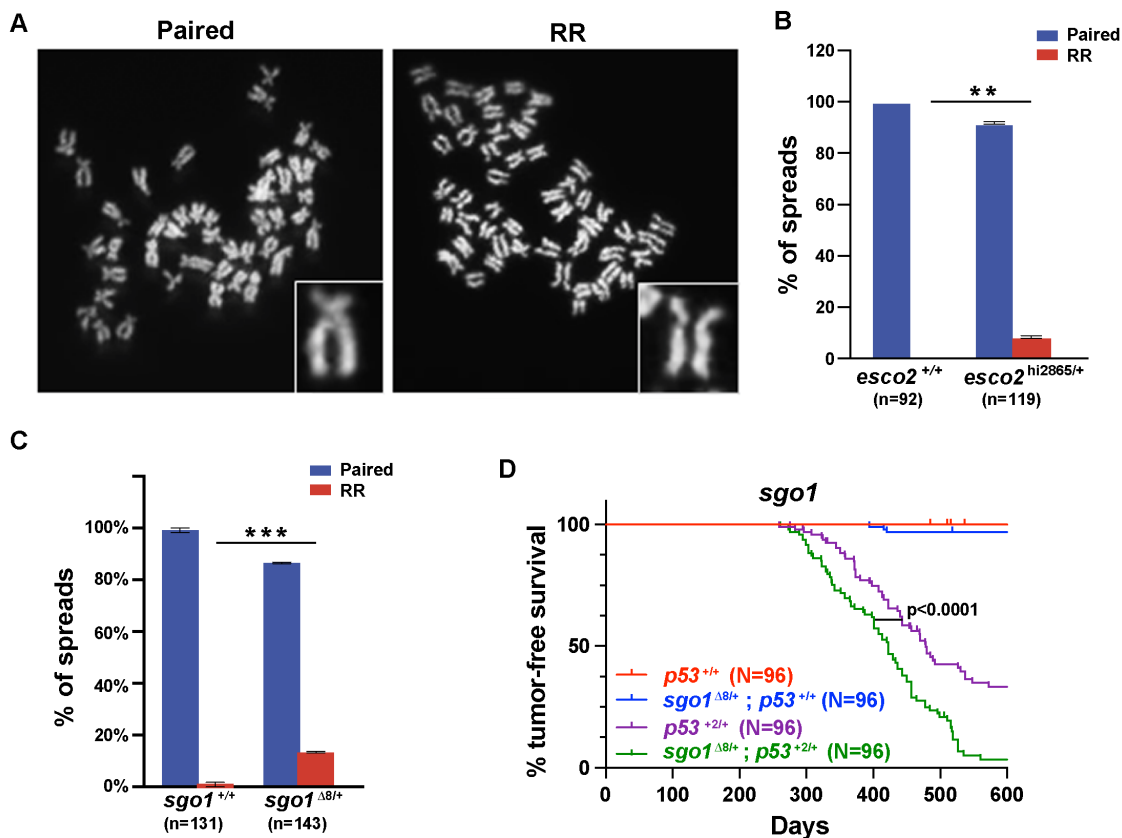


Figure 3. Reduced SCC in *esco2* and *sgo1* haploinsufficient animals correlates with accelerated tumor onset. (A) Representative images of “paired” and “railroad” (RR) metaphase spreads. Inset shows zoomed-in view of each phenotype. (B) The percentage of metaphase spreads in *esco2*^{+/+} and *esco2*^{2865/+} showing paired or RR phenotypes. Two pools of embryos were used for *esco2*^{+/+} and *esco2*^{2865/+} spreads from two independent experiments. A total of 92 *esco2*^{+/+} and 119 *esco2*^{2865/+} spreads were tallied. (C) The percentage of spreads in *sgo1*^{+/+} and *sgo1*^{+/-} showing paired or RR phenotypes. Three pools of embryos were used for *sgo1*^{+/+} and *sgo1*^{m/+} spreads. A total of 131 *sgo1*^{+/+} and 142 *sgo1*^{+/-} spreads were tallied. ** p-value < 0.01 and *** p-value < 0.001 by paired t-test. (D) Kaplan-Meier curves for tumor-free survival for *p53*^{+/+}, *sgo1*^{+/-}; *p53*^{+/+}, *p53*^{+/-} and *sgo1*^{+/-}; *p53*^{+/-} cohorts. Cohorts were established by natural single-pair breeding of *sgo1*^{+/-} X *p53*^{+/+} parents (all cohorts were n=96). P-value = <0.0001 when comparing *p53*^{+/-} with *sgo1*^{+/-}; *p53*^{+/-} curves based on Log-rank (Mantel-Cox) test.

Low-frequency chromosome segregation defect in *esco2* haploinsufficient animals.

Chromosome missegregation is one mechanism by which *p53* LOH has been described to occur in tumors(53-56), and we previously observed high levels of chromosome missegregation in the *esco2*^{hi2865/hi2865} animals(44). To determine if chromosome missegregation occurs in *esco2*^{hi2865/+} animals, we monitored 73 mitoses in six wild-type sibling embryos and 132 mitoses in ten *esco2* heterozygous embryos using a single-cell in-vivo imaging procedure(57). The majority of mitoses in wild-type embryos were error-free (72 of 73; **Figure 4A**) and were of normal duration (74% were 18-26 minutes; **Figure 4B**). We did observe one abnormal mitotic event that resulted in a congression defect, slightly lengthened mitotic duration, but no observable segregation errors (**Figure 4C & Video S1**). We also observed that some wild-type mitoses were mildly longer in length (~25% were 28-36 minutes in length; **Figure 4B**). In *esco2* heterozygous mutant embryos, while the majority of divisions appear normal (120 of 132; **Figure 4A**), we observed 12 mitoses with errors, five (~4%) of which had clear chromosome missegregation events, and two that never exited mitosis within our observation window. These events are summarized in **Figure 4C** and include one anaphase bridge (**Figure 4A & Video S2**), six congression defects (**Video S3**), two multipolar divisions (**Figure 4A & Video S4**), two prolonged delays in metaphase with no division observed (>50min, and >120 min; **Video S5**), and one cell fusion leading to multiple lagging defects (**Video S6**). These events would suggest mild defects in microtubule attachment (lagging chromosomes and congression defects) and/or centrosome duplication (multi-polar divisions). Further, in 3 of 132 (2.3%) mitoses, we observed a severe mitotic delay (60 min, >50 minutes, and >120 minutes; **Figure 4B and 4C**) indicative of mitotic defects

resulting in a prolonged spindle assembly checkpoint. Together these data indicate that as early as embryogenesis, haploinsufficient loss of *esco2* contributes to chromosome instability, which could be the driving force for more p53 LOH events.

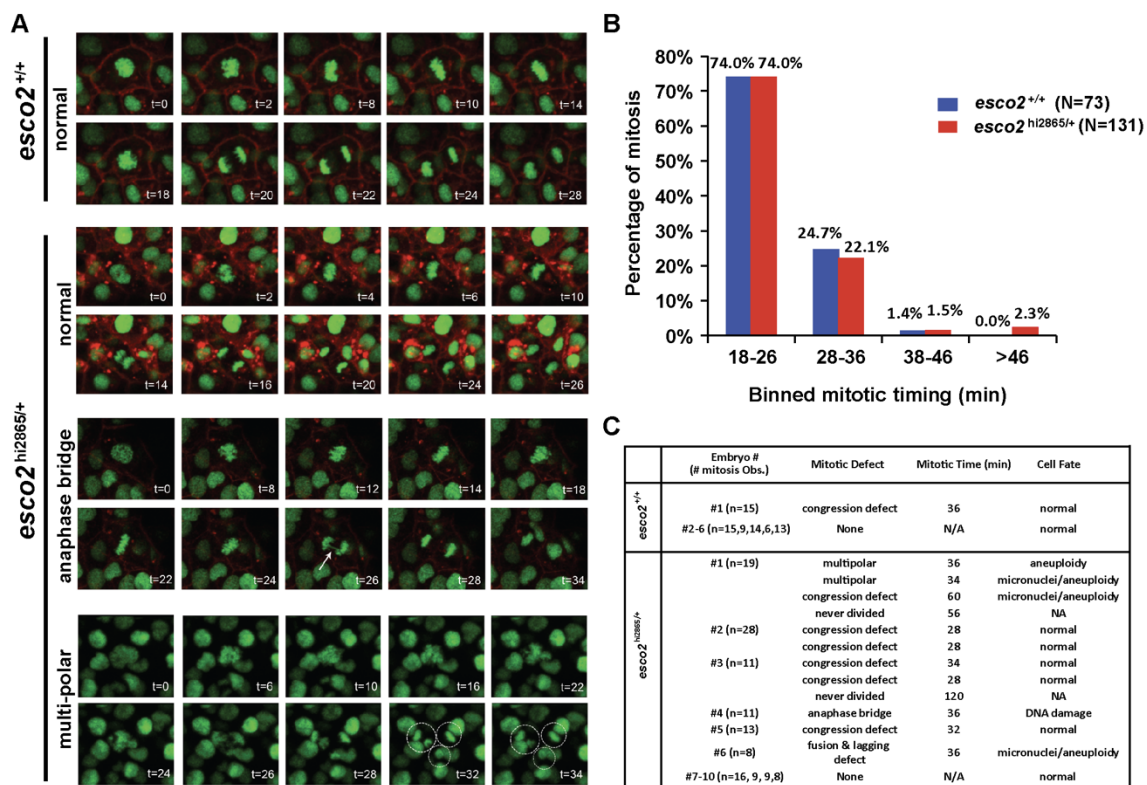


Figure 4. Elevated mitotic segregation errors in *esco2* haploinsufficient embryos. (A) in-vivo confocal imaging of H2A.F/Z-EGFP and CaaX-mCherry mRNA injected embryos at 24 hours post-fertilization (hpf) for two hours. Representative images of normal and defective mitoses in *esco2*^{+/+} and *esco2*^{m/+}. Arrow in anaphase bridge time-lapse points towards the anaphase bridge formed. Dotted circular in tri-polar time-lapse represents the three future nuclei that will occur. CaaX-mCherry was removed in tri-polar time-lapse for better visualization. t=time in minutes. (B) Division time calculated for each division in six *esco2*^{+/+} and ten *esco2*^{m/+} embryos using two-hour imaging time-lapse data from each embryo. The percentage of cells was calculated for each bin category. N=73 for *esco2*^{+/+} and N=132 for *esco2*^{m/+}. (C) Table representing mitotic defects and the associated mitotic timing and cell fate observed in six *esco2*^{+/+} and ten *esco2*^{m/+} embryos.

Somatic micronuclei frequencies during embryogenesis do not correlate with timing of tumor onset.

Micronuclei (MN) are often observed in cancers, and are derived from ungrouped chromosomes, often lagging chromosomes, during telophase when the nuclear envelope is reformed around chromatid material. MN are an indicator of a mitotic chromosome segregation defect, resulting in one cell gaining chromosomes while the sister cell losing chromosomes which could contribute to p53 LOH. Consistent with our chromosome segregation analysis, we observed a significantly higher number of micronuclei in 1 dpf *esco2* heterozygous mutant embryos (Avg. ~6%) versus the wild-type embryos (Avg. ~2%; **Figure 5A**). Interestingly, there was strong variability in the percentage of cells with micronuclei within embryos of the same genotype, ranging from 0-3.9% in wild-type embryos and 1.9%-15% in *esco2* heterozygous-mutant embryos (**Figure 5A**). This is also consistent with there being variations in the number of segregation errors observed between embryos of the same genotype (**Figure 4C**; up to 4 missegregation within a scanned field in embryo No.1 verse no events in 4 embryos (No.7-10)). This MN variability and higher levels of MN in *esco2* heterozygous animals spurred a hypothesis that animals with higher proportion of cells with MN, would have more frequent p53 LOH events in precancerous somatic cells, therefore a larger pool of cells that could become tumor-forming, which would translate into earlier tumor onset (**Figure 5B**). To test this hypothesis, we confocal imaged live 3-dpf p53 heterozygous embryos for the MN frequency using a PhOTO-N chromatin labeling transgenic line (**Figure 5C**). The TG^{PhOTO-N} transgenic lines ubiquitously expressed H2A-dendra fluorescent protein, which allows for imaging chromosome dynamics as well as determining MN frequency. We used the 3-dpf timepoint

to improve viability of embryos following the imaging procedure. We imaged 446 embryos and selected the top 15% MN frequency (0.91% to 3.85% frequency) as the high MN cohort and the bottom 15% (no MN observed) as the low MN cohort (**Figure 5D**). These cohorts as well as an un-imaged *p53* heterozygous cohort (with TG^{PhOTO-N} background) were monitored for tumor formation. Surprisingly we did not observe a significant difference in the high vs low MN cohort (**Figure 5E**). This suggests that chromosome missegregation and elevated MN in embryos are not the driving force behind elevated LOH and earlier tumor onset in *esco2* haploinsufficient animals. Note these experiments do not address the impact of chromosome missegregation and elevated MN that occurs in adult somatic tissues.

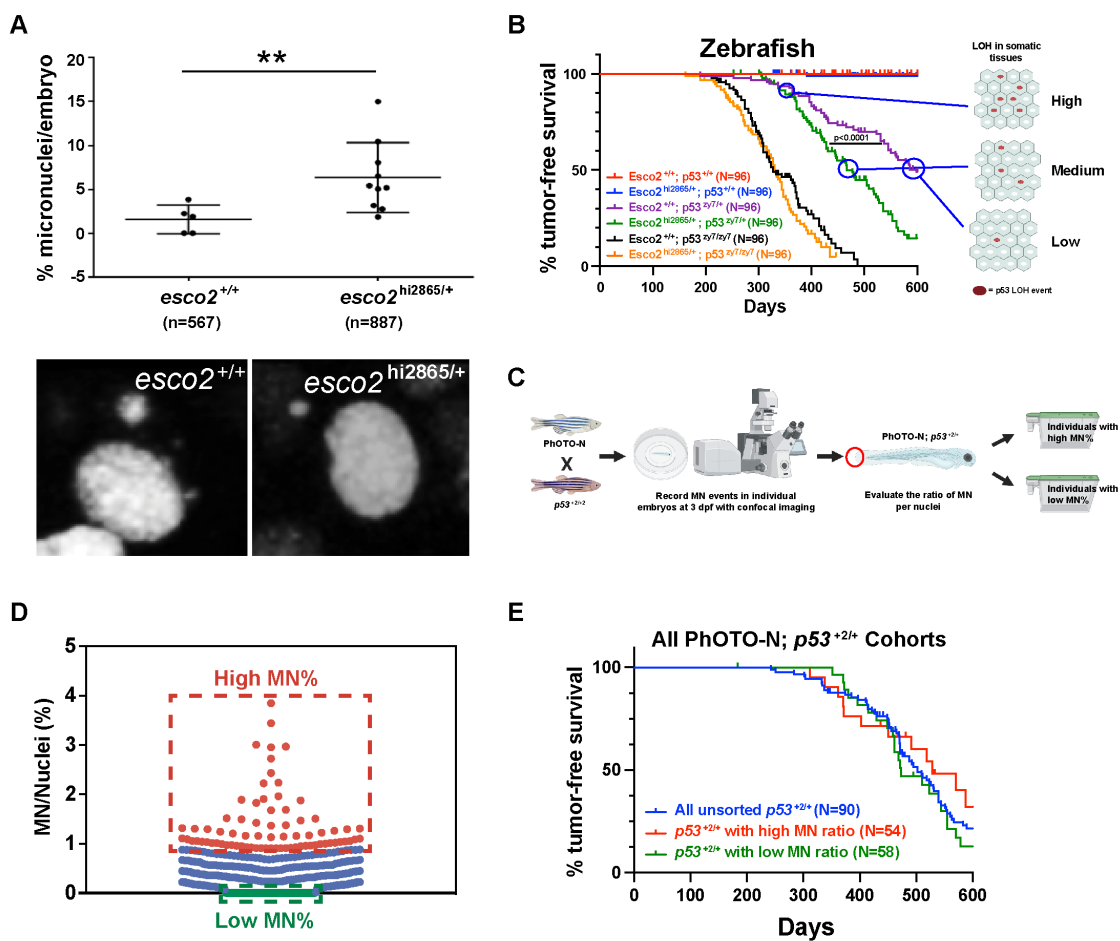


Figure 5. Elevated micronuclei during embryogenesis does not contribute to enhanced tumor onset. (A) Micronuclei (MN) during interphase were counted in six *esco2*^{+/+} and ten *esco2*^{2865/+} H2A.F/Z-EGFP mRNA injected embryos at 24hpf using two-hour live imaging time-lapse data from each embryo. Each dot represents an embryo measured. Percentage MN/embryo was calculated based on the total number of micronuclei per total nuclei present in the time lapse at t=0. Total nuclei are indicated in parenthesis. Mean \pm SD, ** p-value < 0.01 based on unpaired t-test. Representative black and white images of micronuclei in each genotype are shown below. (B) Proposed model where the proportion of cells with MN would correlate with p53 LOH and timing of tumor formation. (C) Experimental workflow to establish high and low MN cohorts, using confocal living-imaging of 3-dpf *p53*^{2/+}; TG^{PhOTO-N/+} embryos. Figure B and C were created with BioRender.com. (D) Dot-blot of Micronuclei frequency in individual 3-dpf *p53*^{2/+}; TG^{PhOTO-N/+} embryos. Individuals deemed part of the high MN cohort were highlighted with red (MN%>0.9%) and individuals in the low MN cohort were highlighted with green (MN%=0). (E) Zebrafish Kaplan-Meier curves for tumor-free survival for *p53*^{2/+}; TG^{PhOTO-N/+} unsorted (n=90), *p53*^{2/+}; TG^{PhOTO-N/+} with high NM ratio(n=54) and *p53*^{2/+}; TG^{PhOTO-N/+} with high NM ratio (n= 58). P-value is not significance when comparing each other based on Log-rank (Mantel-Cox) test.

Elevated mitotic recombination derived LOH.

p53 LOH can also be derived from mitotic recombination (MR) in which the region containing p53 becomes homozygous while the region between the MR site and the centromere as well as the opposite arm remains heterozygous (**Figure 6A**). Since our high and low MN cohort experiment suggested the whole chromosome instability (CIN) is not the driving force behind p53 LOH, we wanted to investigate mitotic recombination as a mechanism of p53 LOH in our *esco2* heterozygous zebrafish tumors. For this we identified a polymorphic SNP in *rabep1* or *cdca5* in normal tissues, that resided on the opposite arm of p53 containing chromosome (**Figure 6A**). Using these markers, we observed an increased rate (37%vs25% ; **Figure 6B**) of heterozygosity maintained at *rabep1* or *cdca5* in tumors derived from *esco2* heterozygous animals, indicative of increased MR. Since we observed the largest difference in the survival curves in the population of animals forming tumors later, we decided to analyze the MR rate of tumors that occur in the first half (<T₅₀) and the second half (>T₅₀) of the tumor cohorts. Interestingly, while in the *esco2* wild-type cohort the rate of MR was 25 % in the first and second half, we observed a much higher MR rate (57%) in the second half of the *esco2* heterozygous derived tumor cohort. These data suggest MR-derived LOH is a driving force for the overall earlier tumor onset in the *esco2* heterozygous cohort (T₅₀=467 days in *esco2*^{hi2865/+}; p53^{zy7/+} cohort vs. 561 days in the p53^{zy7/+} cohort). To determine if human cancers that have ESCO2 deficiencies also have higher MR rates, we analyzed TCGA data to define all LOH loci that maintained a 2N copy number (**Figure 6C**), this would exclude regional deletions or whole chromosome deletion, as well as amplifications. We then plotted these across the chromosome to define MR events. From this analysis we determined that there were more MR events, in multiple

cancer types, in ESCO2 deficient tumors compared to proficient tumors (**Figure 6D**). Together these data suggest that reduced SCC enhances the rate of MR which drives LOH-sensitive tumorigenesis.

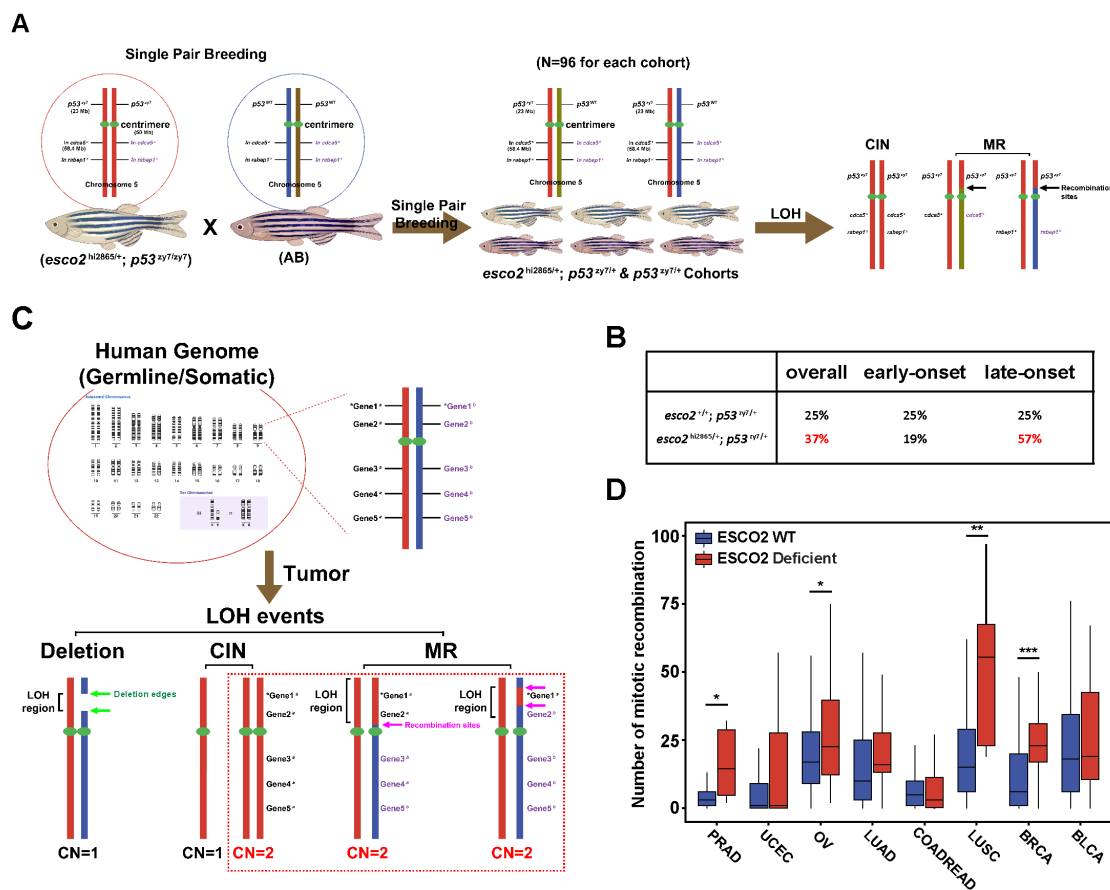


Figure 6. Reduced SCC allows for elevated mitotic recombination derived LOH. (A) Schematic of determining LOH mechanisms/types in *p53* heterozygous tumors. The haplotype of nearby *p53* marker in tumor and normal paired samples, cooccurring with *p53* wild-type or mutant gene are labeled (left). (B) A table showing the percentage of mitotic recombination (MR) in *esco2*^{+/+}; *p53*^{zy7/+} and *esco2*^{hi2865/+}; *p53*^{zy7/+} tumors. (C) Schematic of determining the mitotic recombination with TCGA database. Figure A and C were created with BioRender.com. (D) The number of mitotic recombination in TCGA cancer samples with or w/o ESCO2 mutation/deletion. Genome-wide data was downloaded from NCI Genomic Data Commons. The number of WT and deficient samples in each tumor were indicated: PRAD: 481 WT + 6 Deficient; UCEC: 479 WT + 43 Deficient; OV: 383 WT + 46 Deficient; LUAD: 495 WT + 10 Deficient; COADREAD: 482 WT + 38 Deficient; LUSC: 478 WT + 8 Deficient; BRCA: 935 WT + 29 Deficient and BLCA: 393 WT + 13 Deficient. *, ** and *** indicate $p < 0.05$, $p < 0.01$ and $p < 0.001$ from Mann-Whitney test.

DISCUSSION

These data indicate that gene dose-dependent loss of *esco2* or *sgo1* results in reduction in SCC and enhanced tumor predisposition. Interestingly, amongst viable (majority die in utero or postnatally) Roberts Syndrome (RBS) patients, which are homozygous null of ESCO2, they also display reduced SCC and early onset tumor occurrence(41-43); supporting the fact that reduced SCC is tumor-promoting across species. Further, our analysis of the TCGA data strongly supports that ESCO2 loss in tumors is associated with elevated mitotic recombination and elevated tumor suppressor inactivation. While this study has focused on ESCO2, SCC is a complex network of pro-cohesion factors and anti-cohesion factors (yeast genetics suggests over 350 genes involved)(58), in which the synergistic or antagonistic effects of combined mutations/polymorphisms in these genes can create varying degrees of SCC dysfunction amongst a population of individuals and potentially define variability of tumor penetrance between individuals. Consistent with this, alterations in other SCC factors such as Separase overexpression, STAG2 loss, SGO1 haploinsufficiency, and others have been associated with tumorigenesis(16, 59-61). Additionally, deficiencies in the tumor suppressor retinoblastoma (RB1) have recently been tied to SCC loss and suggestive of a mechanism by which RB loss promotes tumorigenesis (62). SCC involvement in tumorigenesis is also interesting in that there is a yin-yang relationship between the cohesion establishment and antiestablishment processes. In yeast, deletion of Eco1, the homolog of ESCO2, is lethal; while concomitant loss of Eco1 and WAPAL, or PDS5, circumvent this lethality(63-66). This suggests that there could be a window where ESCO2 or another establishment molecule is lost, which would encourage MR and selection, and then a second window

where an anti-establishment factor is lost to restore stability of an aneuploid genome. However, this Yin-Yang relationship is yet to be demonstrated during tumorigenesis. Together these data emphasize that defects in SCC can strongly influence tumorigenesis.

While chromosome instability has been the focus of studies looking at the consequence of defects in SCC, some studies have pointed to increased rates of homolog recombination versus sister chromatid recombination(67, 68). In most normal circumstances, due to the cohesin rings, the sister chromatids are in proximity and therefore the preferred source for homologous recombination and produces a “perfect” repair. However, in situations of reduced SCC, chromosome homologs now have better access to each other, and homologous recombination can occur between homolog chromosomes(10, 69). This can result in multiple repair outcomes, including a crossover event and/or gene conversion events. Following mitosis this recombination between homologs can result in chromosome regions becoming homozygous (mitotic recombination (MR)), resulting in a LOH event. This is consistent with our tumor data in which reduced SCC is associated with elevated MR events. Changes in MR rates are most well demonstrated in recombinase deficient individuals and animal models, such as Bloom syndrome proteins (BLMs) or Werner syndrome helicase (WRN), but we demonstrated that this may also be true for SCC reduced models and syndromes.

Interestingly the variability in the age of tumor onset within LFS is great, with some patients developing tumors within the first year of life, while others have been described to be tumor-free at the age of 74. The timing of tumor onset is influenced by many different factors, including environment and genetic heterogeneity. While these are clearly influential, isogenic animal models under controlled environmental conditions can exclude

these factors and focus on genetic aspects. In a *p53*-centric view, the difference between the survival curves of a $p53^{zy7/zy7}$ and $p53^{zy7/+}$ cohort (at T_{50} , a difference of 241 days vs. 561 days respectively) is rationalized as the time required for the 2nd *p53* hit to occur (*p53* LOH; $p53^{zy7/+} \rightarrow p53^{zy7}$ or $zy7/zy7$). The difference between $p53^{zy7/+}$ and $p53^{+/+}$ curves is the time required for the first *p53* hits to occur ($p53^{+/+} \rightarrow p53^{zy7/+}$). However, the reason that the $p53^{zy7/zy7}$ tumors are not observed immediately at time 0 is due to the time needed for the additional required tumor-promoting mutations to occur (for example Ras and/or other). We demonstrate that reduced SCC through haploinsufficient loss of *esco2* or *sgo1*, decreased the time between $p53^{zy7/zy7}$ and $p53^{zy7/+}$ curves (at T_{50} , a 147-day difference) suggesting that reduced SCC enhances the rate of *p53* LOH events. Further, since there was no change in survival curves in the $p53^{zy7/zy7}$ background, *esco2* haploinsufficiency is not an added oncogenic hit. It is also interesting that in these isogenic and environmentally controlled models that there is a vast difference in the time of tumor onset within these cohorts. For mouse *trp53* heterozygous null in a C57BL6/J background, the first tumors are observed at ~150 days, while the later tumors are at >600 days(48). What influences this difference? We would speculate that the proportion of cells in an organism with stochastically derived *p53* LOH in somatic tissues influences the timing of tumor formation. While measuring *p53* LOH in tumors is relatively easy due to the clonal source of the genomic DNA, the ability to measure *p53* LOH in somatic cells has been close to impossible. However recent advances in single-cell haplotyping might provide a first-time view of *p53* LOH rates in somatic tissue and variability between tissues and individuals. If true, individual evaluations of *p53*, or other tumor suppressor genes, LOH events in somatic tissues of a patient could provide a cancer risk for those individuals.

It is worth noting that some aspects of tumorigenesis with regards to p53 status are different in mouse and zebrafish. In zebrafish, the day distance at the T_{50} between the $p53^{zy7/zy7}$ and $p53^{zy7/+}$ is shorter suggesting they are more prone to LOH of the wild-type allele than mouse. Interestingly, the time for $p53^{-/-}$ mice to form tumors is much earlier than $p53^{zy7/zy7}$ zebrafish and would suggest that these “hits” in mouse are acquired more readily or require less number of hits than in zebrafish. Further, the impact of reduced SCC-derived p53 LOH may have different impact on tumorigenesis between mice and zebrafish. In zebrafish the $p53^{zy7/+}$; $esco2^{hi2865/+}$ and $p53^{zy7/+}$; $sgo1^{D8/+}$ curve progressively diverges from the $p53^{zy7/+}$ curve with time, while in mouse they run parallel. Since the accelerated curves in mouse and zebrafish only occur in the p53 heterozygous animal, inactivation of the wild-type p53 allele is important in the accelerated tumorigenesis. However, potentially the impact that inactivation of p53 has on tumorigenesis is different between species; i.e. inactivation of p53 in zebrafish may continually progresses acquisition of “hits”, while in mouse they are already acquired. Alternatively, increased genomic LOH with reduced SCC maybe adds the additional “hits”, independent of p53 status, such that accelerated tumorigenesis occurs, while the necessary “hits” are already acquired in the mouse. Together this may suggest that the zebrafish model is more strongly influenced by reduced SCC and/or LOH, compared to the mouse model.

MATERIALS AND METHODS

Mouse Lines and Maintenance:

All mouse studies were conducted in compliance with the National Institutes of Health Guide for the Care and Use of Laboratory Animals and approved by the Institutional Animal Care and Use Committee (IACUC) at the University of Alabama at Birmingham. The *Esco2* knockout line was acquired from The European Conditional Mouse Mutagenesis Program (*Esco2*^{tm1a(EUCOMM)Wtsi} EPD0409_6_A03)(52). *Esco2* conditional allele was generated by crossing the *Esco2* Knock out first line to a *Rosa26* flp line (Jackson lab #009086). The *Esco2* null allele was generated by crossing the conditional allele to a *Rosa-CreER* line (National Cancer Institute Mouse Repository Strain #01XAB), and injecting Tamoxifen into the pregnant mom to remove exon 4. All *Esco2* alleles were maintained on a C57BL6/J background. The *p53* KO allele was obtained from Jackson Labs (Strain #002101). The *p53* allele was maintained on a C57BL6/J genetic background.

Zebrafish Lines and Maintenance:

All zebrafish work was performed in the Zebrafish Research Facility (ZRF) of the University of Alabama at Birmingham (UAB). Adult fish and embryos are maintained as described by Westerfield et al (1995) by the ZRF Animal Resources Program which maintains full American Association for Accreditation of Laboratory Animal Care (AAALAC) accreditation and is assured with the Office of Laboratory Animal Welfare (OLAW). All animal studies have UAB Institutional Animal Care and Use Committee (IACUC) approval. The *esco2*^{hi2865} retroviral insertion allele was obtained from Nancy Hopkins and Jacqueline A. Lees (Massachusetts Institute of Technology, Cambridge, MA) and maintained on the AB wild-type background(70). The *p53*^{zy7} allele was obtained from

Dr. Yost at the University of Utah(22) (a thymine to cytosine transition in codon 164), also maintained on an AB background. TG^{PHOTO-N} (pMTB:memb-Cerulean-2A-H2B-Dendra2, a transgenic line ubiquitously expressing membrane-targeted blue fluorescent protein cerulean and chromatin targeted photoconvertible fluorescent protein Dendra2)(71) transgenic fish was obtained from Periklis Pantazis (ETH, Laboratory of Nano Bio Imaging, through Heidi Hehnly-Chang at SUNY upstate as an intermediary). The p53⁺² allele(23) was generated and maintained on an AB background. The *sgo1*^{Δ8} knock-out allele was generated (see below) and maintained on an AB background.

Generation of New Zebrafish Knockout Alleles:

Gene Knockouts were generated as described previously(72). gRNA target sites were identified using the Zhang lab gRNA design tool (gRNA sequencing and target sites listed in **Figure S3**). The CRISPR gRNA sequences were cloned into pDR274 (Addgene NO. 42250). The Cas9 mRNA was transcribed from pT3TS-nCas9n (Addgene No. 46757)(73). After cloning specific target plasmids/guides into pCS2 variant vector, mRNA was generated by in vitro transcription of NotI-HF linearized DNA using the Invitrogen mMACHINE SP6 Transcription Kit (Fisher Scientific AM1340) and purified with the MEGAclean Transcription Clean Up Kit (Fisher Scientific AM1908). 1-2nl of sgRNA/Cas9 mRNA was microinjected into the yolk of one-cell-stage wild-type zebrafish embryos. For indel efficiency evaluation, genomic DNA was extracted from ~24 3dpf injected embryos and evaluated with HRM (see below). The remaining embryos (F0s) from the same clutches were raised. Out-of-frame indels identified in F1 progeny with Sanger sequencing were maintained and propagated. To “clean up” genetic background all lines were bred at least 2 generations to the wild-type strain AB.

Identification of Zebrafish Mutated Alleles:

To determine the mutated allele, a small piece of tail was cut from a single F2 heterozygous progeny (of each allele) to extract genomic DNA through incubation at 98°C for 20 min in 40µl 25mM NaOH in a 96-well plate, then neutralized with 40µl of 40mM Tris-HCl. The PCR amplicons were amplified using Takara Ex Taq DNA Polymerase (Takara Bio, RR001A), purified with the Promega Wizard SV Gel and PCR Cleanup System (Promega, A9282), and examined on a 1% agarose gel (for examining alternative splicing) and sequenced by the UAB Heflin Center for Genomic Sciences Sanger Sequencing Core.

Establishing Zebrafish and Mouse Tumor Cohorts:

The six paired zebrafish tumor cohorts (*esco2*^{+/+} vs *esco2*^{hi2865/+}, *esco2*^{+/+}; *p53*^{zy7/+} vs *esco2*^{hi2865/+}; *p53*^{zy7/+}, and *esco2*^{+/+}; *p53*^{zy7/zy7} vs *esco2*^{hi2865/+}; *p53*^{zy7/zy7}) were established by natural breeding of *esco2*^{hi2865/+} x AB (wild-type strain), *esco2*^{hi2865/+}; *p53*^{zy7/zy7} x AB or *esco2*^{hi2865/+}; *p53*^{zy7/zy7} x *p53*^{zy7/zy7} parents respectively. Four zebrafish tumor cohorts (*sgo1*^{+/+}, *sgo1*^{Δ8/+}, *sgo1*^{+/+}; *p53*^{+2/+}, *sgo1*^{Δ8/+}; *p53*^{+2/+}) were established by natural single-pair breeding of *sgo1*^{Δ8/+} X *p53*^{+2/+} parents. Each paired cohort consisted of 96 fish and was derived from a single set of parents (a single male and female). At 3 months of age, each fish was genotyped for and then separated into 6 tanks of 16 fish each (for *esco2* cohorts) and 4 tanks of ~24 fish each (for *sgo1* and *p53*^{+2/+} micronuclei cohorts). For the micronuclei (MN) study, three zebrafish tumor cohorts (*p53*^{+2/+} unimaged control, *p53*^{+2/+} with high MN ratio and *p53*^{+2/+} with low MN ratio) were established by natural breeding of *p53*^{+2/+2} x TG^{PhOTO-N} transgenic parents multiple times. *P53*^{+2/+} cohort consisted of 90 fish, *p53*^{+2/+} with high NM ratio consisted of 54 fish and *p53*^{+2/+} with low NM ratio

consisted of 58. Six mouse tumor cohorts ($Esco2^{+/+}$, $Esco2^{+/-}$, $Esco2^{+/+}; p53^{+/-}$, $Esco2^{+/-}; p53^{+/-}$, $Esco2^{+/+}; p53^{-/-}$, and $Esco2^{+/-}; p53^{-/-}$) were established by natural breeding of $Esco2^{+/-}; p53^{+/-}$ X 129 mice (first 4 cohorts) and $Esco2^{+/-}; p53^{+/-}$ X $Esco2^{+/+}; p53^{+/-}$ mice (last 2 cohorts). Kaplan-Meier analysis was performed using GraphPad Prism software.

Zebrafish and Mouse Genotyping:

To genotype, tail clippings from each fish were placed in 100 μ l ELB (10 mM Tris pH 8.3, 50 mM KCl, 0.3% Tween 20, 0.3% NP40, 1 mg/ml Proteinase K) in 96-well plates. Tail clips were incubated at 55°C overnight to generate genomic DNA, and the plates were then incubated at 95°C for 10 min to inactivate the Proteinase K. PCR reactions contained 1 μ l of LC Green Plus Melting Dye (BioFire Defense), 1 μ l of enzyme buffer, 0.2 μ l of dNTP Mixture (10mM each), 0.3 μ l of $MgCl_2$, 0.3 μ l of each primer (10 μ M), 1 μ l of gDNA, 0.05 μ l of Genscript Taq, and water up to 10 μ l. For *esco2* allele, PCR amplicons were generated using a universal forward primer: 5'-TTTCACTGTTTCTGCAGGTTG-3', reverse primer 5'-TAAGGTCTTCGAAGTCTTAACG-3' to amplify the wild-type, and reverse primer 5'-GGGGGGGGCCTACAGGTGGGGTCTTTC-3' to amplify the retroviral insertion allele. For *p53* mutant allele (J19), PCR amplicons were generated using forward primer: 5'-GCGCCTGCTGGTCA-3', reverse primer 5'-CTGATTGCCCTCCACTCTT-3'. For *p53* +2 allele, wild-type and mutant amplicons were generated using forward primer: 5'-AGTACTTGCCGGGATCGTTT-3', reverse primer 5'-GTCTCCGGAACAGTGGATGT-3'. For *sgo1* Δ 8 allele, wild-type and mutant amplicons were generated using forward primer: 5'-AGCGTTCAGGCCAACAATAA-3', reverse primer 5'-GCGGGTCTCTCTCTCAGTGT-3'. The PCR reaction protocol was 98°C for

30 sec, then 40 cycles of 98°C for 10 sec, 59°C for 20 sec, and 72° C for 15 sec, followed by 72°C for 1 minute (for *esco2*^{hi2865} allele) and 95°C for 20 sec (for *sgol*^{Δ8}, *p53*^{zy7} and *p53*⁺² allele) and then rapid cooling to 4°C. Following PCR, melting curves were generated and analyzed using the LightScanner instrument (Idaho Technology) over a 65-95°C range. For identifying mouse p53 allele, PCR amplicons were generated using a universal reverse primer for both alleles: 5'-CCCATGCAGGAGCTATTACACA-3', forward primer to amplify the wild-type allele: 5'-GGTCACCTGTAGTGAGGTAGGG-3', and forward primer to amplify the mutant allele: 5'-CCTCTGTTCCACATACTTCA-3', following the Jackson standard protocol for p53 KO stain #002101.

Loss of Heterozygosity Analysis:

DNA was extracted from 22 *esco2*^{+/+}; *p53*^{zy7/+} and 24 *esco2*^{hi2865/+}; *p53*^{zy7/+} zebrafish tumors using the DNeasy Blood & Tissue Kit (Qiagen). LOH analysis was performed for the *esco2* allele using the HRM method described above and for the *p53* allele by sequencing PCR products. Each PCR reaction contained 3 µl Ex Taq Buffer, 2.4 µl dNTPs (2.5mM each), 0.9 ul forward primer (5'-GTGCAGCCCTACTGGAAT-3') and reverse primer (5'-GGTCCTACAAAAGGCTGTGA -3'), 50-100 ng of DNA, 0.15 µl of Ex Taq DNA polymerase and water up to 30ul. PCR conditions were as follows: 98°C for 30 sec, then 40 cycles of 98°C for 10 sec, 56°C for 30 seconds, and 72° C for 30 seconds, followed by 72°C for 4 minutes. Each PCR reaction was analyzed on a 2% agarose gel and purified using the Wizard SV Gel and PCR Clean Up System (Promega). Each sample was sequenced by the UAB Heflin Center for Genomic Science.

Gross Imaging:

Zebrafish embryos were dechorionated at described stages with incubation in 0.03% pronase (Sigma P5147) for 5-7 min and anesthetized using 0.4% tricaine. In a 60 x 15 mm Falcon petri dish, embryos are mounted in 1% low melting agarose and gross images were taken on a Nikon SMZ-18 Zoom Stereo Microscope. All images were acquired at the same magnification, exposure time and gain. After each embryo was imaged, embryos were removed from the agarose to generate genomic DNA for genotyping. Further figure processing and analysis were performed using Nikon NIS Element and ImageJ.

Confocal Time-lapse Imaging:

CaaX-mCherry and H2A.F/Z-EGFP mRNA was transcribed from gift plasmids, pCS2-CaaX-mCherry and pCS2-H2A.F/Z-EGFP from K. Kwan (University of Utah) using mMessage mMachine SP6 kit (Life Technologies). *esco2* heterozygotes were crossed, and zebrafish embryos were microinjected into the yolk of a one-cell-staged embryo with 1 nl of 200 ng/ μ l CaaX-mCherry and 200 ng/ μ l H2A.F/Z-eGFP mRNA. At 24 hours post-fertilization (hpf), embryos were screened for fluorescence. Embryos showing a mutant phenotype were excluded. Embryos were manually dechorionated using tweezers and anesthetized using 0.4% tricaine. In a glass-coverslip-bottomed dish, embryos were embedded in a 1% low-melt agarose. Dishes were placed on the Nikon A1 inverted confocal microscope and Z-stack images were taken at designated intervals. Approximately 40- μ m Z-stacks (with a 2- μ m interval) were obtained every 2 minutes for a total scanning time of 2 hours. After each embryo was imaged, embryos were removed from the agarose to generate genomic DNA for genotyping. All videos were taken using Plan Apo 60x oil 1.4 NA objective. 3D viewing, still shots and videos were assembled and processed using NIS Elements 4.13.00. Division time was calculated by manually counting

how many time intervals encompass the division. This number was then multiplied by the time between each Z-stack (2 minutes). Further details are shown in our video manuscript(74).

Micronuclei Counting:

Zebrafish embryos were injected with H2A.F/Z-EGFP and CaaX-mCherry mRNA and set up for a time-lapse video. An approximately 40- μ M Z-stack was generated with 2- μ m steps using a 60x 1.4 NA objective on a Nikon A1 confocal microscope. Using 3D volume rendering in NIS Elements 4.13.00, the frequency of micronuclei in interphase was calculated by dividing the total number of micronuclei observed in the 3D render by the number of nuclei identified in the 3D render. Representative micronuclei images were pulled from the 3D volume rendering of an *esco2*^{+/+} and *esco2*^{hi2865/+}, CaaX fluorescence was removed, and image was converted to black and white. For the investigation of whether the micronuclei ratio affects the onset of tumor formation, instead of mRNA injection, *p53*^{+2/+2} fish were crossed to TG^{Photo-N} transgenic line which ubiquitously express photoconvertible fluorescent protein Dendra2 fused to H2B to detect micronuclei within a cell. The imaging technique and analysis were identical to that using mRNA injections.

Chromosome Spreads:

Chromosomes spread protocol was adapted from the Lee group(75). Approximately 20-30 zebrafish embryos were dechorionated at 24 hpf. Embryos were incubated in 400 ng/ml nocodazole for 2 h in the dark at 28°C. Embryos were then transferred to 1.1% sodium citrate in a 6-cm dish and deyolked. At this point, for genotyping purposes, tails were removed to be genotyped, whereas the remaining embryo

heads/trunk were transferred to fresh sodium citrate solution and incubated on ice for 8 min. Next, we performed two washes with a cold 3:1 methanol: acetic acid solution for 20 min each followed by storage at -20°C overnight until genotyping was performed. After fixative procedure, embryos were pooled (10-12 embryos/pool) per genotype and then minced using forceps in a 1:1 methanol: acetic acid solution. Using this mixture, 150 μl of pooled embryos were dropped onto a slide, and 3-5 drops of glacial acetic acid were added. The slide was then exposed to hot vapors (we used boiling water) for about 10 s; then allowed to dry on a hot metal surface (approx. 55°C). After the slide was completely dry, a few drops of Prolong Gold with DAPI (Life Technologies) were added, and the slide was covered with a glass coverslip. Chromosomes were imaged with 100x objective on the Zeiss Axio Imager A2 and analyzed with the Zen 2011 Blue Edition software. Although most spreads were clearly delineated into the 'paired' or RR 'railroad' categories, if a spread had multiple phenotypes it was categorized by which was most prevalent in that spread. Chromatid number was counted manually from high-resolution images.

TCGA and Human Tumor Analysis:

To obtain an overview of ESCO2 mutational status across cancers, oncoprint plot of ESCO2 and other SCC-associated genes was generated with cBioPortal (<https://www.cbioportal.org/>) using 10,950 samples from 32 studies under TCGA Pan Cancer Atlas Studies category. The somatic mutation calls, copy number variation calls, and clinical survival data of TCGA samples from all 33 TCGA cancer projects were obtained from TCGA GDC data portal (<https://portal.gdc.cancer.gov/>). Sample number in each analysis was indicated in figure legend. Patients were classified as 'ESCO2 Mutant/Deletion' if there was non-synonymous somatic SNV/indel or copy number loss in

the ESCO2 gene region. Survival analysis was performed with R package ‘survival’ and the differences in patient survival status by ESCO2 mutational status were assessed by log-rank test. Genetic alteration frequency of ESCO2 in different cancer types was plotted with cBioPortal using corresponding studies in TCGA PanCancer Atlas Studies. For deletion frequency analysis, the number of copy number loss was counted in each 100kbp bin on the human reference genome and then divided by the total number of patients in the cohort to calculate deletion frequency. Deletion frequencies in each bin were plotted using the R package ‘ggplot2’ and a smoothed line was generated using the Loess function. For genome-wide LOH analysis, LOH calls were downloaded from <https://gdc.cancer.gov/about-data/publications/pancan-aneuploidy>, which were previously inferred from SNP array and exome sequencing data (76). The LOH status on BRCA1 and other tumor suppressors was classified by comparing the genomic coordinates of each LOH event and tumor suppressor gene. LOH frequency differences by ESCO2 status (WT vs. Mutant) were assessed by Fisher’s exact test(77). Number of LOH events was counted for ESCO2 Mutant/Deletion and ESCO2 WT patients in each cancer type and the differences were assessed with Mann-Whitney test. Mitotic recombination frequencies were inferred from the LOH regions with neutral copy numbers excluding chromosome-level events. For CNV burden visualization, CNVs with focal CNV values smaller than -0.5 were categorized as copy number loss.

Statistical Analysis:

A combination of GraphPad Prism and R statistical packages was used in generation of all graphs and statistical tests. For the zebrafish work, overall statistical significance was calculated using an unpaired t-test with error bars indicating standard

deviation as stated in legend (\pm). All p-values that were determined to be significant are noted in individual figure legends. Unpaired t-test determined the significantly different values. The Log-rank (Mantel-Cox) test was performed for tumor survival studies. Numbers of embryos and significance values are indicated in the figure legends. For analysis of human TCGA data, the R statistical package was used, and the statistical tests are listed in the relevant methods and figure legends.

Data availability:

All relevant data within the manuscript and its Supporting Information are available at <https://doi.org/10.1371/journal.pgen.1010341>.

ACKNOWLEDGEMENT

The UAB High Resolution Imaging Facility is supported by the UAB Comprehensive Cancer Center Support Grant (P30CA013148) and the Rheumatic Disease Core Center (P30 AR048311). JMP is supported by the National Institute of Health (R01 CA216108, R21 CA219546, and U54 OD030167), a pilot grant from American Cancer Society (ACS IRG-60-001-53-IRG) and the UAB Comprehensive Cancer Center (P30CA013148). SMP is supported by the Cell and Molecular Biology T32 Training Grant (5T32GM008111-28). RCR is supported by the UAB MSTP (NIH-NIGMS 5T32GM008361-21). SJC is supported by the Hudson Alpha Tie the Ribbons Fund and the UAB CCTS (NIH 1UL1TR001417-01). ZC is supported by the National Institute of General Medical Sciences (1R35GM138212).

AUTHOR'S CONTRIBUTION

J.M.P. designed and oversaw study. J.W. characterized mutants. H.T.R established and monitored tumor survival curves and performed mitotic spread analysis. Y.C., R.C.R, S.J.C and Z.C. performed TCGA data mining and genomic analysis. S.M.P. performed live mitotic imaging analysis. S.C.W. performed micronuclei analysis. J.W. performed statistical analysis. J.W., with consultation from J.M.P, made all figures. J.M.P. and J.W. wrote the manuscript with revision by all authors.

COMPETING INTERSTS

The authors declare no competing interests.

REFERENCES:

1. Vishwakarma R, McManus KJ. Chromosome Instability; Implications in Cancer Development, Progression, and Clinical Outcomes. *Cancers (Basel)*. 2020;12(4).
2. Thompson SL, Bakhoun SF, Compton DA. Mechanisms of chromosomal instability. *Current biology : CB*. 2010;20(6):R285-95.
3. Bakhoun SF, Silkworth WT, Nardi IK, Nicholson JM, Compton DA, Cimini D. The mitotic origin of chromosomal instability. *Current biology : CB*. 2014;24(4):R148-9.
4. Duijf PH, Benezra R. The cancer biology of whole-chromosome instability. *Oncogene*. 2013.
5. Holland AJ, Cleveland DW. Boveri revisited: chromosomal instability, aneuploidy and tumorigenesis. *Nat Rev Mol Cell Biol*. 2009;10(7):478-87.
6. Baker DJ, Jin F, Jeganathan KB, van Deursen JM. Whole Chromosome Instability Caused by Bub1 Insufficiency Drives Tumorigenesis through Tumor Suppressor Gene Loss of Heterozygosity. *Cancer Cell*. 2009;16(6):475-86.
7. Losada A. Cohesin in cancer: chromosome segregation and beyond. *Nature reviews Cancer*. 2014;14(6):389-93.
8. Onn I, Heidinger-Pauli JM, Guacci V, Unal E, Koshland DE. Sister chromatid cohesion: a simple concept with a complex reality. *Annual review of cell and developmental biology*. 2008;24:105-29.
9. Horsfield JA, Print CG, Monnich M. Diverse developmental disorders from the one ring: distinct molecular pathways underlie the cohesinopathies. *Front Genet*. 2012;3:171.

10. Covo S, Westmoreland JW, Gordenin DA, Resnick MA. Cohesin Is Limiting for the Suppression of DNA Damage-Induced Recombination between Homologous Chromosomes. *Plos Genetics*. 2010;6(7).
11. Gelot C, Guirouilh-Barbat J, Le Guen T, Dardillac E, Chailleux C, Canitrot Y, et al. The Cohesin Complex Prevents the End Joining of Distant DNA Double-Strand Ends. *Mol Cell*. 2016;61(1):15-26.
12. Nigg EA, Stearns T. The centrosome cycle: Centriole biogenesis, duplication and inherent asymmetries. *Nat Cell Biol*. 2011;13(10):1154-60.
13. Wu N, Yu H. The Smc complexes in DNA damage response. *Cell Biosci*. 2012;2:5.
14. Percival SM, Thomas HR, Amsterdam A, Carroll AJ, Lees JA, Yost HJ, et al. Variations in dysfunction of sister chromatid cohesion in *esco2* mutant zebrafish reflect the phenotypic diversity of Roberts syndrome. *Dis Model Mech*. 2015;8(8):941-55.
15. Sakuno T, Tada K, Watanabe Y. Kinetochore geometry defined by cohesion within the centromere. *Nature*. 2009;458(7240):852-8.
16. Barber TD, McManus K, Yuen KW, Reis M, Parmigiani G, Shen D, et al. Chromatid cohesion defects may underlie chromosome instability in human colorectal cancers. *Proceedings of the National Academy of Sciences of the United States of America*. 2008;105(9):3443-8.
17. De Koninck M, Losada A. Cohesin Mutations in Cancer. *Cold Spring Harb Perspect Med*. 2016;6(12).

18. Mai PL, Best AF, Peters JA, DeCastro RM, Khincha PP, Loud JT, et al. Risks of first and subsequent cancers among TP53 mutation carriers in the National Cancer Institute Li-Fraumeni syndrome cohort. *Cancer*. 2016.
19. Varley JM, McGown G, Thorncroft M, Santibanez-Koref MF, Kelsey AM, Tricker KJ, et al. Germ-line mutations of TP53 in Li-Fraumeni families: an extended study of 39 families. *Cancer Res*. 1997;57(15):3245-52.
20. Donehower LA, Harvey M, Slagle BL, McArthur MJ, Montgomery CA, Jr., Butel JS, et al. Mice deficient for p53 are developmentally normal but susceptible to spontaneous tumours. *Nature*. 1992;356(6366):215-21.
21. Lowe SW, Schmitt EM, Smith SW, Osborne BA, Jacks T. p53 is required for radiation-induced apoptosis in mouse thymocytes. *Nature*. 1993;362(6423):847-9.
22. Parant JM, George SA, Holden JA, Yost HJ. Genetic modeling of Li-Fraumeni syndrome in zebrafish. *Dis Model Mech*. 2010;3(1-2):45-56.
23. Wang J, Thomas HR, Li Z, Yeo NCF, Scott HE, Dang N, et al. Puma, noxa, p53, and p63 differentially mediate stress pathway induced apoptosis. *Cell Death Dis*. 2021;12(7):659.
24. Berghmans S, Murphey RD, Wienholds E, Neuberg D, Kutok JL, Fletcher CD, et al. tp53 mutant zebrafish develop malignant peripheral nerve sheath tumors. *Proc Natl Acad Sci U S A*. 2005;102(2):407-12.
25. Venkatachalam S, Shi YP, Jones SN, Vogel H, Bradley A, Pinkel D, et al. Retention of wild-type p53 in tumors from p53 heterozygous mice: reduction of p53 dosage can promote cancer formation. *EMBO J*. 1998;17(16):4657-67.

26. Blackburn AC, McLary SC, Naeem R, Luszcz J, Stockton DW, Donehower LA, et al. Loss of heterozygosity occurs via mitotic recombination in Trp53(+/-) mice and associates with mammary tumor susceptibility of the BALB/c strain. *Cancer Research*. 2004;64(15):5140-7.
27. Suzuki T, Yasui M, Honma M. Mutator Phenotype and DNA Double-Strand Break Repair in BLM Helicase-Deficient Human Cells. *Mol Cell Biol*. 2016;36(23):2877-89.
28. LaRocque JR, Stark JM, Oh J, Bojilova E, Yusa K, Horie K, et al. Interhomolog recombination and loss of heterozygosity in wild-type and Bloom syndrome helicase (BLM)-deficient mammalian cells. *Proc Natl Acad Sci U S A*. 2011;108(29):11971-6.
29. Luo G, Santoro IM, McDaniel LD, Nishijima I, Mills M, Youssoufian H, et al. Cancer predisposition caused by elevated mitotic recombination in Bloom mice. *Nat Genet*. 2000;26(4):424-9.
30. Xue W, Kitzing T, Roessler S, Zuber J, Krasnitz A, Schultz N, et al. A cluster of cooperating tumor-suppressor gene candidates in chromosomal deletions. *Proceedings of the National Academy of Sciences of the United States of America*. 2012;109(21):8212-7.
31. Lebok P, Mittenzwei A, Kluth M, Ozden C, Taskin B, Hussein K, et al. 8p deletion is strongly linked to poor prognosis in breast cancer. *Cancer biology & therapy*. 2015;16(7):1080-7.
32. Matsuyama H, Pan Y, Oba K, Yoshihiro S, Matsuda K, Hagarth L, et al. Deletions on chromosome 8p22 may predict disease progression as well as pathological

- staging in prostate cancer. *Clinical cancer research : an official journal of the American Association for Cancer Research*. 2001;7(10):3139-43.
33. Cooke SL, Pole JC, Chin SF, Ellis IO, Caldas C, Edwards PA. High-resolution array CGH clarifies events occurring on 8p in carcinogenesis. *BMC cancer*. 2008;8:288.
 34. Ciriello G, Gatza ML, Beck AH, Wilkerson MD, Rhie SK, Pastore A, et al. Comprehensive Molecular Portraits of Invasive Lobular Breast Cancer. *Cell*. 2015;163(2):506-19.
 35. Lovat F, Ishii H, Schiappacassi M, Fassan M, Barbareschi M, Galligioni E, et al. LZTS1 downregulation confers paclitaxel resistance and is associated with worse prognosis in breast cancer. *Oncotarget*. 2014;5(4):970-7.
 36. Xue W, Krasnitz A, Lucito R, Sordella R, Vanaelst L, Cordon-Cardo C, et al. DLC1 is a chromosome 8p tumor suppressor whose loss promotes hepatocellular carcinoma. *Genes & development*. 2008;22(11):1439-44.
 37. Berger AH, Niki M, Morotti A, Taylor BS, Socci ND, Viale A, et al. Identification of DOK genes as lung tumor suppressors. *Nature genetics*. 2010;42(3):216-23.
 38. Goringe KL, Ramakrishna M, Williams LH, Sridhar A, Boyle SE, Bearfoot JL, et al. Are there any more ovarian tumor suppressor genes? A new perspective using ultra high-resolution copy number and loss of heterozygosity analysis. *Genes, chromosomes & cancer*. 2009;48(10):931-42.
 39. Rodrigues-Ferreira S, Di Tommaso A, Dimitrov A, Cazaubon S, Gruel N, Colasson H, et al. 8p22 MTUS1 gene product ATIP3 is a novel anti-mitotic protein

- underexpressed in invasive breast carcinoma of poor prognosis. *PloS one*. 2009;4(10):e7239.
40. Beuten J, Gelfond JA, Franke JL, Shook S, Johnson-Pais TL, Thompson IM, et al. Single and multivariate associations of MSR1, ELAC2, and RNASEL with prostate cancer in an ethnic diverse cohort of men. *Cancer epidemiology, biomarkers & prevention : a publication of the American Association for Cancer Research, cosponsored by the American Society of Preventive Oncology*. 2010;19(2):588-99.
 41. Ogilvy CS, Pakzaban P, Lee JM. Oculomotor nerve cavernous angioma in a patient with Roberts syndrome. *Surgical neurology*. 1993;40(1):39-42.
 42. Parry DM, Mulvihill JJ, Tsai SE, Kaiser-Kupfer MI, Cowan JM. SC phocomelia syndrome, premature centromere separation, and congenital cranial nerve paralysis in two sisters, one with malignant melanoma. *American journal of medical genetics*. 1986;24(4):653-72.
 43. Wenger SL, Blatt J, Steele MW, Lloyd DA, Bellinger M, Phebus CK, et al. Rhabdomyosarcoma in Roberts syndrome. *Cancer Genet Cytogenet*. 1988;31(2):285-9.
 44. Percival SM, Thomas HR, Amsterdam A, Carroll AJ, Lees JA, Yost HJ, et al. Variations in sister chromatid cohesion dysfunction in *esco2* mutant zebrafish reflects the phenotypic diversity of Roberts Syndrome. *Disease models & mechanisms*. 2015.
 45. Whelan G, Kreidl E, Wutz G, Egner A, Peters JM, Eichele G. Cohesin acetyltransferase *Esco2* is a cell viability factor and is required for cohesion in pericentric heterochromatin. *The EMBO journal*. 2012;31(1):71-82.

46. Varley JM, Evans DG, Birch JM. Li-Fraumeni syndrome--a molecular and clinical review. *Br J Cancer*. 1997;76(1):1-14.
47. Varley JM, Thorncroft M, McGown G, Appleby J, Kelsey AM, Tricker KJ, et al. A detailed study of loss of heterozygosity on chromosome 17 in tumours from Li-Fraumeni patients carrying a mutation to the TP53 gene. *Oncogene*. 1997;14(7):865-71.
48. Lang GA, Iwakuma T, Suh YA, Liu G, Rao VA, Parant JM, et al. Gain of function of a p53 hot spot mutation in a mouse model of Li-Fraumeni syndrome. *Cell*. 2004;119(6):861-72.
49. Jacks T, Remington L, Williams BO, Schmitt EM, Halachmi S, Bronson RT, et al. Tumor spectrum analysis in p53-mutant mice. *Curr Biol*. 1994;4(1):1-7.
50. Olive KP, Tuveson DA, Ruhe ZC, Yin B, Willis NA, Bronson RT, et al. Mutant p53 gain of function in two mouse models of Li-Fraumeni syndrome. *Cell*. 2004;119(6):847-60.
51. Malkin D, Li FP, Strong LC, Fraumeni JF, Jr., Nelson CE, Kim DH, et al. Germ line p53 mutations in a familial syndrome of breast cancer, sarcomas, and other neoplasms. *Science*. 1990;250(4985):1233-8.
52. Meehan TF, Conte N, West DB, Jacobsen JO, Mason J, Warren J, et al. Disease model discovery from 3,328 gene knockouts by The International Mouse Phenotyping Consortium. *Nat Genet*. 2017;49(8):1231-8.
53. Vanneste E, Voet T, Le Caignec C, Ampe M, Konings P, Melotte C, et al. Chromosome instability is common in human cleavage-stage embryos. *Nat Med*. 2009;15(5):577-83.

54. Johnson DS, Gemelos G, Baner J, Ryan A, Cinnioglu C, Banjevic M, et al. Preclinical validation of a microarray method for full molecular karyotyping of blastomeres in a 24-h protocol. *Hum Reprod.* 2010;25(4):1066-75.
55. Capalbo A, Wright G, Elliott T, Ubaldi FM, Rienzi L, Nagy ZP. FISH reanalysis of inner cell mass and trophectoderm samples of previously array-CGH screened blastocysts shows high accuracy of diagnosis and no major diagnostic impact of mosaicism at the blastocyst stage. *Hum Reprod.* 2013;28(8):2298-307.
56. Vazquez-Diez C, Yamagata K, Trivedi S, Haverfield J, FitzHarris G. Micronucleus formation causes perpetual unilateral chromosome inheritance in mouse embryos. *Proc Natl Acad Sci U S A.* 2016;113(3):626-31.
57. Percival SM, Parant JM. Observing Mitotic Division and Dynamics in a Live Zebrafish Embryo. *Journal of visualized experiments : JoVE.* 2016(113).
58. Stirling PC, Crisp MJ, Basrai MA, Tucker CM, Dunham MJ, Spencer FA, et al. Mutability and mutational spectrum of chromosome transmission fidelity genes. *Chromosoma.* 2012;121(3):263-75.
59. Meyer R, Fofanov V, Panigrahi A, Merchant F, Zhang N, Pati D. Overexpression and mislocalization of the chromosomal segregation protein separase in multiple human cancers. *Clinical cancer research : an official journal of the American Association for Cancer Research.* 2009;15(8):2703-10.
60. Solomon DA, Kim T, Diaz-Martinez LA, Fair J, Elkahloun AG, Harris BT, et al. Mutational inactivation of STAG2 causes aneuploidy in human cancer. *Science.* 2011;333(6045):1039-43.

61. Yamada HY, Yao Y, Wang X, Zhang Y, Huang Y, Dai W, et al. Haploinsufficiency of SGO1 results in deregulated centrosome dynamics, enhanced chromosomal instability and colon tumorigenesis. *Cell cycle*. 2012;11(3):479-88.
62. Manning AL, Yazinski SA, Nicolay B, Bryll A, Zou L, Dyson NJ. Suppression of genome instability in pRB-deficient cells by enhancement of chromosome cohesion. *Molecular cell*. 2014;53(6):993-1004.
63. Toth A, Ciosk R, Uhlmann F, Galova M, Schleiffer A, Nasmyth K. Yeast cohesin complex requires a conserved protein, Eco1p(Ctf7), to establish cohesion between sister chromatids during DNA replication. *Genes & development*. 1999;13(3):320-33.
64. Skibbens RV. Establishment of sister chromatid cohesion. *Current biology : CB*. 2009;19(24):R1126-32.
65. Rolef Ben-Shahar T, Heeger S, Lehane C, East P, Flynn H, Skehel M, et al. Eco1-dependent cohesin acetylation during establishment of sister chromatid cohesion. *Science*. 2008;321(5888):563-6.
66. Sutani T, Kawaguchi T, Kanno R, Itoh T, Shirahige K. Budding yeast Wpl1(Rad61)-Pds5 complex counteracts sister chromatid cohesion-establishing reaction. *Current biology : CB*. 2009;19(6):492-7.
67. Claussin C, Porubsky D, Spierings DCJ, Halsema N, Rentas S, Guryev V, et al. Genome-wide mapping of sister chromatid exchange events in single yeast cells using Strand-seq. *Elife*. 2017;6.
68. Krejci L, Altmannova V, Spirek M, Zhao XL. Homologous recombination and its regulation. *Nucleic Acids Research*. 2012;40(13):5795-818.

69. Lu SA, Goering M, Gard S, Xiong B, McNairn AJ, Jaspersen SL, et al. Eco1 is important for DNA damage repair in *S. cerevisiae*. *Cell Cycle*. 2010;9(16):3315-27.
70. Amsterdam A, Nissen RM, Sun Z, Swindell EC, Farrington S, Hopkins N. Identification of 315 genes essential for early zebrafish development. *Proceedings of the National Academy of Sciences of the United States of America*. 2004;101(35):12792-7.
71. Dempsey WP, Fraser SE, Pantazis P. PhOTO Zebrafish: A Transgenic Resource for In Vivo Lineage Tracing during Development and Regeneration. *Plos One*. 2012;7(3).
72. Thomas HR, Percival SM, Yoder BK, Parant JM. High-throughput genome editing and phenotyping facilitated by high resolution melting curve analysis. *PLoS One*. 2014;9(12):e114632.
73. Hwang WY, Fu Y, Reyon D, Maeder ML, Tsai SQ, Sander JD, et al. Efficient genome editing in zebrafish using a CRISPR-Cas system. *Nat Biotechnol*. 2013;31(3):227-9.
74. Percival SM, Parant JM. Observing Mitotic Division and Dynamics in a Live Zebrafish Embryo. *Jove-J Vis Exp*. 2016(113).
75. Jopling C, Sleep E, Raya M, Marti M, Raya A, Izpisua Belmonte JC. Zebrafish heart regeneration occurs by cardiomyocyte dedifferentiation and proliferation. *Nature*. 2010;464(7288):606-9.

76. Taylor AM, Shih J, Ha G, Gao GF, Zhang X, Berger AC, et al. Genomic and Functional Approaches to Understanding Cancer Aneuploidy. *Cancer Cell*. 2018;33(4):676-89 e3.
77. Cerami E, Gao J, Dogrusoz U, Gross BE, Sumer SO, Aksoy BA, et al. The cBio cancer genomics portal: an open platform for exploring multidimensional cancer genomics data. *Cancer Discov*. 2012;2(5):401-4.

CHAPTER 5

SUMMARY, CONCLUSIONS, AND FUTURE DIRECTIONS

Tumor suppressor gene TP53 is the most frequently mutated gene in various human cancers, with mutations occurring in approximately 50% of cases [115-119]. The significance of TP53 is further underscored by its association with Li-Fraumeni syndrome (LFS). In LFS, individuals often inherit one mutated TP53 allele from germline, resulting in a significantly increased risk of developing malignancies. LFS carries a high penetrance rate, with a lifetime 70% or higher lifetime risk in men and 90% in women [13, 15].

Targeting the p53 protein directly in p53-mutant cancers is challenging due to TP53 mutations that inactivate the wild-type p53 protein [18]. Researchers explore correcting structural and functional defects in mutant p53 to restore tumor-suppressive function. For example, PRIMA-1 can reactivate certain missense mutant p53, restoring its wild-type conformation and tumor-suppressive activity, including apoptosis. RITA works by disrupting heterozygous tetramers that consist of mutant p53, effectively restoring tumor-suppressive function of wild-type p53. However, these approaches might not be effective for all p53 mutations due to structural complexities [18, 42, 63, 120]. As an alternative approach, strategies to focus on enhancing p53 functions in tumor suppression by manipulating downstream effector functions, rather than directly targeting p53 protein, hold promise for the treatment of these cancers.

Further evidence emphasizes the importance of p53 as a transcription factor in its tumor-suppressive function is that patients with Li-Fraumeni syndrome (LFS), harbor primarily missense mutations in the DNA binding domain of the TP53 gene [121]. Despite more than 40 years since p53 was first characterized as a transcription factor [122, 123], the specific targets and effector functions that are essential to p53 tumor suppression remain unknown. For a long period of time, cell-cycle arrest (through p21/CDKN1A) and apoptosis (through PUMA/BBC3 and NOXA/PMAIP1) have been considered the canonical effector functions downstream of p53 tumor suppression [123].

However, recent studies suggest that these functions can be dispensable for p53 tumor suppression. For example, mice with specific p53 mutations in the transactivation domain (TAD) displayed resistance to DNA damage-induced apoptosis and cell-cycle arrest due to defective transcriptional induction of key p53 targets. Surprisingly, these mutant mice did not show accelerated tumor formation in a mutant Ras-driven transgenic model of non-small cell lung cancer, unlike p53-deficient mice [124]. Another p53 mutant strain lacking critical amino acid residues failed to induce apoptosis and cell-cycle arrest but exhibited a low incidence of spontaneous tumor formation occurring late in the mice [125]. Additionally, mice lacking Puma, Noxa, and p21 did not exhibit increased cancer predisposition, unlike p53 mutant or null mice [66]. These findings suggest that other non-canonical p53 target genes and/or effector functions may be more crucial for p53's tumor-suppressive role.

However, it is important to note that the ablation of p53-mediated apoptosis and cell-cycle arrest has only been examined in limited cell types, such as MEFs and thymocytes, in these significant studies [12-14]. Therefore, the loss of p53-regulated

apoptosis and cell-cycle arrest observed in these studies may not necessarily extend to multiple tissues or the whole organism. In our research group, before investigating other non-canonical targets and pathways, we aim to use zebrafish as a model organism to observe *p53*-induced apoptosis and cell-cycle arrest mediated by *puma*, *noxa*, and *p21*. The transparency of zebrafish embryos allows us to visualize apoptosis and cell-cycle arrest markers throughout the entire organism, providing valuable insights for further investigations.

p53-Mediated Apoptosis Mainly Occurs through the Activation of Puma in Response to IR-Irradiation

Apoptosis is primarily observed in the neural tube of 13.5-dpc mouse embryos following irradiation [126]. Similar findings have been demonstrated in zebrafish studies, where robust *p53*-dependent apoptosis occurs in the neural tube of zebrafish embryos at 24-hours post fertilization (hpf) after irradiation [89, 90, 127]. To investigate the role of *puma* and *noxa* in a *p53*-dependent apoptosis, we conducted a series of IR induced apoptosis studies. Our findings indicate the presence of at least two waves of apoptosis within the first 24 hours following irradiation. The initial wave is regulated by *p53*-*puma* axis, while the second wave occurs in *p53*- and *puma*-independent manner. The second wave of apoptosis, independent of *p53* and *puma*, may result from severe and persistent DNA damage. Unrepaired DNA lesions activate pathways like ATM and ATR kinases, leading to a separate wave of apoptosis to eliminate damaged cells. Additionally, mitotic failure caused by extensive DNA damage or replication stress can trigger mitotic cell death pathways, such as mitotic catastrophe, also independent of *p53* and *puma*. Further research

is needed to unveil the mechanisms underlying this second wave of apoptosis. Our findings highlight the significance of studying apoptosis in the neural tube following irradiation and the role of *puma* and *noxa* in p53-dependent apoptosis.

p53-Independent Apoptosis Mainly Occurs through the Activation of Puma in Response to ER and ROS Stress

In our investigations, we have showed the essential role of *p63* and *puma* in ER stress-induced apoptosis, while *p53*, *p73*, and *noxa* do not appear to be involved. Additionally, we have found that oxidative stress-induced apoptosis requires the presence of *p63*, *noxa*, and *puma*, but not *p53*, *p73* or *noxa* (as shown in Figure 1). These findings suggest the existence of distinct and shared molecular pathways in different stress responses, with *puma* acting as a common factor across these pathways.

Importantly, the loss of PUMA does not lead to any discernible morphological or tumorigenic phenotypes. Given this observation, targeting PUMA to restore apoptosis hold promise as a potential therapeutic strategy for cancer treatment.

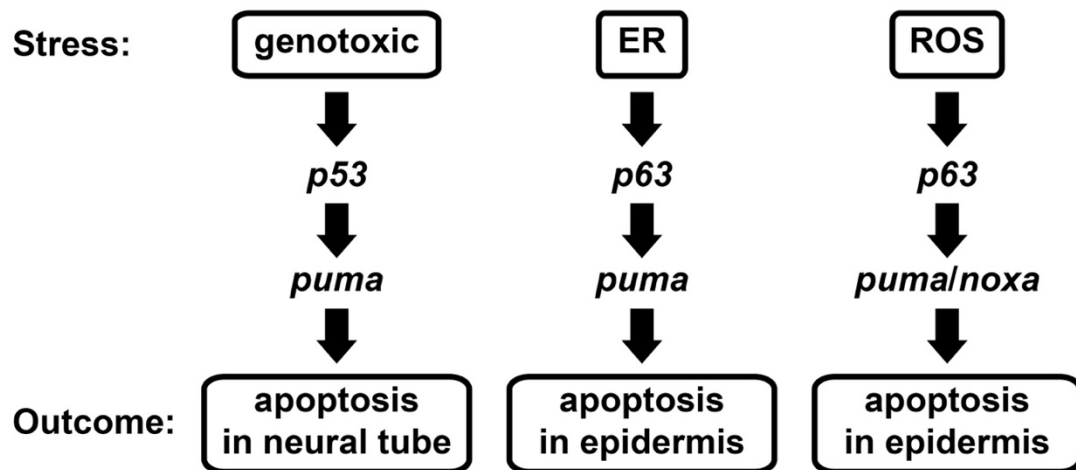


Figure 1. Schematic showing how *p53*, *p63*, *p73*, *puma* and *noxa* in response to different cellular stress in zebrafish.

Investigating Tissue-Specific Puma Expression Patterns after p53 Activation

While the epidermis is predisposed to apoptosis due to ER and ROS stress, p53-dependent apoptosis is almost exclusively induced in neural tube of both mouse and zebrafish embryos. To investigate the underlying mechanism, I first utilized a transgenic zebrafish line, where neural tube cells were labeled with GFP. Using flow cytometry, I sorted cells from the neural tube and non-neural tube regions that were subjected to IR treatment. Subsequently, I performed western blotting to analysis protein expression levels. Surprisingly, I found no significant difference in the elevated 53 protein level between two cell types, indicating that the tissue-specific induction of puma expression is not solely due to differential p53 protein levels.

To gain further insights, I conducted 10x single cell RNA sequencing (scRNA-seq) on zebrafish lacking *puma*, *noxa*, and *p21* with both IR-treated and untreated samples. Through this analysis, I identified 21 clusters in both groups. While canonical *p53* targets such as *p21*, *mdm2*, *ccng1* were significantly induced in all 21 clusters after IR, *puma* induction was observed only in five of them, specifically annotated to various neural cells. These findings suggest that the exclusive *p53*-dependent apoptosis in the neural tube results from the induction of *puma* solely within this tissue.

This raises an intriguing question: Is *p53*-mediated apoptosis not necessary for tumor suppression, considering that *puma* is not induced in cells that initiate tumors? To address this, I generated a transgenic zebrafish model called *puma:OE*, where *puma* is ectopically expressed under the control of ubiquitous promoter and Cre-based recombination. In preliminary experiments, I injected Cre mRNA into 1-cell embryos of both *puma:OE* and GFP:OE (negative control) lines. These results showed that 80%

injected *puma*:OE embryos did not survive beyond 24 hpf, compared to only 2.7% in GFP:OE embryos, suggesting excessive apoptosis induced by *puma* overexpression may occur in multiple tissues beyond the neural tube. In future studies, we plan to breed *puma*:OE with different Cre driver lines to investigate the effects of *puma* overexpression in various tissues. Additionally, we aim to restore *puma* expression in zebrafish with tumor burden that are homozygous null for *p53*, to examine whether the tumors can shrink as a result of *puma* restoration. The findings provide insights into the complex mechanisms of p53-dependent apoptosis and its potential implications for cancer research and therapies.

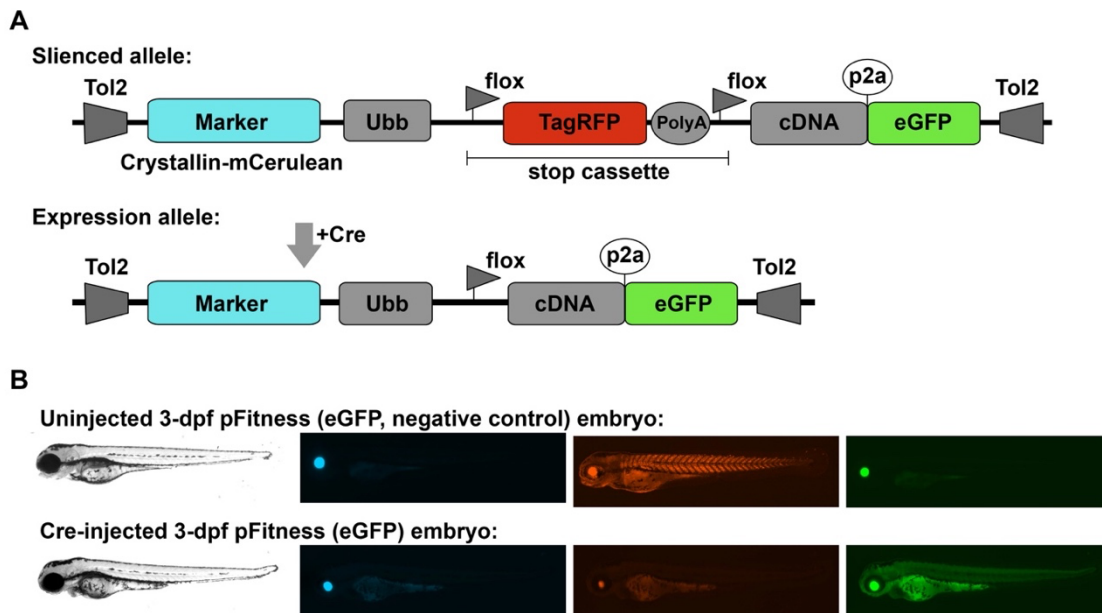


Figure 2. Generation of overexpression (OE) zebrafish line. **A.** Schematic of Cre-induced gene OE cassette. Tol2 transposon system was used for random integration of inducible OE cassette. **B.** Representative images showing the GFP expression after Cre induction at 3-dpf zebrafish embryos.

p21 is Important but Not the Sole Mediator in p53-Mediated Cell Cycle Arrest

Numerous targets of p53 involved in the regulation of the cell cycle have been identified. Among them, p21/CDKN1A, the first discovered p53 target, is considered to be of particular importance. In order to determine if *p21* also is sufficient to induce *p53*-mediated cell-cycle arrest, I quantified the number of pH3-positive cells (indicating mitotic cells) for different genotypes (wild type, *p53*^{-/-}, and *pnp*^{-/-}) in both IR-treated and *mdm2*-null zebrafish embryos over time.

Surprisingly, our findings indicate that *p21* is not the sole downstream target of *p53* in the regulation of the cell cycle, regardless of whether *p53* activation is induced by IR-irradiation or *mdm2*-null mutations. As a next step, our focus is to elucidate the other targets of p53 involved in the regulation of the cell cycle and explore non-canonical effector pathways (as illustrated in Figure 3).

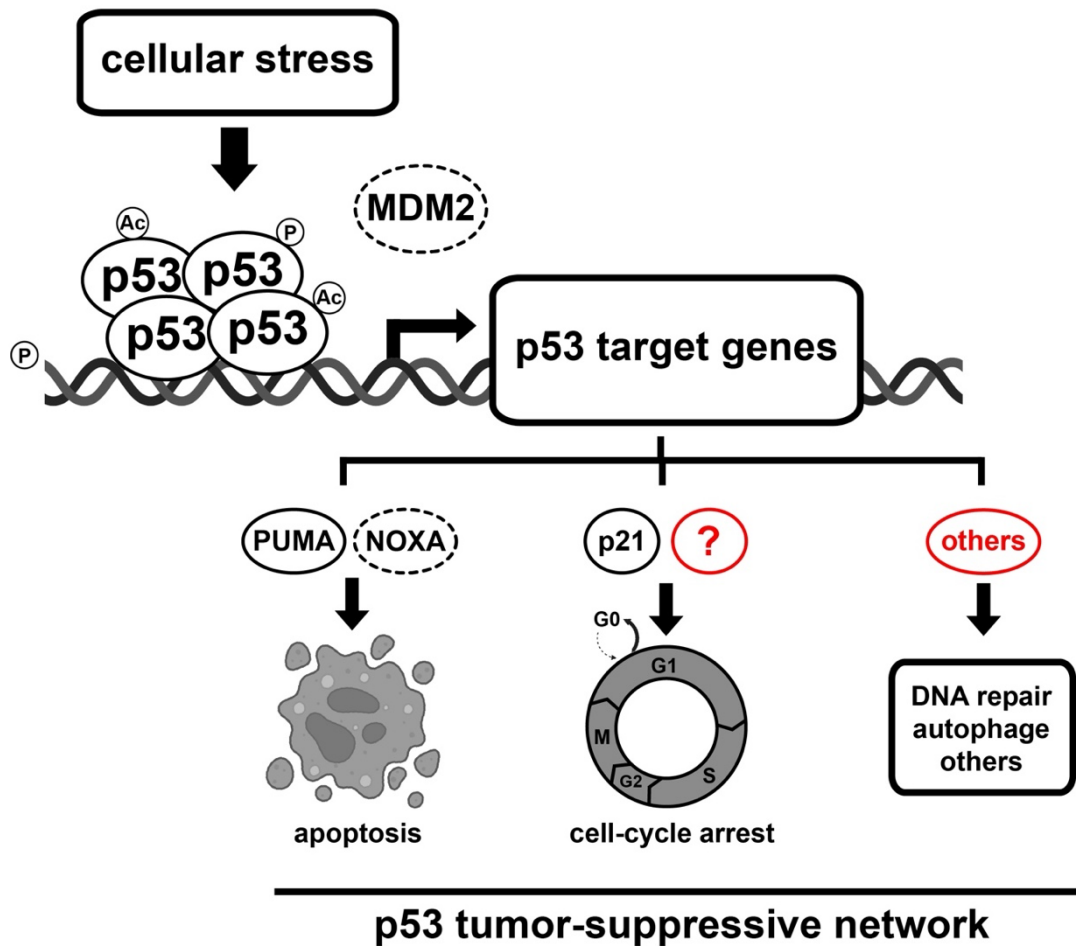


Figure 3. Proposed models depicting p53 downstream tumor-suppressive network.

(P, phosphorylation; Ac, acetylation; dashed circle of MDM2 indicating decreased or modified mdm2 that cannot destabilize p53 protein; dashed circle of NOXA indicating limited function in p53-mediate apoptosis)

Identified Conserved p53 Target Gene Candidates

The key question in the field of p53 research remains unanswered: what are the crucial targets and effector pathways of p53 that contribute to tumor suppression? Numerous effectors have been explored as potential p53 downstream pathways that functions in its tumor suppression. However, consensus has yet to be reached on the most significant downstream targets and biological processes that contribute to p53's tumor prevention capabilities [128-132].

Extensive CHIP-seq and gene expressing sequencing studies have been conducted to define p53 targets. However, upon closer examination of these datasets, it becomes apparent that the thousands of p53 target gene candidates proposed by each group are not entirely consistent. Meta-analyses have been performed to integrate and reconcile the vast amount of sequencing data. While these analyses have successfully reduced the number of candidates from thousands to hundreds, discrepancies in the identified target gene pools persist due to variations in cell types, stimulus durations, nature of stimuli, and analysis techniques employed in these studies. Another concern is that most sequencing data were generated using limited cell types, lacking the diversity found in complex organisms. Although these publicly available studies have provided a pool of potential p53 direct target genes with thousands of candidates, investigating such a large number of genes with the required "criterion" for their contribution to p53 tumor suppression is impractical.

As mentioned earlier, p53-mutant or p53-null zebrafish and mice, similar to human Li-Fraumeni Syndrome (LFS), develop early-onset tumors with 100% penetrance [19-21], indicating a highly conserved p53 regulatory network in tumor suppression among these species. In our study, we did perform a unique cross-species comprehensive analysis of

RNA-seq data to define conserved p53-upregulated across between mice and zebrafish. This analysis to define p53-upregulated genes in between mice and zebrafish led to a 50% reduction in candidate gene pool. Additionally, by analyzing whole zebrafish and mouse embryos, which encompass multiple cell and tissue types, as well as the complexity and physiology of the organism, we sought to capture a comprehensive view of p53 regulation.

To exclude secondary targets downstream of *puma*, *noxa*, and *p21*, we employed *puma*^{-/-}; *noxa*^{-/-}; *p21*^{-/-} zebrafish model for our sequencing analysis. This approach enabled us to effectively reduce the number of genes (~72% deduction) that are influenced by *puma*⁻, *noxa*⁻, and *p21*-mediated signaling pathways. Additionally, to further exclude p53-independent genes, we utilized *p53*^{-/-} zebrafish and mouse models in our analysis. By comparing the gene expression profiles between these p53-deficient models and the p53-wildtype controls, we ruled out those genes that are not influenced by p53. Furthermore, we examined *p53*-upregulated genes at both 1 and 3 hpi, focusing on identifying the earliest-responsive genes, which are more likely to be direct targets of *p53*.

For zebrafish *p53*-upregulated genes, we analyzed both mouse orthologues and paralogues to avoid overlooking important target genes. Interestingly, 79 out of the 132 genes only exhibited *p53*-induced upregulation in zebrafish paralogues, not orthologues in mice. For instance, *sesn1*, *sesn3*, and *sesn4* (*si:zfos-80g12.1*) were among the top *p53*-induced differentially expressed genes (DEGs) in zebrafish, whereas only *Sesn2* showed significant p53 induction in mice. In humans, both *SESN1* and *SESN2* are potential p53 target genes. Fischer et al. demonstrated that *SESN1* is a p53 target gene in 11 out of 16 analyzed human genome-wide datasets, whereas *SESN2* was found in only one dataset [133]. Nguyen et al. observed p53-induced upregulation of *SESN1* in 14 out of 16 analyzed

human datasets combining CHIP-seq and gene expression data, while SESN2 was detected in 5 of them.

Using these criteria and the animal models, we successfully identified 132 conserved p53-unregulated genes shared between mice and zebrafish. These genes may play a significant role in the p53 tumor-suppressive network, regulating critical cellular processes involved in tumor suppression. Their identification offers valuable insights into the molecular mechanisms of p53-mediated tumor suppression across species. More investigation is needed to explore the interactions and regulatory networks among these 132 genes, aiming to uncover essential signaling pathways that intersect with p53 signaling. Additionally, further research is required to determine whether these genes could serve as potential therapeutic targets for the development of novel anti-cancer treatments.

In summary, our cross-species transcriptome analysis significantly reduces the candidate gene pool for p53 tumor suppression targets from thousands to hundreds. These 132 conserved p53-upregulated genes are crucial in unraveling the complexities of p53-mediated tumor suppression. They offer a valuable resource for cancer research, including biomarker discovery, drug development, and a deeper understanding of p53's tumor-suppressive functions.

We next compared the 132 genes with the upregulated DEGs in *mdm2*^{-/-}; *puma*^{-/-}; *noxa*^{-/-}; *p21*^{-/-} (referred to as *mpnp*) zebrafish versus sibling controls, identifying 108 genes that overlapped. This suggests that the p53 regulatory network exhibits relative conservation in response to different stimuli. However, there are still 24 genes that do not appear in the *mpnp* dataset. For example, *myl7* and *myh7* are conserved p53-upregulated genes, yet they were scarcely detected in our *mpnp* data. This discrepancy may be attributed

to the fact that *myl7* and *myh7* encode myosin regulatory heavy chain proteins primarily expressed in the heart, which may not be fully formed at the 18 hpf timepoint when the *mpnp* data were collected. These findings suggest that the response of certain tissues to *p53* activation may not be captured fully, emphasizing the need for further research in this area.

Identification of *ccng1*, *fbxw7* and *foxo3b* as Important

Components of p53-Dependent Cell-cycle Arrest

The most reliable criterion for determining the functional significance of genes and effector pathways in tumor suppression is to assess their impact on timing of tumor onset or progression *in vivo*. [18]. Toward this the most effective approach is to perform gene ablation experiments and closely monitor the resulting tumor cohort for timing of tumor onset and spectrum. If the ablation of a particular gene leads to accelerated tumorigenesis, it indicates that the gene is crucial for p53's tumor-suppressive function. On the other hand, if the ablation does not result in tumor development, the gene can be considered dispensable or redundant. However, it is important to note that generating animal models and monitoring tumor cohorts for such studies can be a time-consuming process, often taking 2-3 years even for the validation of a single gene.

To overcome the time constraints associated with conducting extensive tumor cohort analyses, we utilized the *mdm2*^{-/-}; *puma*^{-/-}; *noxa*^{-/-}; *p21*^{-/-} (referred to as *mpnp*^{-/-}) zebrafish model in our study. This model exhibits morphological lethality and impaired cell-cycle regulation, both of which are p53-dependent. We consider this model ideal for investigating p53 tumor suppression, as it does not rely on external oncogenic or stress signals, allowing us to focus specifically on the regulation of transcriptional and effector

pathways by p53. The systemic effects of p53 in this model reflect its role in preventing tumor initiation and progression. By employing CRISPR/Cas9 gene editing technology, we individually knocked out the top 24 cell cycle related genes of interest (GOIs) in the *mpnp*^{-/-} zebrafish. Through this approach, we identified *ccng1*, *fbxw7*, and *foxo3b* as important genes involved in p53-dependent cell-cycle arrest.

The *ccng1* gene, also known as Cyclin G1, is a member of the cyclin family of protein, which play an important role in the cell cycle machinery and are involved in the activation of cyclin-dependent kinases (CDKs) that control cell progression through different phases of the cell cycle. *ccng1* has been identified as a transcriptional target of p53 in response to various cellular stresses, including DNA damage or oncogenic signaling. Previous studies also have provided evidence suggesting that *ccng1* may have tumor-suppressive functions. Altered expression of *ccng1* has been observed in various types of cancers, highlighting its potential role in tumorigenesis. *ccng1* has been shown to inhibit cell growth and promote cell cycle arrest, preventing the uncontrolled proliferation of damaged or abnormal cells and providing time for DNA repair or other cellular responses.

Indeed, *fbxw7* has been recognized as a tumor suppressor gene due to its role in ubiquitin-mediated protein degradation of a variety of substrates involved in critical cellular processes. One notable target of Fbxw7 is cyclin E, a protein that drives cell cycle progression. Through the degradation of cyclin E, Fbxw7 helps ensure proper cell cycle progression and prevents uncontrolled cell division. The dysregulation of Fbxw7 has been implicated in the development of several types of cancers, including colorectal cancer, gastric cancer, and T-cell acute lymphoblastic leukemia. Additionally, activation of p53 has been shown to upregulate the expression of Fbxw7. In summary, Fbxw7 acts as a tumor

suppressor gene by orchestrating the degradation of critical proteins involved in cell cycle progression, differentiation, and apoptosis.

foxo3b, the zebrafish orthologue of human FOXO3, shares functional similarities with its human counterpart. It belongs to the FOXO family of transcription factors, which is primarily known for its role in promoting cell cycle arrest and inducing apoptosis. Foxo3b, like FOXO3, acts as a transcription factor, modulating the expression of genes involved in these processes. One of the essential functions of FOXO3 is to promote cell cycle arrest by activating cell cycle inhibitors. By upregulating the expression of these inhibitors, FOXO3 can halt cell division, preventing aberrant proliferation of damaged or abnormal cells. Alterations in FOXO3 expression or activity have been observed in various cancers. Furthermore, p53 can physically interact with FOXO3 and influence its transcriptional activity. This interaction between p53 and FOXO3 can result in enhanced transcriptional regulation of target genes, leading to more robust cell cycle arrest and apoptosis induction.

Overcoming Challenges in Identifying p53 Target Genes and Unraveling Tissue-Specific Roles in Tumor Suppression

Studying *ccng1*, *fbxw7*, and *foxo3b* in the context of tumor suppression regulated by p53 can enhance our understanding of the underlying mechanisms of tumor development, progression, and response to treatment. This knowledge may contribute to the development of targeted therapies and improved strategies for cancer prevention and treatment.

One caveat to consider is that even though zebrafish provide advantages for rapid screening of target genes using CRISPR/Cas9 G0 crispants, fully identifying all the targets of *p53* as a transcription factor remains challenging. First of all, the candidate pool of potential target gene is still quite large, and it requires further investigation to determine which genes are directly regulated by *p53*. Secondly, in our study, we utilized a rescue strategy to validate the GOIs one by one, with the expectation that they would act as primary target genes involved in specific *p53* effector functions.

However, it is important to note that *p53* likely regulates multiple target genes simultaneously, and their combined effects may contribute to tumor suppression. If this is the case, we may need to employ guide RNAs to target multiple genes in our future experiments in order to fully understand their contributions to *p53*-mediated tumor suppression. During our validation process, certain genes, such as *fbxw7*, *foxo3b*, and *ccng1*, showed promising results by partially rescue the cell-cycle arrest phenotype. These genes warrant further examination using a combinational injection method. It would be particularly interesting to investigate whether the absence of these three genes in *pnp*^{-/-} animals leads to a tumor onset rate equivalent to that of *p53*-null animals. Although this might seem challenging, due to the requirement to knock out six genes, the advantages of the zebrafish model make it a feasible endeavor. By utilizing the zebrafish model, we can overcome some of the challenges associated with studying multiple gene knockouts and gain valuable insights into the tumor-suppressive functions of *p53*.

In our research, to assess the involvement of the conserved genes in *p53*-mediated cell cycle arrest, we have conducted tests on 24 GOIs and observed that three of them contribute to *p53*-mediated cell cycle arrest. However, none of these genes individually

showed the ability to fully rescue the gross phenotype of *mdm2*-null zebrafish. These findings suggest that multiple downstream pathways of *p53* may be responsible for the rescue of *mdm2*-null induced embryonic lethality. To rescue the lethal phenotype and further investigate these targets in the context of *p53*-mediated tumor suppression, multiplex injection targeting multiple gene concurrently is necessary. By the careful design and execution of multiplex injection experiments, we can simultaneously knockout these genes in zebrafish embryos and assess the collective impact on tumor onset and progression. This strategy allows for the investigation of the synergistic or additive effects of multiple genes, providing a deeper understanding of their contribution of *p53*-mediated tumor suppression. This approach holds the potential to uncover novel mechanisms underlying *p53*-mediated tumor suppression and inform tumor therapeutic strategies.

Moreover, our previous scRNA-seq data has revealed that the induction of *p53* target genes occurs in a tissue-specific manner. This finding highlights the importance of studying the rescue effects of these genes in different tissues. To address this, it would be valuable to generate *mdm2* conditional knockout models that allow for tissue-specific manipulation of *p53* activity. By selectively inactivating *mdm2* in specific tissues, we can examine the extent to which the rescued phenotype is observed in different cellular contexts. This approach will enhance our understanding of the tissue-specific mechanisms underlying *p53*-mediated tumor suppression and pave the way for the development of targeted therapeutic strategies for different types of cancers.

**Reduced Sister Chromatid Cohesion Acts as Modifier for p53 LOH
And Tumor Penetrance in p53 Heterozygous Null Background**

Loss of heterozygosity (LOH) is a common occurrence associated with the inactivation of functional tumor suppressor genes in cancer formation. ESCO2 is required for the establishment of sister chromatid cohesin (SCC) during the S phase. Mutations in ESCO2 are linked to a genetic disorder, known as Robert/SC phocomelia Syndrome (RBS). Patients with a severe form of RBS often die in utero or shortly after birth, while mildly affected patients may live into adulthood, exhibiting reduced SCC and an increased risk of early-onset tumors [134-136]. Our zebrafish model with homozygous mutations in the *esco2* gene results in embryonic lethal due to complete loss of cohesin in most cells [113]. In this study, we demonstrate that *esco2* haploinsufficiency results in reduced SCC and promotes tumor predisposition (without affecting viability) in both mice and zebrafish. These findings suggest that reduced SCC may promote tumors across different species. Another pro-cohesin factor, Shugoshin (SGO1), plays a role in protecting centromeric cohesin and ensuring faithful chromosome segregation [137-140]. Haploinsufficiency of SGO1 is also associated with tumorigenesis in humans [141-144]. Using a zebrafish model with a mutant *sgo1* gene (resulting in embryonic lethality), we found that, similar to *esco2*, haploinsufficiency of *sgo1* leads to reduced SCC and elevates tumor predisposition.

Under normal circumstances, sister chromatids are held together by cohesin, making them an ideal source for homologous recombination. However, reduced SCC allows homologous chromosomes to interact and undergo recombination, potentially leading to homozygosity in specific chromosome regions (known as mitotic recombination) and resulting in LOH events [145, 146].

Interestingly, tumor onset within LFS occurs over a wide range of ages. Some infants with LFS develop tumors within the first year of life, while others remain tumor-

free until their seventies. This variation in timing may be influenced by factors such as genetic heterogeneity and the environment in which individuals live. However, even in research settings where p53 heterozygous-mutant zebrafish and mice share identical environments and heritable backgrounds, variability in tumor onset still exists, suggesting the involvement of stochastic events. Complete inactivation of p53 is typically required for tumorigenesis, so these stochastic events may drive p53 LOH in somatic tissues.

Reduced SCC has the potential to drive p53 LOH by shortening the time window for tumor onset between p53 homozygous and heterozygous mutants, which is necessary for the occurrence of the second p53 hit. Consequently, additional research efforts will focus on investigating the specific role of reduced SCC in promoting tumor formation and elucidating the underlying mechanisms that determine whether p53 LOH plays a key role in this process. Additionally, we explore the impact of LOH events resulting from reduced SCC on the inactivation of p53, in somatic tissues. The frequency and consequences of p53 LOH in various cell types prior to tumor initiation will be examined to assess their implications for tumorigenesis. Furthermore, further research will be conducted to identify and characterize other factors involved in SCC and cohesion protection, and to explore their potential associations with tumor predisposition and LOH events. Given the complexity of human tumorigenesis, including the interplay of genetic and environmental factors, we recognize the importance of investigating these specific mechanisms with human samples to enhance the translational potential of the findings.

Monitoring p53 LOH in Somatic Tissues at Single-Cell Level

The most effective approach is to assess p53 LOH in somatic cells before tumor initiation rather than focusing solely on tumors. While it is relatively straightforward to measure p53 LOH in tumors using bulk-based techniques due to the clonality of genomic DNA, a concern arises as tumors represent the end stages of carcinogenesis. Therefore, it becomes important to determine whether p53 LOH contributes to tumor initiation or is a secondary consequence of tumor development. Surprisingly, our knowledge regarding the frequency of p53 LOH, survival of LOH cells, and the potential tissue-specific differences in LOH rates in somatic tissues remains limited. This limitation primarily arises from the lack of techniques that enable accurate monitoring of p53 LOH events at the single-cell level.

To overcome the limitation, we have developed a transgenic zebrafish model using CRSPR/Cas9 knock-in technology in which the wildtype and null alleles are labeled with different fluorescence proteins. This model labels cells carrying the wild-type p53 allele with eGFP and cells carrying the p53-null allele with mCherry (Figure 4). By employing light-sheeting and confocal imaging, we can easily identify p53 LOH events in individual organisms and cells during embryonic development. We will breed the *esco2* mutation into our transgenic p53 allele to generate *esco2*^{+/-}; p53^{GFP/Cherry} line. With this model, we aim to evaluate whether there is a difference in p53 LOH occurrence in somatic tissues between *esco2*^{+/-}; p53^{GFP/Cherry} and *esco2*^{+/+}; p53^{GFP/Cherry}. We hypothesize that individuals with a higher p53 LOH ratio at a certain timepoint may develop spontaneous tumors at an earlier stage. Furthermore, we will explore p53 LOH rates in different cell and tissue types during somatic tissue development and tumor initiation. In addition, we will investigate other

factors or genetic modifiers that may influence p53 LOH, potentially accounting for the observed variability in tumor-onset timing.

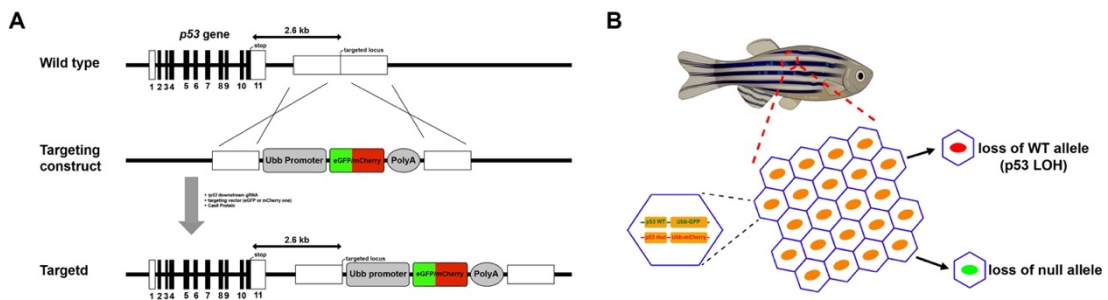


Figure 4. Generation and validation of transgenic fish to visualize p53 LOH in somatic tissues. **A.** Schematic of insertion of ubiquitous promoter driven GFP or mCherry into downstream p53 wildtype or null alleles, respectively. **B.** Cartoon showing loss of WT allele (p53 LOH) and null allele.

Collectively, these studies aimed to address critical questions in the fields of cancer and p53 research. The investigation of PUMA shed light on both convergent and unique molecular pathways involved in cell death, showing that it can be triggered in a p53-dependent or -independent manner in response to different stresses. Additionally, the apoptotic patterns were found to be tissue-specific, driven by distinct signaling pathways. Considering that PUMA is a shared protein in these pathways, it represents a promising target for therapeutic interventions in cancers, particularly those with p53 mutations.

The study on the p53 transcriptome identified a pool of candidate genes downstream of p53 that are conserved across human, mouse, and zebrafish. These genes play a significant role in p53 tumor suppression, highlighting the conservation of p53's tumor-suppressive function across species. The findings provide valuable insights into potential targets for therapeutic strategies aimed at enhancing p53-mediated tumor suppression.

To identify those targets that promote p53-mediated cell-cycle arrest, we developed a zebrafish model system of *mdm2*^{-/-}; *puma*^{-/-}; *noxa*^{-/-}; *p21*^{-/-} (referred to as *mpnp*^{-/-}), which exhibits morphological lethality and impaired cell-cycle regulation in a p53-dependent manner. This model allows us to focus specifically on the transcriptional and effector pathways regulated by p53, without the need for external stress signals. Employing CRISPR/Cas9 gene editing technique, we have individually knocked out the top 24 genes of interest in the *mpnp*^{-/-} zebrafish and identified *ccng1*, *fbxw7*, and *foxo3b* as significant genes involved in the regulation of cell-cycle arrest by p53. These findings provide valuable insights into the transcriptional and effector pathways involved in p53-mediated tumor suppression and its role in preventing tumor initiation and progression.

Furthermore, the *esco2* study provided evidence suggesting that defects in proteins involved in sister chromatid cohesion could be associated with tumor initiation by affecting loss of heterozygosity (LOH) of tumor suppressor genes. Evaluating LOH, such as RB and p53, in somatic tissues could serve as a potent biomarker to predict cancer incidence and risk. Understanding the functions of p53, including its tumor-suppressive network and the dynamics and mechanisms of p53 LOH, is expected to have a positive impact on the field of cancer research, particularly in the treatment of cancers with p53 mutations.

Overall, these studies contribute to advancing our knowledge of the complex roles and mechanisms of p53 in cancer development and provide potential targets for therapeutic interventions, with the ultimate goal of improving cancer treatments, especially for those with p53 mutations.

GENERAL LIST OF REFERENCES:

1. Bailey, M.H., et al., *Comprehensive Characterization of Cancer Driver Genes and Mutations*. Cell, 2018. **174**(4): p. 1034-1035.
2. Cancer Genome Atlas, N., *Comprehensive molecular portraits of human breast tumours*. Nature, 2012. **490**(7418): p. 61-70.
3. Olivier, M., et al., *The clinical value of somatic TP53 gene mutations in 1,794 patients with breast cancer*. Clin Cancer Res, 2006. **12**(4): p. 1157-67.
4. Petitjean, A., et al., *TP53 mutations in human cancers: functional selection and impact on cancer prognosis and outcomes*. Oncogene, 2007. **26**(15): p. 2157-65.
5. Ahrendt, S.A., et al., *p53 mutations and survival in stage I non-small-cell lung cancer: results of a prospective study*. J Natl Cancer Inst, 2003. **95**(13): p. 961-70.
6. Levine, A.J. and E. Vosburgh, *P53 mutations in lymphomas: position matters*. Blood, 2008. **112**(8): p. 2997-8.
7. Samowitz, W.S., et al., *Prognostic significance of p53 mutations in colon cancer at the population level*. Int J Cancer, 2002. **99**(4): p. 597-602.
8. Donehower, L.A., et al., *Integrated Analysis of TP53 Gene and Pathway Alterations in The Cancer Genome Atlas*. Cell Rep, 2019. **28**(11): p. 3010.
9. Sasaki, K., et al., *Different impacts of TP53 mutations on cell cycle-related gene expression among cancer types*. Sci Rep, 2023. **13**(1): p. 4868.

10. Kleihues, P., et al., *Tumors associated with p53 germline mutations: a synopsis of 91 families*. Am J Pathol, 1997. **150**(1): p. 1-13.
11. Varley, J.M., D.G. Evans, and J.M. Birch, *Li-Fraumeni syndrome--a molecular and clinical review*. Br J Cancer, 1997. **76**(1): p. 1-14.
12. Varley, J.M., et al., *Germ-line mutations of TP53 in Li-Fraumeni families: an extended study of 39 families*. Cancer Res, 1997. **57**(15): p. 3245-52.
13. Schneider, K., et al., *Li-Fraumeni Syndrome*, in *GeneReviews((R))*, M.P. Adam, et al., Editors. 1993: Seattle (WA).
14. Varley, J.M., *Germline TP53 mutations and Li-Fraumeni syndrome*. Hum Mutat, 2003. **21**(3): p. 313-20.
15. Chompret, A., et al., *P53 germline mutations in childhood cancers and cancer risk for carrier individuals*. Br J Cancer, 2000. **82**(12): p. 1932-7.
16. Malkin, D., et al., *Germ line p53 mutations in a familial syndrome of breast cancer, sarcomas, and other neoplasms*. Science, 1990. **250**(4985): p. 1233-8.
17. Shieh, S.Y., et al., *DNA damage-induced phosphorylation of p53 alleviates inhibition by MDM2*. Cell, 1997. **91**(3): p. 325-34.
18. Kasthuber, E.R. and S.W. Lowe, *Putting p53 in Context*. Cell, 2017. **170**(6): p. 1062-1078.
19. Kaiser, A.M. and L.D. Attardi, *Deconstructing networks of p53-mediated tumor suppression in vivo*. Cell Death & Differentiation, 2017. **25**(1): p. 93-103.
20. Jones, S.N., et al., *Rescue of embryonic lethality in Mdm2-deficient mice by absence of p53*. Nature, 1995. **378**(6553): p. 206-8.

21. Montes de Oca Luna, R., D.S. Wagner, and G. Lozano, *Rescue of early embryonic lethality in mdm2-deficient mice by deletion of p53*. Nature, 1995. **378**(6553): p. 203-6.
22. Haupt, Y., et al., *Mdm2 promotes the rapid degradation of p53*. Nature, 1997. **387**(6630): p. 296-9.
23. Honda, R., H. Tanaka, and H. Yasuda, *Oncoprotein MDM2 is a ubiquitin ligase E3 for tumor suppressor p53*. FEBS Lett, 1997. **420**(1): p. 25-7.
24. Kubbutat, M.H., S.N. Jones, and K.H. Vousden, *Regulation of p53 stability by Mdm2*. Nature, 1997. **387**(6630): p. 299-303.
25. Wafik S. El-Deiry, T.T., Victor E. Velculescu, Daniel B. Levy, Ramon Parsons, Jeffrey M. Trent, David Lin, W. Edward Mercer, Kenneth W. Kinzler and Bert Vogelstein, *WAF1, a Potential Mediator of p53 Tumor Suppression*. Cell, 1993. **75**: p. 9.
26. Harper, J.W., et al., *The p21 Cdk-interacting protein Cip1 is a potent inhibitor of G1 cyclin-dependent kinases*. Cell, 1993. **75**(4): p. 805-16.
27. Miyashita, T., et al., *Tumor suppressor p53 is a regulator of bcl-2 and bax gene expression in vitro and in vivo*. Oncogene, 1994. **9**(6): p. 1799-805.
28. el-Deiry, W.S., et al., *WAF1/CIP1 is induced in p53-mediated G1 arrest and apoptosis*. Cancer Res, 1994. **54**(5): p. 1169-74.
29. Xiong, Y., et al., *p21 is a universal inhibitor of cyclin kinases*. Nature, 1993. **366**(6456): p. 701-4.
30. Harper, J.W., et al., *Inhibition of cyclin-dependent kinases by p21*. Mol Biol Cell, 1995. **6**(4): p. 387-400.

31. Abbas, T. and A. Dutta, *p21 in cancer: intricate networks and multiple activities*. Nat Rev Cancer, 2009. **9**(6): p. 400-14.
32. Warfel, N.A. and W.S. El-Deiry, *p21WAF1 and tumorigenesis: 20 years after*. Curr Opin Oncol, 2013. **25**(1): p. 52-8.
33. Deng, C., et al., *Mice lacking p21CIP1/WAF1 undergo normal development, but are defective in G1 checkpoint control*. Cell, 1995. **82**(4): p. 675-84.
34. Macleod, K.F., et al., *p53-dependent and independent expression of p21 during cell growth, differentiation, and DNA damage*. Genes Dev, 1995. **9**(8): p. 935-44.
35. Fulda, S., et al., *Cellular stress responses: cell survival and cell death*. Int J Cell Biol, 2010. **2010**: p. 214074.
36. Wang, S. and R.J. Kaufman, *The impact of the unfolded protein response on human disease*. J Cell Biol, 2012. **197**(7): p. 857-67.
37. Lindholm, D., et al., *Recent Insights into the Role of Unfolded Protein Response in ER Stress in Health and Disease*. Front Cell Dev Biol, 2017. **5**: p. 48.
38. Fisher, S.A., B.L. Langille, and D. Srivastava, *Apoptosis during cardiovascular development*. Circ Res, 2000. **87**(10): p. 856-64.
39. Jackson, S.P. and J. Bartek, *The DNA-damage response in human biology and disease*. Nature, 2009. **461**(7267): p. 1071-8.
40. Lowe, S.W. and A.W. Lin, *Apoptosis in cancer*. Carcinogenesis, 2000. **21**(3): p. 485-95.
41. O'Driscoll, M., *Diseases associated with defective responses to DNA damage*. Cold Spring Harb Perspect Biol, 2012. **4**(12).

42. Vousden, K.H. and D.P. Lane, *p53 in health and disease*. Nat Rev Mol Cell Biol, 2007. **8**(4): p. 275-83.
43. Singh, R., A. Letai, and K. Sarosiek, *Regulation of apoptosis in health and disease: the balancing act of BCL-2 family proteins*. Nat Rev Mol Cell Biol, 2019. **20**(3): p. 175-193.
44. Hatok, J. and P. Racay, *Bcl-2 family proteins: master regulators of cell survival*. Biomol Concepts, 2016. **7**(4): p. 259-70.
45. Opferman, J.T. and A. Kothari, *Anti-apoptotic BCL-2 family members in development*. Cell Death Differ, 2018. **25**(1): p. 37-45.
46. Brunelle, J.K. and A. Letai, *Control of mitochondrial apoptosis by the Bcl-2 family*. J Cell Sci, 2009. **122**(Pt 4): p. 437-41.
47. Hekisz, P. and Z.M. Kilianska, *PUMA, a critical mediator of cell death--one decade on from its discovery*. Cell Mol Biol Lett, 2012. **17**(4): p. 646-69.
48. Oda, E., et al., *Noxa, a BH3-only member of the Bcl-2 family and candidate mediator of p53-induced apoptosis*. Science, 2000. **288**(5468): p. 1053-8.
49. Melino, G., et al., *Functional regulation of p73 and p63: development and cancer*. Trends Biochem Sci, 2003. **28**(12): p. 663-70.
50. Levrero, M., et al., *The p53/p63/p73 family of transcription factors: overlapping and distinct functions*. J Cell Sci, 2000. **113** (Pt 10): p. 1661-70.
51. Botchkarev, V.A. and E.R. Flores, *p53/p63/p73 in the epidermis in health and disease*. Cold Spring Harb Perspect Med, 2014. **4**(8).
52. Melino, G., V. De Laurenzi, and K.H. Vousden, *p73: Friend or foe in tumorigenesis*. Nat Rev Cancer, 2002. **2**(8): p. 605-15.

53. Belyi, V.A. and A.J. Levine, *One billion years of p53/p63/p73 evolution*. Proc Natl Acad Sci U S A, 2009. **106**(42): p. 17609-10.
54. Yang, A., et al., *p63, a p53 homolog at 3q27-29, encodes multiple products with transactivating, death-inducing, and dominant-negative activities*. Mol Cell, 1998. **2**(3): p. 305-16.
55. Reimertz, C., et al., *Gene expression during ER stress-induced apoptosis in neurons: induction of the BH3-only protein Bbc3/PUMA and activation of the mitochondrial apoptosis pathway*. J Cell Biol, 2003. **162**(4): p. 587-97.
56. Pyati, U.J., et al., *p63 mediates an apoptotic response to pharmacological and disease-related ER stress in the developing epidermis*. Dev Cell, 2011. **21**(3): p. 492-505.
57. Melino, G., et al., *p73 Induces apoptosis via PUMA transactivation and Bax mitochondrial translocation*. J Biol Chem, 2004. **279**(9): p. 8076-83.
58. Youle, R.J. and A. Strasser, *The BCL-2 protein family: opposing activities that mediate cell death*. Nat Rev Mol Cell Biol, 2008. **9**(1): p. 47-59.
59. Villunger, A., et al., *p53- and drug-induced apoptotic responses mediated by BH3-only proteins puma and noxa*. Science, 2003. **302**(5647): p. 1036-8.
60. Ming, L., et al., *Sp1 and p73 activate PUMA following serum starvation*. Carcinogenesis, 2008. **29**(10): p. 1878-84.
61. Wu, B., et al., *p53 independent induction of PUMA mediates intestinal apoptosis in response to ischaemia-reperfusion*. Gut, 2007. **56**(5): p. 645-54.
62. Qin, J.Z., et al., *p53-independent NOXA induction overcomes apoptotic resistance of malignant melanomas*. Mol Cancer Ther, 2004. **3**(8): p. 895-902.

63. Aubrey, B.J., et al., *How does p53 induce apoptosis and how does this relate to p53-mediated tumour suppression?* Cell Death & Differentiation, 2017. **25**(1): p. 104-113.
64. Klimovich, B., et al., *p53 partial loss-of-function mutations sensitize to chemotherapy.* Oncogene, 2022. **41**(7): p. 1011-1023.
65. Arnoff, T.E. and W.S. El-Deiry, *CDKN1A/p21(WAF1), RB1, ARID1A, FLG, and HRNR mutation patterns provide insights into urinary tract environmental exposure carcinogenesis and potential treatment strategies.* Am J Cancer Res, 2021. **11**(11): p. 5452-5471.
66. Valente, L.J., et al., *p53 efficiently suppresses tumor development in the complete absence of its cell-cycle inhibitory and proapoptotic effectors p21, Puma, and Noxa.* Cell Rep, 2013. **3**(5): p. 1339-45.
67. Sammons, M.A., et al., *Tumor suppressor p53: from engaging DNA to target gene regulation.* Nucleic Acids Res, 2020. **48**(16): p. 8848-8869.
68. Nguyen, T.T., et al., *Revealing a human p53 universe.* Nucleic Acids Res, 2018. **46**(16): p. 8153-8167.
69. Kenzelmann Broz, D., et al., *Global genomic profiling reveals an extensive p53-regulated autophagy program contributing to key p53 responses.* Genes Dev, 2013. **27**(9): p. 1016-31.
70. Li, M., et al., *Distinct regulatory mechanisms and functions for p53-activated and p53-repressed DNA damage response genes in embryonic stem cells.* Mol Cell, 2012. **46**(1): p. 30-42.

71. Tonelli, C., et al., *Genome-wide analysis of p53-regulated transcription in Myc-driven lymphomas*. *Oncogene*, 2017. **36**(21): p. 2921-2929.
72. Postlethwait, J.H., et al., *Vertebrate genome evolution and the zebrafish gene map*. *Nat Genet*, 1998. **18**(4): p. 345-9.
73. Howe, K., et al., *The zebrafish reference genome sequence and its relationship to the human genome*. *Nature*, 2013. **496**(7446): p. 498-503.
74. Langheinrich, U., *Zebrafish: a new model on the pharmaceutical catwalk*. *Bioessays*, 2003. **25**(9): p. 904-12.
75. White, R., K. Rose, and L. Zon, *Zebrafish cancer: the state of the art and the path forward*. *Nat Rev Cancer*, 2013. **13**(9): p. 624-36.
76. Parant, J.M., et al., *Genetic modeling of Li-Fraumeni syndrome in zebrafish*. *Dis Model Mech*, 2010. **3**(1-2): p. 45-56.
77. Stainier, D.Y., et al., *Mutations affecting the formation and function of the cardiovascular system in the zebrafish embryo*. *Development*, 1996. **123**: p. 285-92.
78. Xi, Y., S. Noble, and M. Ekker, *Modeling neurodegeneration in zebrafish*. *Curr Neurol Neurosci Rep*, 2011. **11**(3): p. 274-82.
79. Patton, E.E., et al., *BRAF mutations are sufficient to promote nevi formation and cooperate with p53 in the genesis of melanoma*. *Curr Biol*, 2005. **15**(3): p. 249-54.
80. Neiswender, J.V., et al., *KIT Suppresses BRAF(V600E)-Mutant Melanoma by Attenuating Oncogenic RAS/MAPK Signaling*. *Cancer Res*, 2017. **77**(21): p. 5820-5830.

81. Brodsky, M.H., et al., *Drosophila p53 binds a damage response element at the reaper locus*. Cell, 2000. **101**(1): p. 103-13.
82. Ollmann, M., et al., *Drosophila p53 is a structural and functional homolog of the tumor suppressor p53*. Cell, 2000. **101**(1): p. 91-101.
83. Derry, W.B., A.P. Putzke, and J.H. Rothman, *Caenorhabditis elegans p53: role in apoptosis, meiosis, and stress resistance*. Science, 2001. **294**(5542): p. 591-5.
84. Schumacher, B., et al., *The C. elegans homolog of the p53 tumor suppressor is required for DNA damage-induced apoptosis*. Curr Biol, 2001. **11**(21): p. 1722-7.
85. Lu, W.J. and J.M. Abrams, *Lessons from p53 in non-mammalian models*. Cell Death Differ, 2006. **13**(6): p. 909-12.
86. Donehower, L.A., et al., *Mice deficient for p53 are developmentally normal but susceptible to spontaneous tumours*. Nature, 1992. **356**(6366): p. 215-21.
87. Clarke, A.R., et al., *Thymocyte apoptosis induced by p53-dependent and independent pathways*. Nature, 1993. **362**(6423): p. 849-52.
88. Lowe, S.W., et al., *p53 is required for radiation-induced apoptosis in mouse thymocytes*. Nature, 1993. **362**(6423): p. 847-9.
89. Wang, J., et al., *Puma, noxa, p53, and p63 differentially mediate stress pathway induced apoptosis*. Cell Death Dis, 2021. **12**(7): p. 659.
90. Berghmans, S., et al., *tp53 mutant zebrafish develop malignant peripheral nerve sheath tumors*. Proc Natl Acad Sci U S A, 2005. **102**(2): p. 407-12.
91. Jacks, T., et al., *Tumor spectrum analysis in p53-mutant mice*. Curr Biol, 1994. **4**(1): p. 1-7.

92. Donehower, L.A., *The p53-deficient mouse: a model for basic and applied cancer studies*. Semin Cancer Biol, 1996. **7**(5): p. 269-78.
93. Birch, J.M., et al., *Prevalence and diversity of constitutional mutations in the p53 gene among 21 Li-Fraumeni families*. Cancer Res, 1994. **54**(5): p. 1298-304.
94. Horio, Y., et al., *Predominantly tumor-limited expression of a mutant allele in a Japanese family carrying a germline p53 mutation*. Oncogene, 1994. **9**(4): p. 1231-5.
95. Lubbe, J., et al., *Familial brain tumour syndrome associated with a p53 germline deletion of codon 236*. Brain Pathol, 1995. **5**(1): p. 15-23.
96. Venkatachalam, S., et al., *Retention of wild-type p53 in tumors from p53 heterozygous mice: reduction of p53 dosage can promote cancer formation*. EMBO J, 1998. **17**(16): p. 4657-67.
97. Liu, Y., et al., *Deletions linked to TP53 loss drive cancer through p53-independent mechanisms*. Nature, 2016. **531**(7595): p. 471-475.
98. Shirole, N.H., et al., *TP53 exon-6 truncating mutations produce separation of function isoforms with pro-tumorigenic functions*. Elife, 2016. **5**.
99. Vishwakarma, R. and K.J. McManus, *Chromosome Instability; Implications in Cancer Development, Progression, and Clinical Outcomes*. Cancers (Basel), 2020. **12**(4).
100. Thompson, S.L., S.F. Bakhoun, and D.A. Compton, *Mechanisms of chromosomal instability*. Curr Biol, 2010. **20**(6): p. R285-95.
101. Bakhoun, S.F., et al., *The mitotic origin of chromosomal instability*. Curr Biol, 2014. **24**(4): p. R148-9.

102. Duijf, P.H. and R. Benezra, *The cancer biology of whole-chromosome instability*. Oncogene, 2013.
103. Holland, A.J. and D.W. Cleveland, *Boveri revisited: chromosomal instability, aneuploidy and tumorigenesis*. Nat Rev Mol Cell Biol, 2009. **10**(7): p. 478-87.
104. Baker, D.J., et al., *Whole Chromosome Instability Caused by Bub1 Insufficiency Drives Tumorigenesis through Tumor Suppressor Gene Loss of Heterozygosity*. Cancer Cell, 2009. **16**(6): p. 475-486.
105. Suzuki, T., M. Yasui, and M. Honma, *Mutator Phenotype and DNA Double-Strand Break Repair in BLM Helicase-Deficient Human Cells*. Mol Cell Biol, 2016. **36**(23): p. 2877-2889.
106. LaRocque, J.R., et al., *Interhomolog recombination and loss of heterozygosity in wild-type and Bloom syndrome helicase (BLM)-deficient mammalian cells*. Proc Natl Acad Sci U S A, 2011. **108**(29): p. 11971-6.
107. Luo, G., et al., *Cancer predisposition caused by elevated mitotic recombination in Bloom mice*. Nat Genet, 2000. **26**(4): p. 424-9.
108. Peters, J.M. and T. Nishiyama, *Sister chromatid cohesion*. Cold Spring Harb Perspect Biol, 2012. **4**(11).
109. Onn, I., et al., *Sister chromatid cohesion: a simple concept with a complex reality*. Annu Rev Cell Dev Biol, 2008. **24**: p. 105-29.
110. Tanaka, T., et al., *Cohesin ensures bipolar attachment of microtubules to sister centromeres and resists their precocious separation*. Nat Cell Biol, 2000. **2**(8): p. 492-9.

111. Mannini, L., S. Menga, and A. Musio, *The expanding universe of cohesin functions: a new genome stability caretaker involved in human disease and cancer*. Hum Mutat, 2010. **31**(6): p. 623-30.
112. Losada, A., *Cohesin in cancer: chromosome segregation and beyond*. Nat Rev Cancer, 2014. **14**(6): p. 389-93.
113. Percival, S.M., et al., *Variations in dysfunction of sister chromatid cohesion in esco2 mutant zebrafish reflect the phenotypic diversity of Roberts syndrome*. Dis Model Mech, 2015. **8**(8): p. 941-55.
114. Sakuno, T., K. Tada, and Y. Watanabe, *Kinetochore geometry defined by cohesion within the centromere*. Nature, 2009. **458**(7240): p. 852-8.
115. Baker, S.J., et al., *p53 gene mutations occur in combination with 17p allelic deletions as late events in colorectal tumorigenesis*. Cancer Res, 1990. **50**(23): p. 7717-22.
116. Baker, L., et al., *p53 mutation, deprivation and poor prognosis in primary breast cancer*. Br J Cancer, 2010. **102**(4): p. 719-26.
117. Greenblatt, M.S., et al., *Mutations in the p53 tumor suppressor gene: clues to cancer etiology and molecular pathogenesis*. Cancer Res, 1994. **54**(18): p. 4855-78.
118. Bartek, J., et al., *Aberrant expression of the p53 oncoprotein is a common feature of a wide spectrum of human malignancies*. Oncogene, 1991. **6**(9): p. 1699-703.
119. Kandoth, C., et al., *Mutational landscape and significance across 12 major cancer types*. Nature, 2013. **502**(7471): p. 333-339.

120. Freed-Pastor, W.A. and C. Prives, *Mutant p53: one name, many proteins*. *Genes Dev*, 2012. **26**(12): p. 1268-86.
121. Olivier, M., M. Hollstein, and P. Hainaut, *TP53 mutations in human cancers: origins, consequences, and clinical use*. *Cold Spring Harb Perspect Biol*, 2010. **2**(1): p. a001008.
122. Fields, S. and S.K. Jang, *Presence of a potent transcription activating sequence in the p53 protein*. *Science*, 1990. **249**(4972): p. 1046-9.
123. Raycroft, L., H.Y. Wu, and G. Lozano, *Transcriptional activation by wild-type but not transforming mutants of the p53 anti-oncogene*. *Science*, 1990. **249**(4972): p. 1049-51.
124. Brady, C.A., et al., *Distinct p53 transcriptional programs dictate acute DNA-damage responses and tumor suppression*. *Cell*, 2011. **145**(4): p. 571-83.
125. Li, T., et al., *Tumor suppression in the absence of p53-mediated cell-cycle arrest, apoptosis, and senescence*. *Cell*, 2012. **149**(6): p. 1269-83.
126. Shimada, M., et al., *Induction of Excess Centrosomes in Neural Progenitor Cells during the Development of Radiation-Induced Microcephaly*. *PLoS One*, 2016. **11**(7): p. e0158236.
127. Toruno, C., et al., *Interdependence of Bad and Puma during ionizing-radiation-induced apoptosis*. *PLoS One*, 2014. **9**(2): p. e88151.
128. Moyer, S.M., et al., *p53 drives a transcriptional program that elicits a non-cell-autonomous response and alters cell state in vivo*. *Proc Natl Acad Sci U S A*, 2020. **117**(38): p. 23663-23673.

129. Kon, N., et al., *mTOR inhibition acts as an unexpected checkpoint in p53-mediated tumor suppression*. Genes Dev, 2021. **35**(1-2): p. 59-64.
130. Jiang, L., et al., *Ferroptosis as a p53-mediated activity during tumour suppression*. Nature, 2015. **520**(7545): p. 57-62.
131. Ou, Y., et al., *Activation of SAT1 engages polyamine metabolism with p53-mediated ferroptotic responses*. Proc Natl Acad Sci U S A, 2016. **113**(44): p. E6806-E6812.
132. Janic, A., et al., *DNA repair processes are critical mediators of p53-dependent tumor suppression*. Nat Med, 2018. **24**(7): p. 947-953.
133. Fischer, M., *Census and evaluation of p53 target genes*. Oncogene, 2017. **36**(28): p. 3943-3956.
134. Ogilvy, C.S., P. Pakzaban, and J.M. Lee, *Oculomotor nerve cavernous angioma in a patient with Roberts syndrome*. Surg Neurol, 1993. **40**(1): p. 39-42.
135. Parry, D.M., et al., *SC phocomelia syndrome, premature centromere separation, and congenital cranial nerve paralysis in two sisters, one with malignant melanoma*. Am J Med Genet, 1986. **24**(4): p. 653-72.
136. Wenger, S.L., et al., *Rhabdomyosarcoma in Roberts syndrome*. Cancer Genet Cytogenet, 1988. **31**(2): p. 285-9.
137. Kitajima, T.S., S.A. Kawashima, and Y. Watanabe, *The conserved kinetochore protein shugoshin protects centromeric cohesion during meiosis*. Nature, 2004. **427**(6974): p. 510-7.
138. Salic, A., J.C. Waters, and T.J. Mitchison, *Vertebrate shugoshin links sister centromere cohesion and kinetochore microtubule stability in mitosis*. Cell, 2004. **118**(5): p. 567-78.

139. Kitajima, T.S., et al., *Shugoshin collaborates with protein phosphatase 2A to protect cohesin*. Nature, 2006. **441**(7089): p. 46-52.
140. Hara, K., et al., *Structure of cohesin subcomplex pinpoints direct shugoshin-Wapl antagonism in centromeric cohesion*. Nat Struct Mol Biol, 2014. **21**(10): p. 864-70.
141. Meyer, R., et al., *Overexpression and mislocalization of the chromosomal segregation protein separase in multiple human cancers*. Clin Cancer Res, 2009. **15**(8): p. 2703-10.
142. Solomon, D.A., et al., *Mutational inactivation of STAG2 causes aneuploidy in human cancer*. Science, 2011. **333**(6045): p. 1039-43.
143. Yamada, H.Y., et al., *Haploinsufficiency of SGO1 results in deregulated centrosome dynamics, enhanced chromosomal instability and colon tumorigenesis*. Cell Cycle, 2012. **11**(3): p. 479-88.
144. Barber, T.D., et al., *Chromatid cohesion defects may underlie chromosome instability in human colorectal cancers*. Proc Natl Acad Sci U S A, 2008. **105**(9): p. 3443-8.
145. Covo, S., et al., *Cohesin Is Limiting for the Suppression of DNA Damage-Induced Recombination between Homologous Chromosomes*. Plos Genetics, 2010. **6**(7).
146. Lu, S.A., et al., *Eco1 is important for DNA damage repair in S. cerevisiae*. Cell Cycle, 2010. **9**(16): p. 3315-3327.

APPENDIX
IACUC ANIMAL USAGE APPROVAL

**MEMORANDUM**

DATE: 04-Aug-2022
TO: Parant, John M
FROM: 
Robert A. Kesterson, Ph.D., Chair
Institutional Animal Care and Use Committee (IACUC)
SUBJECT: NOTICE OF APPROVAL

The following application was approved by the University of Alabama at Birmingham Institutional Animal Care and Use Committee (IACUC) on 04-Aug-2022.

Protocol PI: Parant, John M
Title: Understanding Genomic Instability and its Role in Cancer
Sponsor: UAB DEPARTMENT
Animal Project Number (APN): IACUC-09359

This institution has an Animal Welfare Assurance on file with the Office of Laboratory Animal Welfare (OLAW), is registered as a Research Facility with the USDA, and is accredited by the Association for Assessment and Accreditation of Laboratory Animal Care International (AAALAC).

This protocol is due for full review by 03-Aug-2025.

Institutional Animal Care and Use Committee (IACUC)

403 Community Health on 19th | 933 19th Street South